BIOLOGICALLY-INFORMED INVESTIGATIONS TO REDUCE THE FOREIGN BODY RESPONSE TO CENTRAL NERVOUS SYSTEM IMPLANTS

by

Robert Smith Oakes

A dissertation submitted to the faculty of
The University of Utah
in partial fulfillment of the requirements for the degree of

Doctor of Philosophy

Department of Bioengineering

The University of Utah

May 2016

The University of Utah Graduate School

STATEMENT OF DISSERTATION APPROVAL

The dissertation of **Robert Smith Oakes**

has been approved by the following supervisory committee members:

Patrick A. Tresco	, Chair	**11/05/2015** Date Approved
Alan Dale Dorval	, Member	**11/05/2015** Date Approved
David W. Grainger	, Member	**11/05/2015** Date Approved
Vladimir Hlady	, Member	**11/05/2015** Date Approved
Paul A. House	, Member	**11/05/2015** Date Approved

and by **Patrick A. Tresco** , Chair/Dean of

the Department/College/School of **Bioengineering**

and by David B. Kieda, Dean of The Graduate School.

ABSTRACT

Neural recording devices are a therapeutic and diagnostic option for central nervous system (CNS) diseases and a vital component of neuroscience research. However, poor functional longevity is a major hurdle facing this broad class of devices. Decreases in functionality are associated, in part, with the foreign body response (FBR) surrounding chronically implanted recording devices; which includes chronic inflammation, astrogliosis, blood-brain barrier (BBB) leakiness, and neuronal cell death. Two potential areas for intervention were explored including the initial hemorrhage that results from device insertion and the neuroinflammatory sequela. Researchers have shown that cellular interactions with extracellular matrix (ECM) are able to affect both of these aspects of the FBR. The central hypothesis driving this work is that ECM coatings which target the initial hemorrhage, should decrease the FBR. This was investigated by coating silicon microelectrode arrays (MEAs) with ECM and implanting them into motor cortex of rats. Two ECM coatings were investigated, including the xenogeneic clinically-used Avitene Microfibrillar Collagen Hemostat and allogeneic astrocyte-derived ECM. Results show that the allogeneic astrocyte-derived ECM decreased astrogliosis within the recording zone at the 8-week time point. This decrease in astrogliosis may improve device functionality, as indicated by previous studies that correlated recording metrics to histology. Interestingly, the xenogeneic Avitene coating increased IgG within the recording zone at the 8-week time point. Collectively, these results show that ECM coatings with different genetic backgrounds and compositions are able to differentially affect specific aspects of the FBR. To broaden the knowledge on the FBR to neural recording devices, the FBR of headstage components used to anchor CNS devices to the skull was analyzed. Results showed that the FBR to fixation screws and fixation anchoring adhesive illicit a chronic FBR that has all of the hallmarks described for MEAs implanted in brain tissue. Moreover, results show evidence of persistent neuroinflammation below a variety of fixation screws including chronic macrophage

activation, demyelination, and neural tissue loss. Understanding the FBR of fixation techniques, which is common to a wide variety of CNS devices, may improve the biocompatibility of existing devices and provide a reference for future biologically-informed device designs.

For my brother, Sam.

TABLE OF CONTENTS

LIST OF FIGURES

Figure

LIST OF ABBREVIATIONS

Abbreviations

ALS ..... Amyotrophic Lateral Sclerosis

BBB ..... Blood Brain Barrier

CD-68 ..... Pan Macrophage Marker (Center of Differentiation-68)

CNS ..... Central Nervous System

CSF ..... Cerebral Spinal Fluid

DBS ..... Deep Brain Stimulation

DMAC ..... Dimethylacetamide

DARPA ..... Defense Advanced Research Projects Agency

ECM ..... Extracellular Matrix

FBGC ..... Foreign Body Giant Cell

FBR ..... Foreign Body Response

FDA ..... Food and Drug Administration

GFAP ..... Glial Fibrillary Acidic Protein

IBA-1 ..... Ionized Calcium Binding Adaptor Molecule 1

NDD ..... Neurodegenerative Disease

NIH ..... National Institutes of Health

MEA ..... Microelectrode Array

MS ..... Multiple Sclerosis

PD ..... Parkinson Disease

PU ..... Polyurethane

SCI ..... Spinal Cord Injury

TBI ..... Traumatic Brian Injury

TGFβ1 ..... Transforming Growth Factor β1

TNF-α..... Tumor Necrosis Factor – alpha

UEA ..... Utah Electrode Array

ACKNOWLEDGMENTS

I would like to sincerely thank my advisor and mentor, Dr. Patrick Tresco, who offered me a research position in the summer of 2011. His mentorship has strengthened many facets of my professional development, especially my scientific approach as a research assistant and educational approach as a teaching assistant. I also want to acknowledge my advisory committee members: Drs. Chuck Dorval, David Grainger, Vladimir Hlady, and Paul House for their mentorship in regards to my projects as well as in the classroom and various department events. I would like to thank other members of the Tresco Lab for their support and companionship during my studies including Dr. Elena Budko, Dr. Ben Christiansen, Dr. John Skousen, Dr. Fan-Wei Meng, Nick Nolta, Michael Polei, and Bharath Velagapudi as well as the many other undergraduates and high school students who have come through the lab as volunteers. I would like to thank Defense Advanced Research Projects Agency and the National Institutes of Health for funding parts of my research through grants N66001-11-1-4120 / N66001-12-C-4002 and 5R21NS088737-02, respectively. I would like to thank the University of Utah's Department of Bioengineering and previous chair Dr. Rick Rabbitt and present chair Dr. Patrick A. Tresco for facilitating my teaching assistantships throughout my graduate student career. Along with the teaching assistantships, I would like to thank the wonderful students whom I instructed in Fundamentals of Bioengineering and Introduction to Modern Biomaterials, both were great teaching as well as learning experiences. Thanks to Troy D'Ambrosio who gave me the opportunity to work at the Lassonde New Venture Development Center where I was able to improve communication and personal management skills.

I would like to thank all of the members of my family. Special thanks to my parents, Marty and Toni, who have always supported my pursuits both academically and personally. They are the greatest teachers I have ever had, in the most important subject of all, life. I especially want to express my appreciation for my best friend and wife, Amelia, who encourages and

inspires me. As both of us are graduate students, many of our date nights included homework and paper writing, with the occasional email proofread. Lastly, I want to thank my late brother Sam for being my inspiration to pursue a career with an emphasis on improving the lives of others. He always saw the best in people and made every effort to help those in need, whether that was through charitable work or by providing laughter and a warm smile.

CHAPTER 1

INTRODUCTION

This introduction establishes the background necessary to understand the studies that follow including a discussion of the pathogenesis and prevalence of central nervous system (CNS) injuries and diseases, their treatment with chronically implanted devices, the limitations and concerns associated with those devices with a special focus on the foreign body response (FBR), and previous efforts to mitigate the FBR in brain tissue. Special emphasis is placed on silicon microelectrode arrays (MEAs) as this was the model system used in the experimental aspects of the dissertation. This also included associated components used to anchor such device to the skull, hemorrhage in the brain due to device implantation, immunomodulatory potential of ECM, and the influence of neuroinflammation on global brain function. Finally, section 1.9 introduces the rationale, hypotheses, and results for this dissertation as a whole.

1.1 CNS Diseases and Injuries

Diseases and injuries to the CNS, which includes the brain and spinal cord, are currently some of the most debilitating conditions for patients and healthcare systems as a whole. Due to the wide array of CNS diseases and injuries, an accurate measure of the collective prevalence and economic burden is not available. However, some of the most common diseases and injuries are detailed below to establish a point of reference for the impact of the experimental work that follows.

1.1.1 Neurodegenerative diseases

Neurodegenerative diseases (NDD) make up a large subset of CNS diseases, especially in the elderly population. Alzheimer disease is the most common NDD and cause of dementia in the United States (US). Alzheimer disease results from plaques and neurofibrillary tangles, that

are similar to implanted devices or foreign bodies, in the cerebral cortex which are associated with synaptic dysfunction, neuronal degeneration, and progressive cognitive decline [1]. In 2015, the prevalence of Alzheimer disease in the US was approximately 5.1 million people and the estimated economic burden (health care, long-term care, hospice) is expected to reach $226 billion for Alzheimer disease and other types of dementia [2]. Parkinson disease is the second most common NDD. Parkinson disease results from the death of dopamine-producing neurons in the pars compacta of the substantia nigra [3]. The symptoms are characterized by the unilateral onset of resting tremor in combination with varying degrees of rigidity and bradykinesia. As of 2010, the prevalence of Parkinson disease is approximately 630,000 people in the US with a projected economic burden exceeding $14.4 billion [4]. Lastly, a third NDD which is less prevalent but has a profound effect on the health individuals is amyotrophic lateral sclerosis (ALS), also known as Lou Gehrig Disease. ALS results from axonal denervation and neuronal cell death in lower motor neurons in the brainstem and spinal cord as well as the upper motor neurons in the motor cortex. This leads to muscle atrophy and weakness, fasciculations, and spasticity [5]. In 2012, there were 12,187 individuals identified as suffering from ALS in the US with a majority of individuals dying within 2-5 years following symptom onset [6]. The prevalence and economic burden of all NDDs is expected to scale with the ever-increasing elderly population, which is compounded by the baby boomer population who will all be 65 years of age or older by 2029 (approximately 20% of the total US population) [7].

1.1.2 Hydrocephalus

Hydrocephalus is a disease that most often affects infants and children. It is defined as an active distension of the ventricular system of the brain resulting from inadequate passage of cerebrospinal fluid (CSF) from its point of production within the cerebral ventricles to its point of absorption into the systemic circulation [8]. The consequence of this inadequate passage in infants is often an increase in head circumference that is accompanied by severe cognitive or motor dysfunction. Hydrocephalus may also develop in adults following brain injury. The prevalence of hydrocephalus has not been regularly assessed, however, one report estimates that there were 39,904 pediatric hospital admissions related to hydrocephalus based on data in

2003, which accounted for healthcare costs of approximately $2 billion [9].

1.1.3 Stroke and aneurysm

Stroke is the leading cause of long-term CNS-related disability in the US. A stroke is a disruption of the vasculature and the subsequent lack of perfusion in downstream brain tissue, which leads to a loss of neural tissue and its associated function. The two forms of stroke include ischemic, caused by arterial obstruction, and hemorrhagic, caused by vascular rupture. As of 2015, approximately 6.6 million people over 20 years of age have had a stroke in the US. In 2013, the estimated direct and indirect cost of stroke was $33.6 billion [10]. Analogous concerns to hemorrhagic stroke are brain aneurysms. An aneurysm is a ballooning or bulging of vasculature and can potentially lead to a hemorrhagic stroke, however, a majority do not rupture. Between 2002 and 2010, there were 54,589 admissions for unruptured intracerebral aneurysms [11].

1.1.4 Traumatic brain injury and spinal cord injury

Traumatic brain injury (TBI) occurs when any external force creates damage to brain tissue or causes neural dysfunction. The most common cause of TBI is motor vehicle accidents. Due to the varying levels of TBI (mild, moderate, and severe), there are a wide range of physical and psychological symptoms. As of 2005, the estimated prevalence of TBI was 3.32 million people in the US and the estimated economic burden of TBI in 2013 was approximately $78.1 billion [12]. Spinal cord injury (SCI) is another form of injury to the CNS, specific to the spinal cord. Similar to TBI, the most common cause of SCI is motor vehicle accidents [13]. Individuals with SCI experience a partial or complete loss of motor function in lower extremities depending on the location of the injury. In 2012, the estimated prevalence of SCI was 236,000-327,000, with an associated economic burden of $9.7 billion [12].

All indices of prevalence and economic burden presented in this section were based on estimates available in literature. It should be noted that these examples are not exhaustive and estimates of prevalence and economic burden vary between various academic studies as well as dedicated health organizations, which may use different methods for reaching their estimates.

1.2 Therapeutic Implants for CNS Diseases and Injuries

A number of therapeutic strategies have been developed to address the diseases and injuries listed in section 1.1. One of the most common strategies, along with pharmaceutical intervention, is medical device implantation. The medical devices detailed below range from clinically utilized to investigational.

1.2.1 Deep brain stimulators

Deep brain stimulators (DBS) are a successful therapeutic brain implanted device, which become particularly beneficial for patients that suffer from Parkinson disease and essential tremor where it is able to significantly decrease tremor severity. DBS has been beneficial for modulating several other neurological conditions including pain, epilepsy, addiction, and depression [14-16]. The device includes an implantable pulse generator and stimulating electrode array consisting of several platinum-iridium contacts [17]. This electrode is considered a macroelectrode given its size (0.06 cm^2). Experimental findings from Magariños-Ascone et al. suggest that the therapeutic benefit for Parkinson disease is a result of DBS' high frequency stimulation suppressing the action potentials of subthalamic neurons [18]. However, the specific mechanisms of action for DBS are still poorly understood. Regardless, the clinical benefit has overshadowed these unknowns and led to DBS' increasing adoption as a therapeutic device, with the DBS market projected to increase yearly at 8.9% (compound annually) between 2014 and 2020 [19].

1.2.2 Cell encapsulation and drug elution implants

Another device which has been proposed as a therapeutic for Parkinson disease is cellular encapsulation devices. In one set of studies, encapsulated dopamine-secreting PC12 cells were able to elicit functional recovery in Parkinsonian rats (6-OHDA hydrobromide lesion in substantia nigra) as determined by quantification of rotational behavior [20, 21]. The cell encapsulation approach has been postulated for a large variety of CNS diseases, with some approaches reaching clinical trials. However, while clinical trials have shown that cell encapsulation devices are relatively safe, their clinical progress has been hindered due to low efficacy [22]. Along the same lines as cell encapsulation devices, drug releasing implants also

aim to modulate the neural environment with various soluble factors, and have been investigated for NDDs and brain cancer [23, 24]. One of the most clinically successful examples are carmustine wafers (bis-chloroethylnitrosourea, Gliadel®) used in the treatment of patients with malignant gliomas and other intracranial malignancies [24].

1.2.3 Hydrocephalic shunts

Shunts, or intraventricular catheters, have proven efficacious for the treatment of hydrocephalus. Alleviation of elevated CSF pressure is achieved through a silicon elastomer catheter implanted in the ventricular space and draining into the peritoneal cavity. The passage of CSF is controlled with an inline siphon-preventing backflow, or a flow control device, which has seen a considerable amount of development over the past two decades. The most notable design improvement is the advent of adjustable pressure valves which can be set following implantation [25].

1.2.4 Aneurysm clips and endovascular coils

Aneurysm clips or endovascular coils are the two device options for individuals who have a ruptured aneurysm. This clipping or coiling is intended to limit the risk of a subsequent rupture and hemorrhage. Clips are typically made of titanium whereas the detachable coils are mostly platinum. Some newer coil designs are integrating polymers and thrombogenic agents to promote clotting inside the aneurysm [26, 27]. Coiling is the most recently developed of the two options and has shown better outcomes in comparison to surgical clipping. In a clinical study, which focused on subarachnoid hemorrhage as a result of aneurysm, coiling significantly decreased the risk of re-hemorrhage as compared to clipping [28]. Another major advantage of coiling is that a craniotomy is not required which improves patient recovery time.

1.2.5 Microelectrode arrays

Microelectrode arrays (MEAs) are used for high resolution stimulation and recording from neuronal cell bodies or cell clusters. They are an emerging technology used in the treatment of NDDs, Stroke, TBI, and SCI [16]. The most powerful form of stimulation and recording occurs at the cellular level. Specific to recording, single-unit action potentials (APs) acquired from

intracortical microelectrodes provide the highest neural signal resolution. Other modes of recording including electroencephalography (EEG), electrocorticography (ECoG), and local field potentials (LFP) have many potential benefits and have been reviewed extensively [29-32]. However, unlike the intracortical microelectrodes needed for single-unit APs, the requisite devices for these other modalities do not penetrate brain tissue. Additionally, these other modalities have a lower potential for recording resolution and do not experience the same *in vivo* complications as intracortical microelectrodes. For these reasons, devices that do not penetrate the brain are not a focus of this dissertation. For measuring single-unit APs the most common devices are microwires or microfabricated silicon microelectrode arrays.

Microwires are historically the most utilized device for single-unit AP recordings [29]. To the best of my knowledge, their use currently is limited to neurophysiology research. These wires are commonly 30-50 μm in diameter (after insulation) with the electrical conduit being a pure metal (tungsten or gold) or an alloy (stainless steel or platinum/iridium). Typical materials used to electrically insulate the wire include polyimide, poly-para-xylylene (Parylene), or polytetrafluoroethylene (Teflon) [33]. Some labs fabricate microwires into arrays in-house, which enables a high degree of customization and affordability. The Nicolelis Lab (Duke University) detailed some of the advantages of customization such as contour mapping and specificity of tip geometry [34]. There are also a number of commercial options which have more recently allowed for higher levels of customization, with the added benefit of guaranteed device tolerances (electrode length, impedance, etc.). An example is Tucker-Davis Technologies (Alachua, FL) who have a web applet that allows neurophysiology researchers to design custom microelectrode arrays [35].

Microfabricated silicon MEAs are a commercially available neural recording device option. The high cost, inaccessibility of equipment, and advanced techniques required for their fabrication restrict the in-house customization afforded to microwire arrays. However, similar to commercial microwire arrays, highly customizable silicon arrays are available from manufacturers in two-dimensional and three-dimensional configurations.

Two-dimensional or planar silicon arrays are most associated with the University of

Michigan, where their development has been extensive and led to the company Neuro-Nexus. To the best of my knowledge, their use currently is limited to neurophysiology research. These planar devices may be single or multishanked and are made through photolithography processes similar to semiconductors and microelectromechanical systems. In brief, the microfabrication process begins with a silicon substrate which is boron-doped and etched (deep-reactive ion etch) to define the MEAs profile. The processed silicon shank is then functionalized with metallic deposition of gold, platinum, or iridium oxide recording and stimulating sites depending on intended application. The probe is then separated from the silicon wafer and the shanks are insulated via a low-pressure chemical vapor deposition. Several organic materials have been investigated for final packaging including polyimide and Parylene. All dimensions are lithographically controlled with tolerances well below 1 μm [36].

Three-dimensional silicon arrays are most associated with the University of Utah, where their development has been extensive and are now marketed by the company Blackrock Technologies, Inc., located near the University of Utah. To the best of my knowledge and according to the National Institutes of Health (NIH, clinicaltrials.gov) these are the only cortically implanted MEA approved by the Food and Drug Administration (FDA) for use in human clinical trials, with the patient condition limited to tetraplegia, spinal cord injury, and brainstem stroke. The microfabrication of the UEA is quite different in nature to the lithography methods used for the 2D MEAs. First, a silicon block is processed via thermomitigation which dopes the silicon with aluminum creating tracts of highly conductive p^+ silicon. A micro-sawing technique followed by etching creates high aspect ratio individual shanks. Each shank is electrically isolated from one another at the base as a result of the regionalized p^+ silicon being encased in nonconductive n-type silicon. Each shank tip is then sputtered with iridium oxide (originally platinum was used) and insulated with Parylene-C (originally polyimide was used) [37]. This design of the UEA is roughly the same in 2015 as it was in 1990 when fabricated by Dr. Richard Normann's lab [38, 39]. Some of the most promising design modifications to the UEA are variable shank length (Utah Slanted Electrode Array) and the packaging of a wireless telemetry system on the UEA's base [40].

Sensory loss and limb amputation are two injuries not specific to CNS tissue but could benefit from stimulating and recording microelectrodes. Individuals suffering from sensory loss could benefit from stimulation of a specific brain region, thus bypassing the defunct sensory cells or pathway [41]. Example diseases include blindness or deafness, which may result from injury or degeneration of peripheral sensory cells or pathway.

One disease that exemplifies this scenario is macular degeneration which results from degradation of the central portion of vision due to photoreceptor inhibition or death. These photoreceptors are then unable to provide stimulation to brain's visual cortex, which results in large scale reorganization of visual processing [42]. Macular degeneration is currently the leading cause of blindness in the developed world. In addition, whole limb amputees could also benefit from recording MEAs implanted in the motor cortex, thus enabling control of high resolution robotic prostheses. In 2006 Hochberg et al. provided the proof-of-principle experiments for human control of robotic apparatuses when a tetraplegic patient was able to control a computer mouse and robotic hand with a UEA implanted in motor cortex [43].

1.3 Limitations and Concerns of Current and Investigational Devices

Of the device classes discussed in section 1.2, all have limitations in efficacy or safety concerns [22, 44-49]. One broad concern is infection, as with all surgical procedures and implanted devices [50]. While infections are problematic everywhere in the body, they can be particularly difficult to treat in the brain. One study looked at the effect of prophylaxis, an antibiotic, on patients with meningitis (infection of the tissue surrounding the brain). Of the 6243 patients with craniotomies (no device insertion), it was shown that prophylaxis did not significantly decrease meningitis, even though it significantly decreased the infection rate of the dermal incision site [51]. One way that hydrocephalic shunt technology has combated infection is with impregnated antibiotics, which have been shown to decrease the incidence of shunt-related infections [52]. While infection is a uniform concern for all devices, other device-specific concerns including intracortical hemorrhage, shunt occlusion, recording device reliability, and deep-brain stimulation efficacy, all contribute to poor functional longevity. Two devices that have been

especially troubled by poor functional longevity are hydrocephalic shunts in clinical use and cortically-implanted recording MEAs in research, which has inhibited their clinical use.

1.3.1 Failure of hydrocephalic shunts

In a study on hydrocephalic shunts which tracked 64 patients, ages ranged from days old to adolescence, it was shown that 84.5% of patients required at least one shunt revision surgery and 4.7% of patients required 10 or more revision surgeries [53]. The most prevalent cause was catheter occlusion, which accounted for 42% of all failures. Other common causes of failure were catheter disconnection (11%) and infection (9%). More than half of shunt failures and revisions occur within the first year. Following these acute failures, revisions were still required at time points beyond 15 years for some patients. Of all the revisions, 65.5% required replacement of the brain implanted proximal catheter. Proximal catheter occlusion occurs when tissue encapsulates the perforated catheter tip and invades the lumen of catheter through the drainage holes [54]. This tissue encapsulation and lumen infiltration is driven by various reactive cell types (inflammatory and glial) [45, 55].

1.3.2 Failure of recording microelectrode arrays

A majority of the knowledge about shunt failure has been obtained through clinical observations, explanted device analysis, and *in vitro* material analysis. Conversely, the majority of knowledge about chronic recording MEA failure has been obtained from animal experiments. This results from the neuroscience communities' extensive use of recording MEAs as a basic research tool. To date they have only been used in a limited number of clinical trials, due to a lack of device reliability and longevity [56]. In various *in vivo* neural recording studies using various species (rat, guinea pig, cat, nonhuman primate, and human) all have shown that recording quality fluctuates unpredictably and decreases over time [49, 57-65].

A retrospective study which exemplifies many of the concerns with recording MEAs was put together by the Donoghue group covering two decades of neural recording experiments in nonhuman primates (NHP). It represents one of the most comprehensive failure analyses conducted to date in nonhuman primates [49]. The studies used the UEA described in section

1.2, with a common set of measures to evaluate recording performance failure. Overall, 78 UEAs were implanted in 27 NHPs with failures grouped into acute or chronic and sorted based on failure type within the four categories which included material, mechanical, biological, and unknown mechanisms. The mean recording duration was 387 days (range of 0 to 2104 days) with a majority of the recording failures occurring within the first year of implantation. Acute mechanical failures were most prevalent at acute time points 48%, and macroscopic biological response (meningeal encapsulation) led to 53% of all chronic failures. One aspect of the mechanical and material failures that was not considered in these categories was the influence of biological factors. For instance, headstage loosening was grouped under mechanical failure, however, it was noted that a major factor of the failure was the tissue response to the headstage material. Another example was the failure of insulating material, which may be influenced to the corrosive nature of physiological environment [66, 67]. An area of failure that was not extensively investigated in this study was those induced by tissue responses on the cellular level.

A recent study focused on the FBR as it relates to single unit recording quality and longevity using a 16-shank (4 x 4) UEA implanted in rats. Results showed that a lesion/cavity formed below the implanted UEA, near the center of the implant. Single unit recording performance of microelectrodes in the center of the electrode array performed significantly worse than those located at the edge of the array. The reduction of recording performance in the center of the UEA was associated with elevated FBR, astrogliosis, and blood-brain barrier (BBB) leakiness [68]. Lastly, given that applied sciences tend to outpace the progress of basic sciences (biology, physics, etc.), it is reasonable to believe that improvements in device design and manufacturing will limit mechanical and material failures, thus increasing the likelihood that biological failures will dominate in the future [69].

While hydrocephalic shunts and recording MEAs have drastically different therapeutic applications, there are similarities between their failure modes. First, the majority of failures for both occur within the first year following implantation. Second, revision of the device usually requires removal or replacement. Finally, a majority of failures for shunts (acute and chronic time points) and for MEAs (chronic time points) are attributed to the FBR. Additionally, enhanced

astrocyte reactivity and cell attachment to the device is a common failure mode for both types of devices [45, 68]. For these reasons, understanding and reducing the FBR in brain tissue has been the primary focus of many studies seeking to improve the biocompatibility of this class of devices [70-77].

1.4 The Foreign Body Response to Implanted Devices

There are a number of differences in the CNS FBR compared to other tissues such as loose connective tissue or bone. For brevity, this section will focus on the FBR to chronically implanted devices in brain tissue. The relationship between the CNS and non-CNS tissue response has been detailed in several reviews [78, 79]. The tissue response in the CNS can be roughly classified into four phases: hemostasis, inflammation, proliferation, and remodeling [78]. The divisions between these phases are not stringently demarcated and it is important to recognize that the tissue response is a continuum. The moment of injury is the first aspect of the response to consider as it leads to mechanical damage of cells and their resulting apoptosis, necrosis, or inflammatory activation. Injury severity has influence on the scale of the four following phases [80, 81].

1.4.1 CNS hemostasis

Hemostasis is the first phase of the tissue response following injury or the implantation of a biomedical device. It is the process of stopping the initial hemorrhage, which is facilitated through activation of the coagulation cascade and formation of a blood clot, in which platelets play crucial role. The process of hemostasis begins immediately following breakage of vasculature, and can last for several hours depending on the severity of the insult. Hemorrhage can be pronounced in brain tissue due to its dense vascularization and is accompanied by neuronal death caused by nutrient deprivation, activation of the complement cascade, activation of neutrophils, and macrophages [82, 83]. Dense vascularization, detailed in Fig. 1.1, is required to maintain the metabolic activity of neural tissue [84].

The initial hemorrhage is the major complication in stroke, ruptured aneurysms, and traumatic brain injury. For larger penetrating implants, DBS and shunts, vasculature networks are

approached with great caution during insertion due to the dangers of hemorrhage [85]. Few studies have examined the hemorrhage that results from the implantation of MEAs but it is commonly indicated as a concern [56, 86-89]. Given this dissertations focus, a more detailed background on hemorrhage and hemostasis is reviewed in section 1.6.

1.4.2 Neuroinflammation

Following injury or the implantation of a biomedical device, inflammation is initiated during the process of hemostasis and continues for variable lengths of time depending on the severity of the injury or the indwelling period of the implant [90]. This process is directed by neutrophils initially, and then by macrophages, which are influenced by signaling molecules that result from cellular damage or from various phases of the hemostasis process (e.g., platelet degranulation) [91]. The first inflammatory cells to respond are neutrophils, which flood into the extracellular space during vessel rupture. They are also recruited from the surrounding intact vasculature through binding to various intravascular adhesion receptors, activated following injury, and intravascular rolling that facilitates extravasation through the endothelial wall [92]. Neutrophils at the wound site release proteolytic enzymes and reactive oxygen species during the phagocytosis and degradation of damaged tissue or at the surface of the foreign body (biomedical device) [93]. Following the initial influx of neutrophils, they undergo apoptosis after several days and are phagocytized by activated macrophages [94]. From that point on the inflammatory process is mostly dictated by extravasation of circulating monocytes, which then differentiate into macrophages and activation of tissue-specific macrophages called microglia (discussed in detail below). Unlike neutrophils which undergo apoptosis, macrophages traffic in and out of the wound to remove necrotic and foreign debris [95]. This clean up continues at the current level until the blood-brain barrier (BBB) is restored. In the absence of a foreign body, once the BBB is restored the trafficking of monocytes to the wound site is inhibited by down regulation endothelial cell selectins [96].

Another factor which potentially plays a large role in these initial events is complement activation. Complement activation evolved to removed pathogens and microbes through various pathways (classical, lectin, alternative) [97]. Complement activation is important for implanted

devices as it has been shown that artificial surfaces activate the complement system *in vitro* and *in vivo* [98, 99].

Other reactive cell types in neural tissue include tissue-resident macrophages (microglia), mast cells, and astrocytes. Microglia cells are the tissue-resident macrophage of the brain [100]. They are derived from the yolk sac unlike other circulating monocytes and blood-borne macrophages which originate from the bone marrow [101]. In an effort to delineate the role of tissue-resident and blood-borne macrophages some approaches use chimera mice, where the bone marrow is irradiated and replaced with labeled bone marrow. These experiments show that yolk-sac derived microglia may have a larger role in debris clearance at the acute time points (0-4 d) as compared to blood-borne macrophages [102]. Conversely, another study with a similar mouse model showed that blood-derived macrophages dominate the chronic biotic/abiotic interface of an implanted device [103]. However, these approaches do not account for the population of bone-marrow derived macrophages that infiltrate and reside in the CNS. To address this, a recent approach used genetic markers to label bone marrow derived cells (via HOXB8). This genetic approach has shown that even in the healthy brain there is a distributed population of bone-marrow derived tissue-resident macrophages, which accounts for approximately 40% of all brain tissue-resident macrophages [104].

Mast cells, another tissue-resident inflammatory cell type, are most associated with their role in anaphylaxis. They are mostly present in the perivascular space in the brain and in the meninges surrounding the brain. Mast cell activation during neural injury and neuroinflammation is hypothesized as a contributing factor to neuronal death following injury, especially due to their release of vasoactive mediators and other soluble factors during degranulation [105].

Astrocytes, while most associated with scarring in the injured brain, can also secrete proinflammatory cytokines and contribute to neuroinflammation [106]. The inflammatory phase is essentially resolved when all damaged/necrotic tissue is removed and the presence of proinflammatory macrophages ceases at the site of injury. Macrophages are not limited to a proinflammatory phenotype, their phenotypes exist across a wide spectrum and some contribute to the next phase, proliferation [107].

1.4.3 CNS proliferation

Proliferation is the next phase of the tissue response in the CNS and is sometimes denoted as the repair phase. The cells most associated with this phase in the CNS are astrocytes. Following injury, astrocytes encircle the injury site which is occupied by neutrophils and macrophages. This astrocyte response is often denoted as astrogliosis, where astrocytes develop a hypertrophic cytoskeletal morphology that is believed to develop a barrier around the injury site. At chronic time points this response is denoted as the glial scar. The degree of astrogliosis and glial scarring is related to the initial amount of hemorrhage and tissue damage [108]. The glial scar is a particular focus of intervention for SCI patients. Following injury in the spinal cord, the glial scar formation and secretion of inhibitory proteins (e.g., chondroitin sulfate proteoglycan or CSPG) prevents axonal regeneration, thus limiting functional recovery [109]. Similar to neuronal outgrowth inhibition in the spinal cord, cortical neurons cannot transverse the glial scar due to these inhibitory molecules. While this is detrimental for regeneration, strictly eliminating astrogliosis is not an option as it has also been shown to be protective. This protective nature was show in a study that looked at the tissue response in the spinal cord when reactive astrocytes were selectively deleted in transgenic mice by administration of viral agent ganciclovir, which showed that reactive astrocytes are required for wound healing, protected neuron, and oligodendrocyte function, and preserved motor function in mild or moderate SCI [110].

Unlike other cells involved in CNS injury, differentiated neurons established in the cerebral cortex are unable to proliferate and retract their processes or die as a result of the high levels of inflammation [76, 111, 112].

1.4.4 CNS remodeling

Remodeling, like neuronal proliferation, is limited in the CNS as compared to peripheral tissues. One reason is the chronic nature of the glial scar, which does not resolve and remains above background at chronic time points [76, 77]. When an area of damage is large a CSF filled cavity often develops that is encapsulated by hypertrophic astrocytes [113]. The lack of neural remodeling and reconstruction is a critical limitation for diseases such as stroke and

neurodegenerative diseases, which has prompted interventions that range from growth factor to stem cell delivery to promote functional recovery [113, 114]. Additionally, this means that iatrogenic injury must be minimized to preserve as much of the natural architecture as possible.

1.4.5 The foreign body response

The tissue response detailed above is relevant to a transient injury, however, when a device is chronically left indwelling, there is a deviation from this process known as the foreign body response (FBR). The FBR is observed around all chronically implanted biomedical devices, materials or research tools including those devices introduced in section 1.2, [44-46, 76, 115]. In an effort to understand and improve biocompatibility, FBR to recording MEAs (Fig. 1.2) has been an area of considerable focus in recent years. For this reason, and given the focus of this dissertation, the FBR description below focuses on the FBR surrounding intracortical MEAs. The first notable difference in the FBR is that it does not resolve. A layer of activated, phagocytic macrophages is observed adjacent to the interface over the entire indwelling period irrespective of the type of device, its material makeup or the species studied. The response has been called frustrated phagocytosis, which eventually leads the fusion of macrophages and the formation of multinucleated, foreign body giant cells (FBGC) at the biotic abiotic interface [116-118]. Our lab has previously shown that on explanted brain implants these activated proinflammatory macrophages release a number of proinflammatory cytokines including monocyte chemotactic protein-1 (MCP-1) and tumor necrosis factor-alpha (TNF-α) [76]. A more recent study showed the presence of multinucleated FBGCs on the base of a chronically implanted UEA in rat cortex [68]. The surface adherent macrophages are believed to be a driving force behind the FBR as they secrete a wide array of cytokines, chemokines, and effector molecules which affect tissue remodeling and may damage surrounding neural tissue [111, 118-122].

Immediately beyond the macrophage layer is a layer of hypertrophic astrocytes. Similar to the glial scar that forms following injury, the astroglial scar associated with device interfaces does not resolve and is known to secrete proinflammatory cytokines [106, 123]. Associated with this persistent inflammation is a leaky blood-brain barrier (BBB) as identified by plasma proteins that are present in the brain parenchyma throughout the indwelling period [124, 125]. This sets

up a recurring loop as plasma proteins can induce inflammation in the brain and inflammation, in turn, causes BBB leakage due to monocyte recruitment [126, 127].

Neurons are highly susceptible to mechanical damage as well as changes (ionic, osmotic, metabolic, effector molecules, etc.) in the complex extracellular milieu [128-131]. Most researchers have reported a loss of neuronal cell bodies and their processes adjacent to the electrode-tissue interface [76, 132]. Furthermore, altered excitability in the tissue surrounding the device may also influence recording MEA functionality [76, 133]. This is particularly problematic for the advancement of neural recording devices, as single unit AP measurements require a distance of less than 140 μm between the electrode and adjacent neuronal cell bodies [134, 135]. Following these observations, a leading theory to improve the long term efficacy of recording devices is to decrease the FBR [68, 132, 136, 137].

The brain's FBR is the most common focus for improving the chronic single unit recording of cortically implanted MEAs. However, most of the devices detailed in section 1.2 require supporting components that exist outside of the cranial vault which require anchorage to the skull and must transverse several layers of noncortical tissue.

One example of noncortical tissue that significantly influences the functional longevity of recording MEAs is the meningeal layers. The meninges include the dura, arachnoid, and pia maters. Although these layers exist inside of the cranial vault and support neural function, they are mostly composed of fibroblasts and fibrous collagen, unlike the brain [138]. As noted in section 1.3, a failure mechanism of cortically-implanted UEAs is fibrous encapsulation by meningeal layers, which are originally removed above the implantation site and grow back. This thick fibroblast driven encapsulation can cause the MEA to be completely isolated from all neural tissue [49, 63, 139, 140]. Lastly, an issue which is seldom discussed as a biological problem in literature is the failure and dislodgment of headstage components [49, 58]. Headstage dislodgement is often categorized as a mechanical failure, even though the etiology is partially biological due to animal grooming but can also occur due to osteolysis surrounding bone screws which results in bone screw loosening. Additionally, the influence of these components on the underlying neural tissue was previously unknown, but is addressed in section 1.9 and Chapter 3.

1.5 Previous Efforts to Minimize the FBR to CNS Implants

Improved biocompatibility is the ultimate goal of studies that seek to minimize the FBR. Towards this end, a number of studies have focused on systemic pharmaceutical intervention, local drug elution, modification to the device geometry, and surface coatings. The majority of the techniques are directed towards recording MEAs to establish the contemporary work for the model system used in this dissertation.

1.5.1 Systemic pharmaceutical administration

Systemic pharmaceutical interventions have focused on the inflammatory response to cortical implants [141, 142]. One investigation analyzed the influence of systemic anti-inflammatory treatment on MEA recording function by orally administering minocycline, a tetracycline antibiotic. The rationale for using minocycline, a tetracycline antibiotic, is its neuroprotective effects when administered following CNS injury or for neurodegenerative diseases. While the exact mechanism of this neuroprotection is unknown, it has been postulated that the root cause is inhibition of microglia activation and excitotoxicity [143]. Their results showed that the minocycline treated group had a higher signal-to-noise ratio, more functional recording channels, and a lower area of astrocyte (GFAP) immunolabeling [144]. Drawbacks of this approach were the limited time points and that minocycline is not a viable chronic solution due to side effects. Regardless, the experiment indicates a relationship between the FBR, specifically astrogliosis, and functional performance.

1.5.2 Local drug and small molecule elution

Local drug elution is another technique which builds off of the concept of influencing the FBR through anti-inflammatory agents or growth factors but avoids the systemic complications. A number of studies have investigated elution of dexamethasone (DEX) as a means to decrease the FBR [145, 146]. The rationale for using dexamethasone, an anti-inflammatory glucocorticoid hormone, is based on studies using systemic injections which decreased astrogliosis around CNS implants [141]. The mechanism of action for this decrease in astrogliosis is attributed to dexamethasone's immunosuppressant/anti-inflammatory properties. However, systemic

administration has a number of dangerous side effects, thus prompting its incorporation into a coating for elution [147]. A study from the Bellamkonda lab showed that MEAs with DEX eluting coatings significantly decreases astrogliosis (GFAP) at both 1 and 4 weeks. However, while inflammation was significantly decreased at 1 week, the benefit was lost at 4 weeks [148]. Another study on DEX elution focused on electrical impedance and showed that impedance did not increase within the first 2 weeks surrounding DEX eluting coating, as compared to uncoated controls which approximately tripled [149]. Other small molecules eluted from the interface include alpha-melanocyte stimulating hormone (α-MSH) and Interleukin-1 receptor antagonist (IL-1ra) that both act as anti-inflammatory agents, and nerve growth factor (NGF) that would supposedly influence neurite growth and neuronal survival [150-152]. One problem with the drug elution approach is the finite supply and lifespan of the eluted drug. A different proposed method to circumvent this and provide unlimited local drug elution is the integration of drug infusion cannula into 2D planar MEA [153]. For injuries to the spinal cord a great deal of work has focused on altering the glial scar to be permissive for neuronal regeneration. These techniques include injectable hydrogels which target either the degradation or alteration of CSPG sulfation or cellular grafts which promote axonal growth via neurotrophic factors [154-157]. Additionally, the implantation of scaffolds to instruct neuronal pathfinding via growth factors or genetic manipulation has been investigated [158, 159].

1.5.3 Device geometry and constitutive modification

Device geometry and constitutive property modification includes alterations of shank size, spacing, inclusion of barbs to maintain position and organization (i.e., braided microwires), and device stiffness [34, 160-162]. There are two primary rationales for modifying the architecture and constitutive properties of MEAs. The first rationale is based on surface-adherent macrophages, which secrete factors that shape the FBR, being influenced by device geometry and permeability that facilitate clearance of proinflammatory cytokines [76, 136, 163]. The second rationale is based on notion that mechanical mismatch between the stiff device and soft neural tissue continuously damages tissue at the biotic-abiotic interface due to micromotion [164, 165]. The influence of surface area was investigated by creating a lattice designed electrode with

openings along the shank [163]. The important feature of this lattice design was that it maintains the same penetrating profile as a solid MEA, which resulted in an equivalent iatrogenic injury. The FBR around the lattice MEA was significantly less, with macrophage activation (CD68) and BBB leakiness (IgG) being significantly less than solid controls and neuronal density (NeuN) being significantly higher than solid controls. A proposed source of this improvement was the decreased amount of surface adherent macrophages (due to less surface area) and an increase in the clearance of proinflammatory factors secreted by the surface adherent macrophages. Interestingly, the level of astrogliosis was not influenced at chronic time points. Along with other studies which look at the time course of astrogliosis, this indicates that the acute factors are influential in the chronic astrogliosis [73].

A concept related to surface area and increased cytokine clearance is that of interfacial permeability [136]. To test this, a 400 μm thick hydrogel (alginate) coating was applied to a MEA and compared to uncoated controls. Results showed that even though this coating had a larger surface area than an uncoated control, the level of macrophage activation (CD68), astrogliosis (GFAP), and BBB leakiness (IgG) was significantly less and neuronal density (NeuN) was significantly higher than solid controls. Another aspect of the hydrogel coating to consider is its pliable nature. Low modulus MEAs are proposed by several groups as means to limit the mechanical mismatch between the stiff device and compliant brain tissue [164-166]. However, dissecting the relationship between permeability and mechanical mismatch has been challenging due to the innate permeability of compliant materials. Recent and future material science developments in nanoporous materials (i.e., silicon and gold) should allow for a better understanding of the relationship between permeability, surface area, and device modulus [167, 168].

1.5.4 Synthetic polymer and protein coatings

Lastly, device surface coatings composed of either synthetic polymer or proteins have been investigated for their influence on the FBR [169-171]. The approach of many of these coatings is unclear as they list vague mechanisms of action or rationales which are not biologically-centric. One study on synthetic insulator, Parylene-C, does list a rationale of reducing

microglia cell attachment [73, 121]. In this study on the electrode insulator Parylene-C, which facilitates significantly less cell attachment than bare glass *in vitro*, there was no influence on the FBR. This contributes to the view that an inert coating does not alter the FBR. Alternatively, a number of groups have investigated bioactive single protein coatings which were not designed for elution, but are tethered to the interface. These include neural adhesion molecule L1 and CDPGYIGSR peptide (facilitate cell adhesion and neurite extension), gelatin (acts a degradable support), and IL-1ra (binds inflammatory molecules) [172-176]. In one study laminin-1 (polyanion) was coated onto the surface of a MEA via a layer-by-layer (LbL) deposition with polyethyleneimine (PEI, polycation) with the general rationale of promoting tissue integration [177]. Compared to uncoated controls, the LbL laminin-1/PEI coating significantly increased macrophage activation (CD68) at 24 h, no difference at 1 week, and a significantly decreased macrophage activation at 4 weeks. Astrogliosis (GFAP) surrounding this coating was no different than controls at 24 hr and 1 week, however, it was significantly decreased at the 4-week time point. There was no observed difference in the neuronal density.

These strategies have had mixed results in regards to their influence on the FBR. The vast majority have focused on the inflammatory and proliferative process, with a few focusing on neurotropism and cell adhesion. The similar nature of the above quantification approaches most likely originates from the referencing of the qualitative Szarowski 2003 and quantitative Biran 2005 publications [76, 178]. For these previous studies, the typical indwelling endpoints range from 1 week to 16 weeks, and cohort sizes range from 4-9 animals. While inflammation was a common target for strategies discuss in this section, none of these approaches specifically addressed the first instigator of inflammation, the initial hemorrhage.

1.6 Hemorrhage and Hemostasis in the CNS: Background for Hemostatic ECM Coatings

Cerebrovascular damage occurs during the insertion of any device into the brain. The resulting hemorrhage is evident following the acute insertion of a MEA into human cortical tissue, as shown in Fig. 1.3. Hemostatic mechanisms stabilize the hemorrhage and limit neuronal cell death [82]. During hemostasis, platelets play many critical roles following their adhesion,

activation, and aggregation. Platelets form the primary hemostatic plug and undergo degranulation; releasing factors which directly accelerate the coagulation cascade [179]. The initial adhesion and subsequent activation of platelets is induced by specific binding motifs located on extracellular matrix (ECM) proteins, which compose the vascular basement membrane. Of these proteins, collagen and laminin are known to initiate adhesion and activation through the platelet glycoprotein VI receptor pathway [180, 181]. Collagen, the most abundant protein in the ECM, specifically induces platelet activation through the recognition of Gly-Pro-Hyp peptide sequence [182]. Laminin, via integrin $\alpha_6\beta_1$, supports extensive platelet spreading and specifically stimulates the formation of filopodia and lamellipodia [183]. Other ECM proteins known to aid in platelet adhesion are fibronectin and vitronectin [184].

In the clinical setting, collagen powders and sponges have served as the gold standard for managing bleeding. *In vitro* studies using clinically-available topical hemostatic agents indicate that noncrosslinked collagen is the most effective mechanical inducer (no thrombin) of hemostasis when compared to gelatin and cellulose [185]. To leverage these hemostatic abilities, investigational endovascular coils have been coated with ECM proteins to promote coagulation of blood inside of an aneurysm [27]. Cumulatively, these studies indicate that mimicking the heterogeneous protein composition and available binding motifs of the vascular basement membrane would be an effective strategy for accelerating hemostasis.

1.7 The Role of ECM in Immunomodulation and CNS Wound Healing: Background for Immunomodulatory ECM Coatings

Acellular tissue engineering scaffolds composed of ECM proteins have demonstrated an ability to direct the tissue response towards a proregenerative phenotype. This, in part, is attributed to the immunomodulatory abilities of ECM. Brown et al. showed that implanted biologically-derived meshes induce a higher ratio of alternatively activated, proregenerative macrophages to classically activated, proinflammatory macrophages. The initial ratio of proregenerative to proinflammatory macrophages was correlated to differences in chronic tissue remodeling [186]. Furthermore, acellular ECM constructs are able to induce a higher ratio of proregenerative macrophages in comparison to cellular constructs; even autologous cellular

constructs resulted in a dominant proinflammatory macrophage response [187]. When ECM was used as a coating for subdermal implants, the degree of fibrosis was significantly decreased 180 days post implantation [188].

Modulating macrophage phenotype and their secreted factors may be especially beneficial in the CNS since proinflammatory macrophages are neurotoxic and proregenerative macrophages promote axonal regeneration and dendritic pruning [189-191]. Injection of a hydrogel ECM in the CNS following traumatic brain injury was able to attenuate local damage [192]. Additionally, studies have shown that nonsoluble factors, such as ECM proteins, secreted from cells alter the morphology and inflammatory processes of CNS tissue-resident macrophages [193-196]. Taken together, these studies indicate that ECM may improve the tissue remodeling following CNS injury through immunomodulation.

1.8 Fixation and Neuroinflammation of Chronic CNS Devices: Background for Headstage FBR Analysis

As mentioned in section 1.4.5, devices implanted in the CNS require anchorage to other tissues in order to perform their intended function. This is especially true for *in vivo* animal studies due to animal interactions or specific grooming behaviors, which might loosen or remove the device. For the most part, all investigational devices in section 1.2 are fixed to the skull with similar techniques (Fig. 1.4).

1.8.1 Fixation techniques for chronic CNS devices

These techniques include anchorage to screws attached to the skull, and encapsulation of the screws and transcutaneous connector in a cement or adhesive to form a headstage [58, 70, 197, 198]. One reason for this similarity in device anchorage is, especially in recording devices, the comparable size and design of the electrical connectors. The standard nature of the connectors is an important aspect as it allows a group to easily connect several different types of recording devices to the same testing or recording apparatus [70]. The size of the animal dictates the number of implants and the corresponding size of the headstage [198]. For example, the size of the nonhuman primate (NHP) brain and skull enables the use of larger MEAs as well as a

larger pedestal and screws for anchorage [49]. The NHP skull is also significantly thicker, which allows for better thread engagement between the screw and bone. Conversely, in rodents, headstage fabrication is limited to the use of screws and adhesive encapsulation to anchor the MEA to the skull [60, 68, 197, 199-202]. Similar screw and adhesive encapsulation techniques are used experimentally for deep brain stimulators, hydrocephalic shunts, optogenetic fiber optic probes, microdialysis probes, push-pull cannulas, tubing for drug infusion, and cranial windows used in advanced microscopy studies [119, 139, 203-206]. The skulls of rodents are much thinner and vary with age, which limits the strength of screw fixation in comparison to NHPs. Furthermore, the primary device component (recording or stimulating MEA, optogenetic probe, microdialysis cannula, etc.) makes up a small percentage of the entire implanted surface area.

While significant attention has been directed to studying the FBR to MEAs implanted in cortex, little attention has been directed to studying the FBR associated with the other headstage components that are used to secure MEAs to the skull during chronic use. Fixation screws (Fig. 1.5) are of special interest as they generally penetrate the skull to make contact the meninges and the underlying brain tissue.

1.8.2 Neuroinflammation and neural function

Emerging evidence on neuroinflammation and its impact on opening the BBB, decline in neurogenesis, and reductions in cognitive function suggest that the scientific community should consider the headstage and its associated components an integral part of the MEA [203, 207, 208]. One group employed a cortically-implanted electrode and cannula to directly stimulate neuroinflammation via lipopolysaccharide (LPS) infusion, and showed that the treatment decreased hippocampal neurogenesis [208]. Moreover, other groups have shown that chronic inflammation outside the CNS has detrimental effects on neurogenesis [207, 209, 210] as well as on neural connectivity [211]. One study mapped the widespread macrophage and glial activation using autoradiography of [3H]PK11195 in the rat brain accompanying the use of a deep brain stimulator (DBS). The DBS was fixed to the skull with multiple screws and acrylic dental cement. The results showed widespread and persistent neuroinflammation over an 8-week indwelling period that was accompanied by cognitive deficits, as determined by an object recognition test

[203]. Studies which have looked at the impact of a craniotomy alone showed neuroinflammation notion that inflammation resulting from an indwelling device or surgical procedure, either located and functional deficits 2 weeks following surgery [212, 213]. Together, such studies support the notion that inflammation, within the brain or systemically, can impact global brain function and not just at the environment surrounding the implanted MEA. In an effort to improve the biocompatibility of the device as a whole, an understanding of FBR to all of the components of the device may be required to maximize biocompatibility.

1.9 Introduction to This Dissertation

CNS implanted devices are an important therapeutic option for CNS diseases and a vital investigative tool used in basic neuroscience research. However, poor functional longevity has limited its impact in research and in clinical medicine. It is currently held within the scientific community that the decreases in single unit recording function is associated, in part, with the foreign body response (FBR) that surrounds implanted devices; which includes persistent inflammation, astrogliosis, BBB leakiness, demyelination, and neuronal cell death. Two potential areas for intervention are in limiting the initial hemorrhage that results from device insertion and the subsequent neuroinflammatory sequela. As already discussed, cellular interactions with extracellular matrix (ECM) have been shown to promote hemostasis and possess immunomodulatory properties. The central hypothesis driving this work was that ECM coatings which target initial hemorrhage and aspects of neuroinflammation will decrease the FBR at chronic time points. This was investigated by coating silicon MEAs with ECM proteins and implanting them into the cortex of Sprague-Dawley rats. The approach was identical to that used in previous studies from our lab that investigated device geometry modifications and hydrogel coatings [136, 163], and was similar to other studies who have investigated the foreign body response (FBR) to MEAs implanted in the rat CNS [73, 136, 145, 148, 150-152, 169-173, 175-177, 214-222].

First, based on the rationale of promoting hemostasis (section 1.6), it was hypothesized that a coating developed from a FDA-approved neurosurgical hemostatic agent, Avitene™ Microfibrillar Collagen Hemostat (MCH), would decrease aspects of the FBR including

inflammation, astrogliosis, BBB leakiness, and neuronal death over the chronic time point. *In vitro* assays on Avitene coatings confirmed its hemostatic properties, but showed no immunomodulatory potential using a microglial activation assay *in vitro*. Quantitative immunohistochemistry of the FBR to chronic implanted Avitene coated MEAs showed that there was a significant increase in IgG within the recording zone. Additionally, there was no significant influence on CD68, GFAP, or NeuN density compared to uncoated controls. To the best of my knowledge the Avitene coating is the first protein coating applied to a recording MEA that did not result in a significant decrease in any of the classic FBR hallmarks. Interestingly, the increase in IgG may indicate an enhancement of late phase neuroinflammation or possibly an unresolved provisional matrix.

Second, based on the rationale of using a hemostatic agent that also possesses immunomodulatory properties (section 1.7), it was hypothesized that a coating developed from an allogeneic tissue-specific ECM would decrease the FBR including inflammation, astrogliosis, BBB leakiness, and neuronal death over the chronic time point. The ECM for this coating was derived from allogenic astrocytes harvested from the cortex of postnatal Sprague-Dawley rats. *In vitro* assays showed that astrocyte-derived ECM possessed hemostatic properties similar to Avitene, and, unlike the Avitene coating, showed an ability to reduce the activation of microglial in an *in vitro* assay. It was found that the astrocyte-derived ECM coating, decreased the amount of GFAP within the recording zone compared to uncoated controls but found no additional benefits of its use on reducing other aspects of the FBR. This decrease in astrogliosis may improve device functionality, as previous studies have shown that elevated astrogliosis is associated with poor single unit recording performance [45, 55, 60, 68, 124].

Collectively, the results of these studies show that ECM coatings with different genetic background and compositions are able to differentially affect specific aspects of the FBR surrounding single-shank, silicon MEAs. Given the relationship between the Avitene MCH and the astrocyte ECM coatings, their methods and results have been combined to present one body of work in Chapter 2.

The third study presented in this dissertation focuses on the FBR to CNS devices as a

whole. While the electrode-tissue interface has been studied extensively, the FBR to other essential headstage components was unknown. In this study the central hypothesis was that headstage components used to anchor microelectrode arrays to the rodent skull contribute to the neuroinflammatory burden. To address this, a retrospective analysis that included 38 rats implanted with neural recording devices correlated screw locations with FBR in underlying cortical tissue. Results showed that, macroscopic damage associated with the headstage components occurs beneath 86% of bone fixation screws and characterized the associated FBR on the cellular and molecular levels. The impact of understanding how fixation techniques, common for a wide variety of neurological studies, influence the cerebral cortex and provide a reference for future biologically-informed device design. The results shown in Chapter 3 are compounded by emerging data on device-related neuroinflammation and the subsequent decline in neurogenesis and cognitive function [203, 207, 208].

In summary, the dissertation as a whole endeavors to first, decrease the known detrimental aspects of implanted CNS devices through biologically-inspired coatings, and second, further the field's understanding of the FBR to device components to provide a foundation for future biologically-inspired designs.

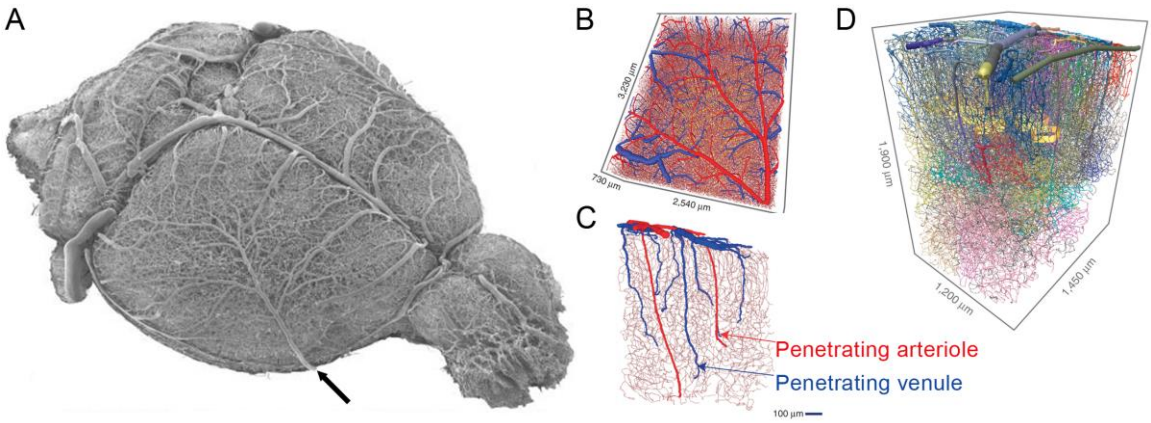

Fig. 1.1. Vasculature of the rodent brain. (A) SEM image of vascular corrosion cast of whole mouse brain with the olfactory bulb on the right side. Visible are the ascending middle cerebral artery of the right cortex (black arrow) and the venous drainage at the surface [223]. (B-D) Histological reconstruction and vectorization of neurovasculature networks in mouse brain. (B) Top view of reconstructed pial arteriolar and venular networks that feed and drain the (C) penetrating arteriole and venules, respectively. These penetrating vessels supply and drain the dense subsurface microvasculature which is (D) organized into different communities throughout the depth and breadth of the cortex. ***(A) Reprinted by permission from John Wiley and Sons: Microscopy Research and Technique, T. Krucker, A. Lang, E. P. Meyer, New polyurethane-based material for vascular corrosion casting with improved physical and imaging characteristics, Microsc. Res. Tech. 69 (2006) 138-147. http://dx.doi.org/10.1002/jemt.20263. [223], Copyright 2006. (B-D) Reprinted by permission from Macmillan Publishers Ltd (Nature Publishing Group): Nature Neuroscience, P. Blinder, P. S. Tsai, J. P. Kaufhold, P. M. Knutsen, H. Suhl, D. Kleinfeld, The cortical angiome: an interconnected vascular network with noncolumnar patterns of blood flow, Nat. Neurosci. 16 (2013) 889-897. http://dx.doi.org/10.1038/nn.3426. [224], Copyright 2013.***

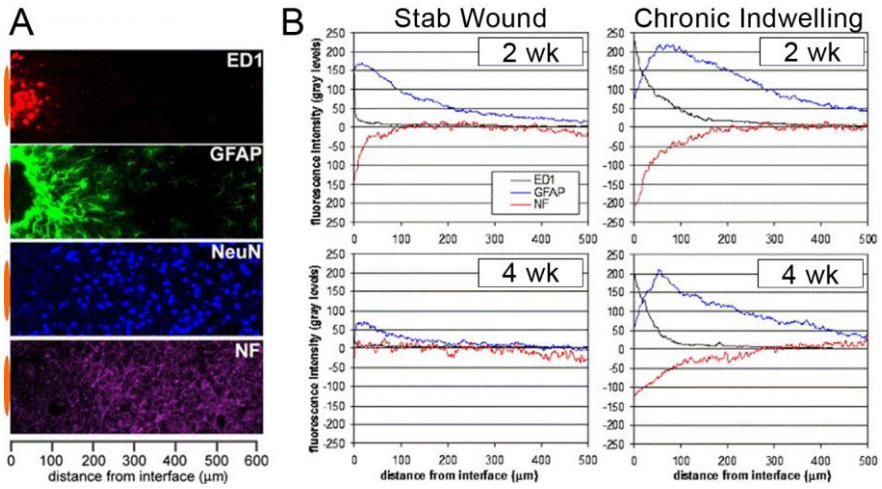

Fig. 1.2. Stereotypical FBR in the rodent brain. Biomarker immunoreactivity and quantification using cell-type-specific markers at the microelectrode–brain tissue interface. (A) Representative images collected from two adjacent sections of an animal with a 4-week microelectrode implant illustrate the general appearance of the foreign body response characterized by inflammatory (ED1) and astrocytic (GFAP) cell phenotypes adjacent to the implant interface. The area of inflammation and intense astrocyte reactivity contains a reduced number of NeuN+ neuronal bodies and a loss of neurofilament (NF) density. The position of the microelectrode is illustrated by the orange oval (drawn to scale) at the left of each image. (B) Quantitative line profile intensity analysis of ED1 (blue line), GFAP (black line), and neurofilament (red line). Mean pixel intensity per distance point for 2-week (top row) and 4-week (bottom row) time points for stab wounds (left column) and chronic microelectrodes (right column). The average standard error of the mean around each data point ranged from 4% to 14% of the mean value. Note that the GFAP response does not return to background levels at 4 weeks following a transient stab wound injury.

Reprinted by permission from Elsevier: Biomaterials, R. Biran, D. C. Martin, P. A. Tresco, Neuronal cell loss accompanies the brain tissue response to chronically implanted silicon microelectrode arrays, Exp. Neurol. 195 (2005) 115-126. http://dx.doi.org/10.1016/j.expneurol.2005.04.020. [76], Copyright 2005.

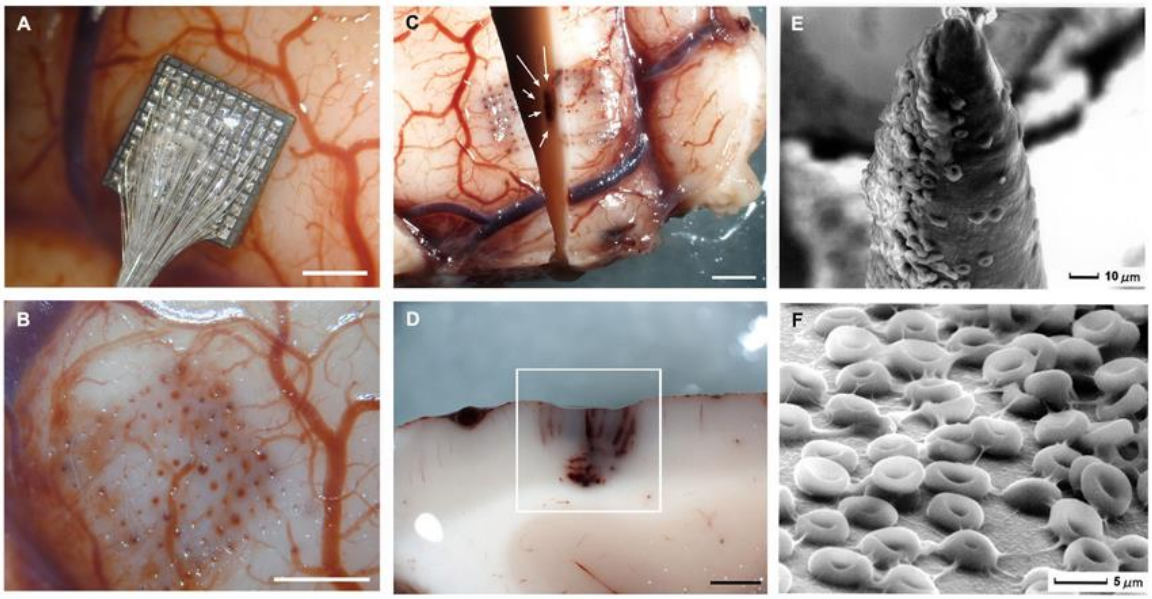

Fig. 1.3. Acute hemorrhagic response to cortically implanted MEAs. Gross specimens of human temporal lobe implantations and scanning micrographs of the surface of the UEA after acute implantation in human brain. (A) Placement of an electrode array in temporal cortex. (B) Hemorrhages in electrode tracks following array removal. (C-D) Horizontal section showing blood in the electrode tracks and petechial hemorrhages (white arrows and box) located below the tip of the electrodes. (E-F) Scanning electron micrograph of a MEA tip shows red blood cells adherent to the surface. Scale bars A, B, C and D = 2 mm. ***Reprinted by permission from Frontiers: Frontiers in Neuroengineering in accordance with open-access article terms, E. Fernandez, B. Greger, P. A. House, I. Aranda, C. Botella, J. Albisua, et al., Acute human brain responses to intracortical microelectrode arrays: challenges and future prospects, Front. Neuroeng. 7 (2014) 24. http://dx.doi.org/10.3389/fneng.2014.00024. [56], Copyright 2014.***

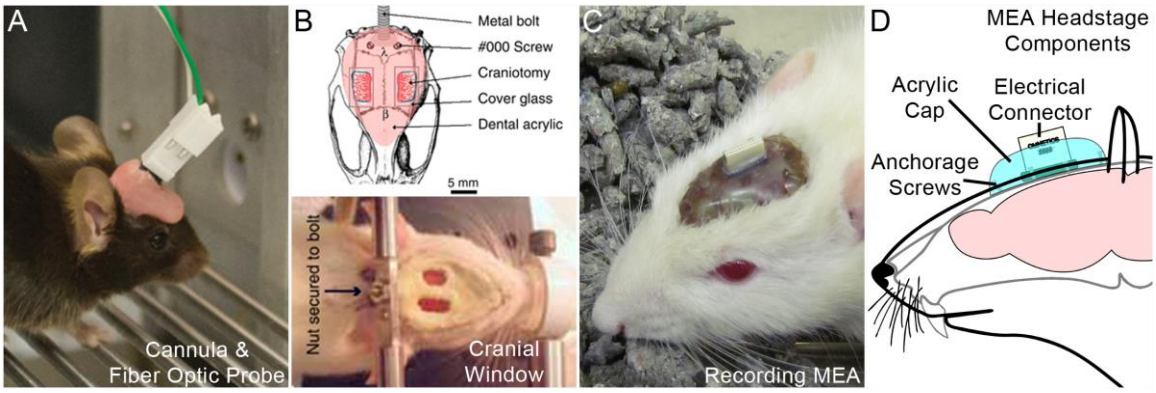

Fig. 1.4. Representative headstages for various CNS experiments in rodents including (A) cannulation and fiberoptic light delivery for optogenetics, (B) cranial windows for *in vivo* cellular and molecular imaging, and (C-D) MEAs for recording and stimulation of single neurons or neuronal clusters. While the implanted devices have dramatically different investigational uses, the techniques to secure them are essentially the same.
(A) Adapted by permission from Macmillan Publishers Ltd (Nature Publishing Group): Nature Protocols, J. G. McCall, T. I. Kim, G. Shin, X. Huang, Y. H. Jung, R. Al-Hasani, et al., Fabrication and application of flexible, multimodal light-emitting devices for wireless optogenetics, Nat. Protoc. 8 (2013) 2413-2428. http://dx.doi.org/10.1038/nprot.2013.158. [204], Copyright 2013. (B) Adapted by permission from Macmillan Publishers Ltd (Nature Publishing Group): Journal of Cerebral Blood Flow & Metabolism, A. Y. Shih, J. D. Driscoll, P. J. Drew, N. Nishimura, C. B. Schaffer, D. Kleinfeld, Two-photon microscopy as a tool to study blood flow and neurovascular coupling in the rodent brain, J. Cereb. Blood Flow Metab. 32 (2012) 1277-1309. http://dx.doi.org/10.1038/jcbfm.2011.196. [206], Copyright 2012.

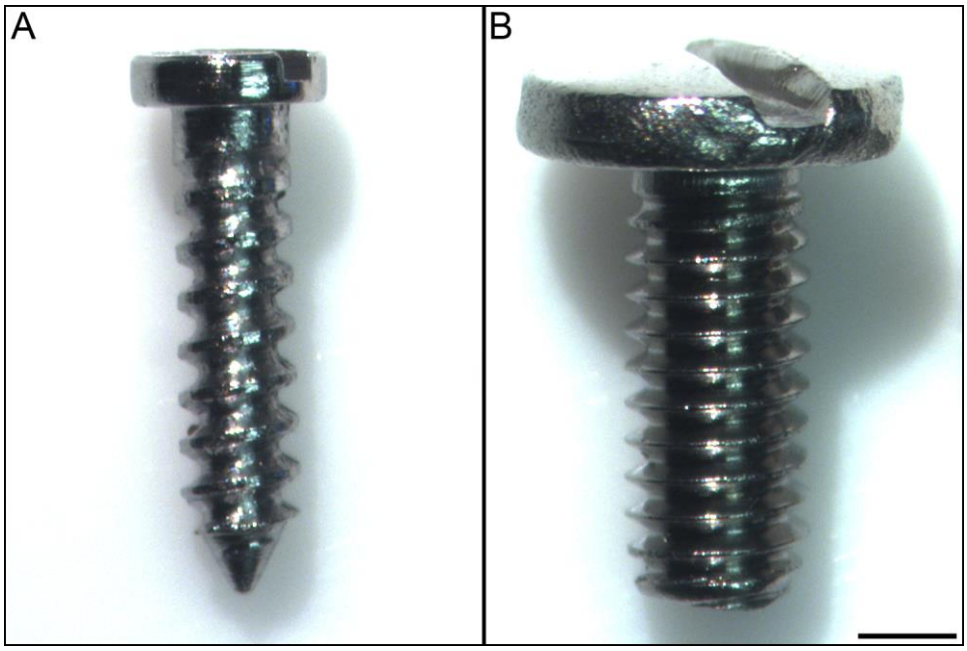

Fig. 1.5. Representative stainless steel anchorage screws used for headstage fabrication in rodents include a (A) self-tapping bone screw (#19010-00, 1.17 mm diameter, 18/8 grade SS, Fine Science Tools (FST), Foster City, CA) and (B) blunt machine screw (#B-MX-172-3, 1.85 mm diameter, 18/8 grade SS, Small Parts Inc., Miami Lakes, FL). Scale bar 1 mm.

CHAPTER 2

A COMPARISON OF THE BRAIN TISSUE FBR TO ECM PROTEIN COATED AND UNCOATED SILICON MICROELECTRODES

The format of this chapter is based on the Biomaterials journal. Authors of the prepared manuscript include Robert S. Oakes, Michael D. Polei, Dr. John L. Skousen, Dr. Michael B. Christensen, and Dr. Patrick A. Tresco.

2.1 Introduction

The foreign body response (FBR) negatively impacts the biocompatibility of various devices chronically implanted in the brain, including hydrocephalic shunts, deep brain stimulation electrodes, and intracortical recording microelectrode arrays (MEAs) [44, 45, 49]. Several efforts have targeted the inflammatory sequela of the FBR with bioactive agents, either delivered locally or systemically [141, 144, 148, 215]. This inflammatory sequela is initiated by bleeding that occurs following device insertion [225]. In particular, plasma proteins including complement and immunoglobulins activate macrophages and initiate the downstream events involved in wound healing and the FBR [226, 227]. For over a century, it has been known that products of hemorrhage elicit a phagocytic response [228]. In particular, plasma proteins including complement and coagulation components activate macrophages and initiate the downstream events involved in wound healing and the FBR [226, 227]. A recent report using two-photon *in vivo* imaging in neural tissue showed that serum protein leakage through the blood-brain barrier (BBB) induced a rapid inflammatory reaction which was correlated with areas of axonal damage and reactive oxygen species release [129]. Furthermore, the plasma protein fibrinogen has been shown to specifically activate astrocytes and drive the glial scar through modulation of TGF-β availability [229]. Several studies have shown that both the size and type of damaged

vasculature has a significant influence on the degree of damaged neural tissue [230]. These effects of hemorrhage on the health of surrounding brain tissue is a major concern [82], which applies to all implanted devices irrespective of the type of implant, species studied, or implantation method [88, 178]

To the best of my knowledge, no one has investigated the use of extracellular matrix (ECM), which naturally regulates hemorrhage, as a coating to see if promoting hemostasis can modulate the FBR to devices implanted in the CNS. Additionally, emerging evidence indicates that ECM from a number of sources is able to modulate macrophage activity towards a proregenerative phenotype [231, 232]. Therefore, an ECM surface coating that promotes hemostasis and modulates macrophage activity may lower the FBR, and by definition improve device biocompatibility. To address this hypothesis, we chose to study the effect of a coating developed from Avitene™, a FDA-approved absorbable microfibrillar collagen hemostat (MCH) derived from bovine dermis [185, 233]. Additionally, we choose to investigate an ECM derived *in vitro* from rat cortical astrocytes. The influence of these two ECM coatings on the FBR hallmarks was immunohistochemically quantified surrounding a single-shank silicon MEA implanted in Sprague-Dawley rat motor cortex, which has been used as a model system for such studies [73, 76, 103, 125, 132, 136]. Moreover, the presented work seeks to address the FBR, which has been identified as an obstacle to the widespread clinical use of intracortical recording MEAs [49, 68, 74, 124].

2.2 Methods

2.2.1 Allogeneic astrocyte ECM derivation

Cell-specific ECM was derived from primary rat astrocytes as previously described [234]. First, open-celled polymeric foams were fabricated by dissolving pellets of medical grade polyurethane (PU) elastomer (Tecoflex SG-80, Thermedics, Woburn, MA) in dimethylacetamide (DMAC) (1:10 w/v) overnight at 60°C [234-236]. A poloxamer solution (Pluronic 10R5, BASF, Germany) is then added to the dissolved PU (1:2 v/v) and thoroughly mixed. The solution is then cooled to its cloud point at 46°C, and pipetted it into polyoxymethylene (Delrin) molds. The solution and molds are then rapidly cooled through surface contact in a dry-ice/ethanol bath to

induce a phase inversion. The molded, phase-inverted solution is then precipitated in DI H_2O overnight. Following precipitation, the resulting foams are removed from the molds, rinsed with multiple washes of DI H_2O, frozen to -80°C, and lyophilized. Lyophilized foams are sectioned into strips (30 mm x 10 mm x 2 mm) and attached to biaxially-oriented polyethylene terephthalate (Mylar) mounts using a medical grade, UV curable adhesive (MD 1180-M, Dymax, Torrington, CT). Mounted foams were sterilized using ethylene oxide (EtO). Following EtO sterilization foams are soaked in 70% ethanol for 20 min to promote wetting followed by rinsing in sterile DI H_2O. To promote cellular attachment, foams are incubated in a fibronectin (FN) solution (20 μg/mL in PBS) overnight.

Following FN incubation, PU substrates were seeded with primary astrocytes, harvested from Sprague-Dawley rat pups as previously described, at two million cells/cm^3 [237]. Astrocyte seeded substrates were cultured for 3 weeks in DMEM F12 supplemented with 10% fetal bovine serum (FBS), with media exchanged every 2 to 3 days.

Following culture, samples were rinsed in DI H_2O and frozen to -80°C. PU removal was performed as described previously with samples being soaked in the solvent DMAC for 72 h. The solvent was exchanged 7 times during the 72-hr period, 3 times on the first day and then twice daily thereafter.

The extracted material (Fig. 2.1) was then processed with decellularization techniques as previously described [234, 238]. First, samples were immersed in hypotonic Tris-Hcl buffer (10 mM, pH 8.0) with 0.1% EDTA and 10 KIU/mL aprotinin (Sigma) for 1-2 hr at room temperature (RT) to disrupt integrin-ECM interactions and deactivate proteases that were released due to cell lysis. Second, samples were immersed in Tris-Hcl buffer containing 0.1% SDS (10 mM, pH 8.0) on a rocker at 100 rpm at RT overnight to remove lipids. Third, samples were rinsed in PBS (3 times, 30 min each), then immersed in Tri-Hcl buffer (50 mM, pH 7.5) containing ribonuclease (1 U/mL, Sigma) and deoxyribonuclease (50 U/mL, Sigma) on a rocker at 37°C for 3 hr to remove nuclear material. Samples are then rinsed again in PBS on a rocker (3 times, 30 min each). To assess the effectiveness of the decellularization process, samples were stained with DAPI (4',6-Diamidino-2-Phenylindole, Dihydrochloride, Life Technologies, Carlsbad, CA, 10 μM) and

immunolabeled for the astrocyte cytoskeletal component GFAP (DAKO, Carpinteria, CA, 2.9 μg/mL). Following PU removal and decellularization steps, the remaining material was rinsed 7 times in DI H2O, frozen, and lyophilized.

2.2.2 Proteomic characterization of astrocyte-derived extracellular matrix

The ECM of the FDA-approved Avitene MCH has been extensively characterized and is composed primarily of type-1 collagen, which is essential for blood clotting [185, 233]. To identify extracellular matrix components in the astrocyte-derived ECM with similar properties, samples were analyzed with tandem mass spectroscopy (MS/MS) using similar methods as described previously [234]. In brief, the cell derived material sample was washed with 50 mM ammonium bicarbonate, denatured (Protease Max, Promega, Madison, WI) for 30 min at room temperature, trypsin (20 ng/μl) digested overnight at 37°C, and purified (Ziptip, Milipore, Billerica, MA). The MS/MS analysis was performed by the University of Utah Mass Spectroscopy & Proteomic Core Facility using a hybrid mass spectrometer (LTQ-FT, Thermo Scientific, Waltham, MA). Primary peptide molecular mass spectra were acquired by Fourier transform ion cyclotron resonance. The sequencing of individual peptide spectra was performed by collision-induced dissociation in the linear ion trap. Sample proteins were identified by comparison of MS/MS measured peptide sequences to a trypsin-cut specific protein database (Mascot version 2.2.1, Matrix Science Inc., Boston, MA).

In addition, samples of the ECMs, Avitene and astrocyte-derived, were analyzed using indirect immunohistochemistry for fibronectin (CFN; Sigma, St. Louis, MO, 14 μg/mL), laminin (LN; Sigma, St. Louis, MO, 1.38 μg/mL) and chondroitin sulfate (CS-56; Sigma, St. Louis, MO, 3.2 μg/mL). In brief, antibodies were diluted in a detergent-free blocking solution consisting of 4% (v/v) goat serum (Invitrogen, Carlsbad, CA) and 0.1% (w/v) sodium azide in PBS. Free-floating material samples were batch treated for 1 hr in a detergent-free blocking solution at room temperature, followed by incubation with primary antibodies overnight at 4°C. After 3 washes in PBS to remove excess antibody (1 h/rinse), appropriate fluorescently labeled secondary antibodies (Molecular Probes, Eugene, OR) were applied in block for 1 hr at room temperature, followed by three washes in PBS (1 h/rinse). Fluorescent images were captured with a Coolsnap

digital camera on a Nikon Eclipse E600 microscope. Immunoreactivity was compared to no primary controls to confirm specificity.

2.2.3 Nanoscale morphological assessment of adsorbed Avitene MCH

Transmission electron microscopy (TEM) images were obtained using a FEI Tecnai T12 microscope (FEI, Hillsboro, OR) operating at 120 kV. To prepare TEM samples, 10 µL of Avitene in DI H2O was adsorbed onto the surface for 1 min, excess fluid was removed with blotting paper. Next, 10 µL of 2% uranyl acetate solution was applied to the adsorbed Avitene to stain the sample on a copper grid covered with a thin carbon film. The sample was then dehydrated overnight at room temperature (RT).

2.2.4 Extracellular matrix coating solution

Both Avitene, microfibrillar collagen purified from bovine corium (dermis) and sterile processed [239], and astrocyte-derived ECM were suspended in 0.25 M acetic acid solution (sequencing-grade aldehyde-free BP1185, Fisher Scientific Company, Ottawa, Ontario) at a concentration of 1 mg/mL in a 50 mL conical tube and stirred at room temperature for 24 h. A nylon 70 µm cell strainer was used to remove large aggregates of material. All processing steps utilized sterile reagents and were performed in a sterile environment.

2.2.5 Lee-White clotting time assessment

Human blood drawn into 105 mM sodium citrate solution (1 mL citrate / 9 mL blood) was transferred to a 37°C water bath until testing. 100 µL of the suspended Avitene or astrocyte-derived ECM was pipetted against the inner wall of a 1.5 mL conical centrifuge tube and dried under sterile nitrogen flow. Citrated blood was added (450 µL) to coated and uncoated control tubes. Then 50 µL of 100 mM CaCl2 was added to the tube, which signified the start of the clotting time measurement. Vials were incubated in water bath and tilted every 30 seconds until the blood formed a solid clot that remained adhered to inverted tube. The time until this clot formation was recorded for all groups and repeated for accuracy. Data sets were normalized to the longest time-point and expressed as percent relative clotting time.

2.2.6 In vitro microglial activation assay

Microglial activation was assessed as previously described [121, 195]. Avitene and astrocyte-derived ECM suspensions were used to coat 12 mm glass coverslips by adding 50 µL to the coverslip surface, allowing them to air dry in a sterile hood, and rinsing them in sterile 1x PBS for 45 min in an incubator. Primary P2 rat microglia were then seeded on control glass coverslips or ECM coated samples in a 24-well plate at a density of 8,000 cells/cm2 in DMEM/F12 supplemented with 10% FBS. Microglia morphology was assessed with indirect immunohistochemistry for CD68 (ED-1, AbD Serotec, Raleigh, NC, 0.25 µg/mL) and IBA1 (WAKO, Richmond, VA, 0.5 µg/mL) then counterstained with DAPI (4',6-Diamidino-2-Phenylindole, Dihydrochloride, Life Technologies, Carlsbad, CA, 10 µM). Using a 20x objective IBA1+ microglia cells were morphologically classified as either ramified or amoeboid as previously described [195]. In brief, Ramified cells had 2+ branches that were equal to at least 0.5 diameter of cell body. If only 2 branches were present then at least 1 branch had to be ramified. Each field of view was considered a sample (n = 8 for uncoated controls, n = 11 for Avitene coated, and n = 12 astrocyte-derived ECM coated). Cohort means were calculated as a percentage of cells that were ramified. Astrocyte-derived ECM coatings were also seeded with primary dorsal root ganglion cells (DRGs) at a density of 20,000 cells/cm^2 to assess neuronal viability and neurite extension with Calcein AM and NeuroFilament 160 (NF 160), respectively.

2.2.7 Microelectrode arrays

Planar 300 µm wide silicon MEAs, identical to those used previously [136, 163], were supplied by the Professor Ken Wise, Center for Wireless Integrated Microsystems, at the University of Michigan. To facilitate handling, MEAs were attached to a 0.25 mm diameter stainless steel wire with a medical-grade solvent-free ultraviolet-light (UV) curable acrylated urethane adhesive (MD-1187-M, Dymax, Torrington, CT). The MEAs were cleaned by immersion in 70% ethanol followed by several rinses in sterile DI water. Following cleaning, the MEAs were sterilized with ethylene oxide (EtO) in the University Hospital Surgical Processing Department and were allowed to outgas for at least 48 hr prior to implantation or sterile coating. Sterile packets containing the MEAs remained sealed until the time of implantation or were only opened

within the sterile environment (biosafety level 2 hood) for coating application.

2.2.8 Microelectrode array extracellular matrix coatings

In order to coat batches of substrates in a reproducible manner a custom dip coating apparatus was designed with controlled actuation for optimized insertion and retraction speeds. A sterile-filtered, nitrogen jet was used as an air knife to maintain coating uniformity. Batches of planar single-shank silicon MEAs were coated with ECM suspensions. For both coatings, 10 insertion and retraction cycles were used. Following the coating process each MEA was rinsed with sterile ultrapure water to neutralize the surface. The coated devices were then allowed to air dry sealed within the sterile environment and remained in that condition until implantation.

2.2.9 Animal surgery

All procedures involving animals were approved by the University of Utah Institutional Animal Care and Use Committee (IACUC) and similar to those described previously [75, 76, 136, 163]. Briefly, male Sprague-Dawley rats (10 week old ± 2 weeks, 350 g ± 50 g) were anesthetized via inhalation of vaporized 5% isoflurane/oxygen to induce anesthesia and then maintained at 2.5% isoflurane/oxygen during the procedure. During the procedure, animal body temperature was regulated (ATC1000, World Precision Instruments, Sarasota, FL). After reaching a full level of anesthesia as assessed by lack of response to a tail/toe pinch, the animal's head was shaved, and the scalp was disinfected with 70% isopropanol and betadine. Animals were then transferred to a stereotaxic frame, and a midline incision extending the length of the skull was made. The skin was retracted and the fascia was removed with a scalpel blade. The exposed skull was then thoroughly dried with cotton tipped applicators. A craniotomy was then cut with a pneumatically-driven burr under sterile PBS irrigation, with the center of the hole positioned above the right hemisphere motor cortex at 0.2 mm rostral of Bregma, and 3 mm lateral to Bregma. Using a stereomicroscope, the exposed Dura was then opened with a 25 G needle and deflected to the side to expose the cortical surface. A custom fabricated polyurethane (ST-1085 A/B, BJB Enterprises, Inc., Tustin, CA) grommet was positioned into the craniotomy to maintain electrode position over the chronic time point. The electrode was stereotactically

positioned over the affixed grommet's annular opening. The electrode was lowered into cortical tissue to a depth of 2 mm and UV-curable adhesive was used to bond the electrode to the grommet (Fig. 2.2). A UV lamp (50W, Dymax) was used to cure the UV curable adhesive. Following these procedures, the skin was closed over the fixed electrode with suture (Vicryl Plus, Ethicon, Somerville, NJ). An antibiotic ointment, Neosporin (Johnson & Johnson, New Brunswick, NJ), was applied to the closed incision. The animals were allowed to recover in individual cages under observation. Sutures were monitored and those which were not removed by the animal during normal grooming were removed after approximately 2 weeks [68]. Each animal received a single implant in the right motor cortex that was either coated with ECM or an uncoated control.

2.2.10 Euthanasia and tissue preparation

Animals were deeply anesthetized with 5% isoflurane and transcardially perfused with PBS followed by 4% paraformaldehyde in PBS. For astrocyte-derived ECM coated and its control cohort, microelectrodes were carefully dissected from brain tissue using microdissection forceps under stereoscopic observation. Immunolabeling and imaging of the MEA surface showed little cell adhesion (data not shown). For Avitene coated MEAs and its control cohort, MEAs were left in brain tissue. Retrieved brains were postfixed with 4% paraformaldehyde for 24 hr at 4°C. Brains were then equilibrated in 30% sucrose. Following equilibration, brains were embedded in Tissue Freezing Medium (Triangle Biomedical Sciences, Durham, NC), serially sectioned in the horizontal plane (tangent to the cortical surface and perpendicular to the electrode tract) at 30 μm thickness with a cryostat (Leica Microsystems, Bannockburn, IL).

2.2.11 Histology

Tissue sections from Avitene- and astrocyte-derived ECM coating cohorts were processed in batch with sections from uncoated control cohorts. Horizontal sections were processed using indirect immunohistochemistry and primary antibodies against CD68 (ED-1, AbD Serotec, Raleigh, NC, 0.25 μg/mL) to assess activated microglia/macrophages; GFAP (DAKO, Carpinteria, CA, 2.9 μg/mL) to localize intermediate filaments of astrocytes; rat IgG (Southern

Biotech, Birmingham, AL, 0.5 µg/mL) as an indicator of BBB permeability; and NeuN (Chemicon/Millipore, Billerica, MA, 2.0 µg/mL) to label neuronal cell bodies [72, 136, 190]. Antibodies were diluted in a blocking solution consisting of 4% (v/v) goat serum (Invitrogen, Carlsbad, CA), 0.5% (v/v) Triton-X 100, and 0.1% (w/v) sodium azide. Free-floating (0.5 mL solution in 24-well plates) tissue sections were batch treated for 1 hr in blocking solution at room temperature, followed by incubation with primary antibodies for 18 hr at room temperature. After 3 washes in PBS at room temperature to remove excess antibody (1 h/wash), appropriate fluorescently labeled secondary antibodies (Invitrogen, Carlsbad, CA) were applied in block for 18 hr at room temperature, followed by 3 washes in PBS (1 h/wash). During the secondary antibody incubation, sections were isolated from light to prevent photobleaching. All sections were also counterstained with DAPI (4',6-Diamidino-2-Phenylindole, Dihydrochloride, Life Technologies, Carlsbad, CA, 10 µM) to identify cell nuclei. Tissue sections were mounted on microscope slides with Fluormount-G (Southern Biotech, Birmingham, AL) and cover-slipped [72].

2.2.12 Quantitative image analyses

Fluorescent images of tissue sections from layers IV-VI of the cortex were captured in batch with a Coolsnap digital camera on an Eclipse E600 microscope (Nikon) with a 10x air objective, using identical exposure times between coated and uncoated control MEAs. Imaging conditions were optimized for each immunomarker. All fluorescent images were light-field corrected [5]. The staining intensity for each immunomarker was quantified using a custom LabView-based image analysis program (National Instruments, Austin, TX) as previously described [72, 73, 136, 163, 240]. In brief, fluorescent intensity as a function of distance from the implant site was extracted using an array of line profiles spanning the implant site. At each point along the lines, an anti-alias pixel extraction algorithm was used to derive the pixel intensity of the line profile arrays in each section. The intensity profiles for a given immunomarker from each layer, IV-VI, were normalized to background levels. In order to quantify changes in neuronal cell body distribution, the numbers of NeuN/DAPI+ cells were manually counted in discrete bins every 50 µm from the device interface. The number of neuronal nuclei per bin were then divided by the bin area to determine the average neuronal nuclear density as an estimate of the number of

neuronal cell bodies surrounding the device. Neuronal density was then normalized to background levels. Representative images were taken on a confocal microscope (Fluoview FV1000, Olympus America Inc., Center Valley, PA) with either a 10x air or 60x water immersion objective. Representative images were arithmetically chosen from animals which best represented the cohort means.

2.2.13 Statistics

For the Lee-White clotting time and the microglia activation assay, cohorts were compared using one-way ANOVAs and Tukey post-hoc analysis by means of an SPSS software package (IBM, Somers NY), with $p < 0.05$ considered as a significant difference. All data are mean and standard error of the mean.

For the quantitative image analysis, to minimize variability and develop a more accurate cohort mean, discrete points were compared against each other as a function of distance from the biotic/abiotic interface with an outlier analysis (1.5 * interquartile range). Outlying points were automatically removed. The outlier analysis was run three consecutive times on each cohort's rostral and caudal profiles. In some cases the automatic outlier removal resulted in an animal being removed from the cohort, which is reflected in the quantification figure legends. Following outlier removal, section profiles were averaged to obtain an average intensity profile for a given animal. The average intensity profile for a given animal was then averaged with other animal profiles receiving the same type of implant to obtain an average intensity profile for each cohort. The average area under the curve of each cohort's intensity profile for each immunomarker as well as the average neuronal nuclear density at 50 mm intervals from the device interface compared uncoated controls with each ECM coated cohort, Avitene $n = 7$ and astrocyte-derived ECM $n = 6$, using a Student's t-test with $p < 0.05$ considered as a significant difference. All data are mean and standard error of the mean.

2.3 Results

2.3.1 Characterization of ECM

The Avitene MCH Flour was white and cotton- or powder-like in appearance and had an innate cohesiveness that aided manipulation (Fig. 2.3). Similar to Avitene and ECM derived from other sources, the ECM derived from astrocytes was a white, insoluble, solid biomaterial (Fig. 2.4). Following decellularization no cell nuclei or cytoskeletal structures were found within the astrocyte-derived ECM. Furthermore, all ECM components investigated with immunohistochemistry and MS/MS remained following decellularization.

Purification of the microfibrillar collagen in Avitene is detailed in several patents. The general process includes enzymatic-treatment (elastases, ficin, etc.) of sliced bovine dermis, alkaline borohydride washes, and a 1% salt solution to remove impurities, and finally precipitated by increasing the pH results in a purified collagen [241, 242]. Proteomic analysis of the astrocyte-derived ECM with MS/MS (Table 2.1) identified a variety of extracellular proteoglycans and glycoproteins. Example proteins and their influence on wound healing are described in Table 2.1. Astrocyte-derived ECM samples were processed using indirect immunocytochemistry for various ECM components found in the CNS. The astrocyte-derived ECM was immunoreactive for antibodies against fibronectin, laminin, and chondroitin sulfate gycosoaminoglycans (CS GAGs). Representative fluorescent images of these ECM components found in astrocyte-derived material are shown in Fig. 2.4B-D. Avitene coatings on the other hand showed no specific immunoreactivity for the same antibody fibronectin, laminin, and chondroitin sulfate gycosoaminoglycans (CS GAGs), but were immunoreactive for antibodies against collagen type I.

Lee-White clotting time was assessed for each of the coatings in 1.5 mL plastic conical tubes. Both the Avitene and astrocyte-derived ECM coatings had a significantly shorter time-to-clot, as compared with uncoated controls (Fig. 2.5A-B). There was no difference in the clotting time between the 2 ECM coatings.

2.3.2 In vitro microglial activation assay

The phenotype of microglia cultured on glass, Avitene, and astrocyte-derived ECM was quantified following Iba-1 immunolabeling. Fig. 2.5C-D shows the representative microglial

morphology when cultured on glass and astrocyte-derived ECM coatings in the presence of serum. Similar to studies examining microglial morphology on fixed astrocyte monolayers, a significant number of microglia cultured on the astrocyte-derived ECM coating showed a more ramified, resting phenotype (Fig. 2.5D) than those cultured on glass. There were few ramified microglia on the Avitene coating, which was not statistically different than uncoated controls.

Cytocompatibilty studies also showed the astrocyte-derived ECM to be nontoxic and adhesive to primary CNS cells. NF160 immunolabeling of P1 rat primary DRGs cultivated for 48 hr on astrocyte-derived ECM showed facilitation of neurite outgrowth (data not shown). Furthermore, Calcein AM viability staining of the DRGs showed no signs that the astrocyte-derived ECM was cytotoxic (data not shown).

2.3.3 Coating morphology and uniformity

Compared to uncoated controls both the Avitene and astrocyte-derived ECM coating were evident under stereoscopic microscopy following 10 cycles of dip coating (Fig. 2.6). Nitrogen jets aided in the uniformity of the coating, in their absence the coating appeared heterogeneous and thicker near the tip due to droplet formation. Immunolabeling of collagen type I following Avitene dip coating showed evidence of collagen microfibrils interwoven on the 300 μm wide MEA faces (Fig. 2.6D-E). The thickness of the coating visualized by stereomicroscopy appeared less than 1 μm on average. There was no evident change in either of the coatings dimensions when hydrated.

2.3.4 Immunohistological quantification of the foreign body response

GFAP was greatest along the 300 μm face of the planar silicon MEA, as opposed to the 12 μm edges. In comparison to uncoated controls, quantitative image analysis (Fig. 2.7) showed a significant reduction in GFAP immunoreactivity surrounding astrocyte-derived ECM coated MEAs within the presumptive recording zone. There was no significant difference in GFAP immunoreactivity between uncoated controls and Avitene coated MEAs. Higher magnification images (Fig. 2.8) indicated that astrocyte intermediate filaments appeared similar in thickness and distribution to those in astrocytes located in normal cortex when compared to either uncoated

or Avitene coated MEAs. This was particularly pronounced when viewed by eye using stereoscopic magnification.

In comparison to uncoated controls, quantitative image analysis (Fig. 2.9) showed a significant increase in IgG immunoreactivity surrounding the Avitene coated MEA within the presumptive recording zone. There was no significant difference in IgG immunoreactivity between uncoated controls and astrocyte-derived ECM coated MEAs. Additionally, although IgG immunoreactivity was elevated surrounding all implants it was rarely symmetrically distributed around the electrode in horizontal sections and was higher surrounding blood vessels.

In horizontal sections, CD68 immunoreactivity was observed surrounding all implants. CD68 immunoreactivity returned to background levels beyond 100 μm for all cohorts. In comparison to uncoated controls, there was (Fig. 2.10) no significant difference in CD68 immunoreactivity surrounding astrocyte-derived ECM coated or Avitene coated MEAs.

In comparison to uncoated controls, there was no significant difference in the spatial distribution of NeuN immunoreactivity between the cohorts (Fig. 2.11).

2.4 Discussion

Using a simple model system, it was shown that an allogeneic ECM coating developed from rat cortical astrocytes *in vitro*, with hemostatic and immunomodulatory properties, was sufficient to lower astrogliosis surrounding a planar silicon MEA 8 weeks after implantation. In contrast, it was shown that a xenogenic hemostatic coating developed from FDA-approved Avitene™ MCH was not sufficient to lower any aspect of the FBR 8 weeks after implantation.

GFAP labels the cytoskeleton of astrocytes and is used as a marker of astrocyte hypertrophy and astrogliosis. It has been frequently used as a biomarker of tissue reactivity [76]. In this study, a significant decrease was observed in the spatial distribution and intensity of GFAP immunoreactivity surrounding the astrocyte-derived ECM coated as MEAs compared to uncoated or Avitene™ coated MEAs (Fig. 2.7). The difference was particularly striking when viewed by eye with a binocular, stereomicroscope where the thickness of the majority of astrocyte intermediate filaments near the astrocyte-derived ECM coated interface more closely resembled that observed in unimplanted cortex at the same cortical level. The mechanism driving this difference likely

occurred acutely as the level of gliosis surrounding similar devices does not progress following the first 2 weeks of implantation and is observed at chronic time points following stab wound injuries in which the MEA was retrieved immediately following insertion [73, 76]. In cases of stab wounds made with a device or resulting from surgery or trauma the neuroinflammatory biomarkers (CD68, IgG) eventually resolve, while the astroglial scar remains [243].

IgG is an antibody present in blood and generally is not present in the extracellular space of brain tissue due to the blood brain barrier (BBB), which restricts its presence to the vascular lumen except in cases of neuroinflammation, following injury or surrounding chronically implanted biomedical devices. BBB leakiness, a hallmark of neuroinflammation, is signaled by the presence of IgG immunoreactivity in the extracellular space of brain tissue [124]. An unexpected finding in the current study was that the immunoreactivity for IgG was elevated surrounding the Avitene™ coated MEAs compared to the other cohorts. Given the presence of phagocytic macrophages in the acute phase of the FBR it is doubtful that the increased IgG represents a remnant from the initial hemorrhage that followed implantation. Studies on provisional matrix formation and its turnover suggest that it would be removed by 8 weeks [244]. Given the small quantity of material used for coating it also seems unlikely that the original ECM coatings would persist over the 8-week indwelling period [245]. It is, therefore, unclear why the observed IgG surrounding the Avitene™ coated implants was more compared to the other cohorts.

CD68 labels a lysosomal-associated membrane glycoprotein in macrophages and in tissue specific macrophages like microglia. CD68 is upregulated in areas of neuroinflammation, thus, it is commonly used as an indicator of macrophage/microglial activation [76, 132]. Neither the Avitene™ nor the astrocyte-derived ECM coatings had an influence on CD68 compared to uncoated controls. This suggests that neither coating was effective in modulating late stage or chronic inflammatory sequela of the FBR. A possible explanation for this could be that such protein-based coatings were degraded soon after implantation and only have an impact on early phase downstream events like astrogliosis.

NeuN labels the nucleus of neurons and can be used to quantify the density of neurons. Similar to the CD68 results, neither the Avitene™ nor the astrocyte-derived ECM coatings had an

influence on NeuN spatial density compared to uncoated controls. The loss of neuronal cell bodies was similar to previous reports from our lab and others that show a decrease of approximately 50% within the recording zone, which did not change over time for simple single-shank devices that cause a minimal penetrating injury [73, 136, 163]. One caveat of neuronal density is that it is not necessarily an indicator of neuronal activity. Neuron excitability is influenced by changes in the ionic balance of the extracellular milieu which is disturbed BBB leakiness. Thus, while neuronal density may have been similar after use of the ECM coatings the increase in BBB leakiness surrounding the Avitene™ coated MEA may affect recording performance [73, 130]. It will be interesting to see how such coatings influence neuronal density and macrophage activation in the FBR of more clinically relevant higher density multi-shank MEAs, such as the UEA, where the amount of vascular damage following implantation is orders of magnitude greater than that caused by single-shank MEA designs.

The decrease in astrogliosis surrounding the astrocyte-derived ECM is perhaps the most important observation from this study. This is important as the level of astrogliosis has been correlated with single unit recording performance [68]. Thus, the impact of a decrease in GFAP surrounding astrocyte-derived ECM coatings may potentially increase the functional longevity of devices implanted in the brain. Interestingly, a prior study from our group using an identical uncoated control and model system showed that by reducing surface area with a lattice architecture, which maintained the same penetration profile and initial injury, there was a reduction in chronic macrophage activation, BBB leakiness, and an increase in neuronal density at 8 weeks [163]. However, the decrease in surface area had no influence on the degree of astrogliosis at 8 weeks. Combining results from the ECM coating study with those from the surface area study, given their identical controls and analysis technique, indicates a divergent pathway in the development of the FBR where constitutive properties, such as surface area, have a more prominent impact on the chronic levels of macrophage activation, BBB leakiness, and neuronal density while bioactive coatings, such as the astrocyte-derived ECM, have a more prominent impact on the chronic level of astrogliosis.

The results and deductions from this study agree with reports of other groups which have

shown that anti-inflammatory drug eluting and single protein coatings are able to influence GFAP intensity [148, 175-177]. One unique difference, to the best of my knowledge, is the Avitene™ coating being the first protein coating applied to a recording MEA that did not show a significant decrease in any biomarker associated with the FBR.

An area for future consideration is the extensive implantation induced injury, as demonstrated by a stab wound model, observed following implantation of the Utah Electrode Array (UEA), a high density, multi-shank silicon MEA. Implantation induces a prominent lesion with extensive tissue loss that looks like an inverted pyramid with the largest area of the lesion occurring below the base of the UEA [68]. Lesions of this nature, which resemble lesions from stroke injury are not observed following stab wounds with single-shank, silicon MEAs likely due to their small penetrating profile and the lesser amount of vasculature damage following implantation. It would therefore be interesting to see whether such hemostatic coatings would lower the lesion volume that accompanies the implantation of a higher density MEA.

Another future question to investigate at greater depth is why the two ECM coatings performed differently. The hemostatic ability of Avitene™ is well documented in research and clinically [185, 233]. Immunohistochemical and proteomic analysis of the astrocyte-derived ECM revealed a number of proteins which have varying influences on biological processes. The collagens identified, VI and XII, both possess hemostatic potential, which likely is the source of the hemostatic ability observed in the clotting assays (Fig. 2) [180]. While both of the ECM coatings examined here had equivalent hemostatic properties only the allogeneic astrocyte-derived hemostat showed influence in the microglial activation assay (Fig. 2C-E). An unknown is what specific contribution the astrocyte-derived ECM's species- and tissue-specificity may have had, as both characteristics have been indicated as contributors to tissue-appropriate remodeling [246, 247]. This is compounded by the antiscarring and anti-inflammatory aspects of the astrocyte-derived ECM proteins found in the proteomic analysis and detailed in Table 2.1. Importantly, previous studies have shown that each of the identified ECM components are found in brain tissue and are produced by astrocytes [248-250]. This suggests that such coatings may have decreased the neuroinflammatory components of the FBR, however, this influence may be

limited to the acute inflammatory phase.

2.5 Conclusions

The results of this study show that ECM coatings derived from different genetic backgrounds differentially affect the FBR to single-shank, silicon MEAs. From a general biomedical device perspective, this study provides the first evidence that an allogeneic *in vitro* cell-derived ECM coating is able to decrease the degree of astrogliosis surrounding a chronically implanted single-shank MEA, presumably due to immunomodulatory effects on acute microglial activation. In concert with previous work on constitutive modification, results support the concept of divergent pathways within the FBR and decreasing the overall FBR to further improve biocompatibility will require a multifaceted approach.

Acknowledgements

Funding for this work was provided by the National Institutes of Health (NIH 5R21NS088737-02). Thanks to Dr. Vladimir Hlady and his group for generously providing human blood for the *in vitro* studies and Mr. Colin Eichinger for his assistance.

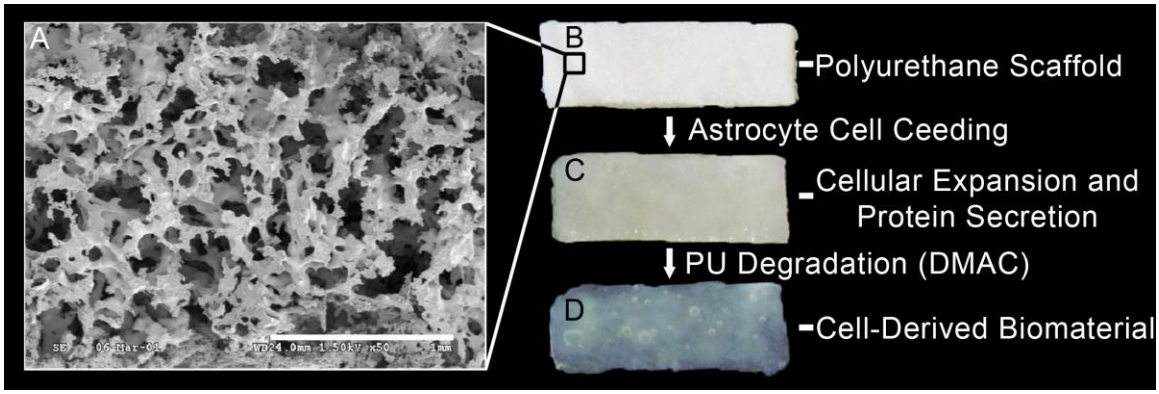

Fig. 2.1. Cell-derived biomaterial process schematic. (A) Representative SEM of sacrificial PU scaffold. Scale bar 1 mm. The cell-derived material is develop through seeding cells onto the (B) porous PU scaffold. This dissertation's cell type of focus was primary rat astrocytes which (C) expand and secrete proteins within the pores of the PU scaffold. The PU scaffold is then degraded with multiple rinses of DMAC which results in (D) a cell-derived material which is then further processed with detergent and enzymatic decellularization techniques and/or lyophilized. (B-D) For scale, scaffold width is 2 mm.
(A) Adapted by permission from Elsevier: Biomaterials, K. Webb, W. Li, R. W. Hitchcock, R. M. Smeal, S. D. Gray, P. A. Tresco, Comparison of human fibroblast ECM-related gene expression on elastic three-dimensional substrates relative to two-dimensional films of the same material, Biomaterials 24 (2003) 4681-4690. http://dx.doi.org/10.1016/s0142-9612(03)00368-5. [251], Copyright 2015.

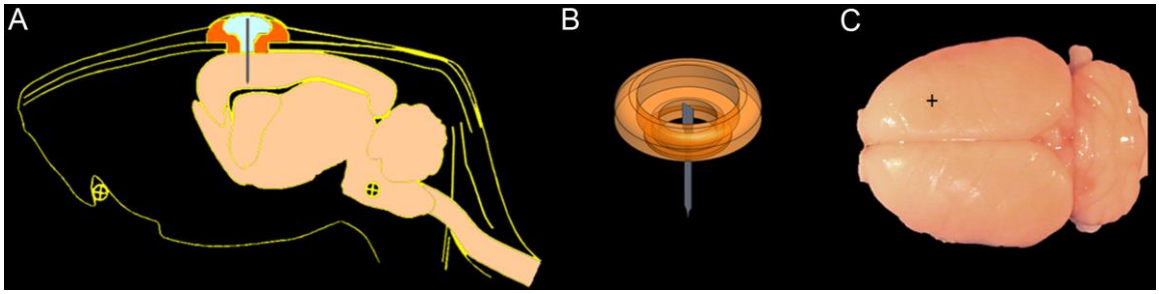

Fig. 2.2 Rat cortical implantation schematic. (A) Side profile CAD drawing of a mid-sagittal section of rat head showing approximate location of implanted silicon MEA and anchoring (B) polyurethane grommet. All MEAs were lowered stereotactically to a controlled depth of 2 mm below the surface of the cortex, and attached to a soft polyurethane grommet (orange) using a UV-curable adhesive (cyan) as shown. (C) Top view of stereotactic implantation position (+) in the right motor cortex at coordinates +0.2 mm Bregma, 3 mm lateral, and 2 mm depth.
(A) Adapted by permission from Elsevier: Biomaterials, B. D. Winslow, P. A. Tresco, Quantitative analysis of the tissue response to chronically implanted microwire electrodes in rat cortex, Biomaterials 31 (2010) 1558-1567. http://dx.doi.org/10.1016/j.biomaterials.2009.11.049. [72], Copyright 2010.

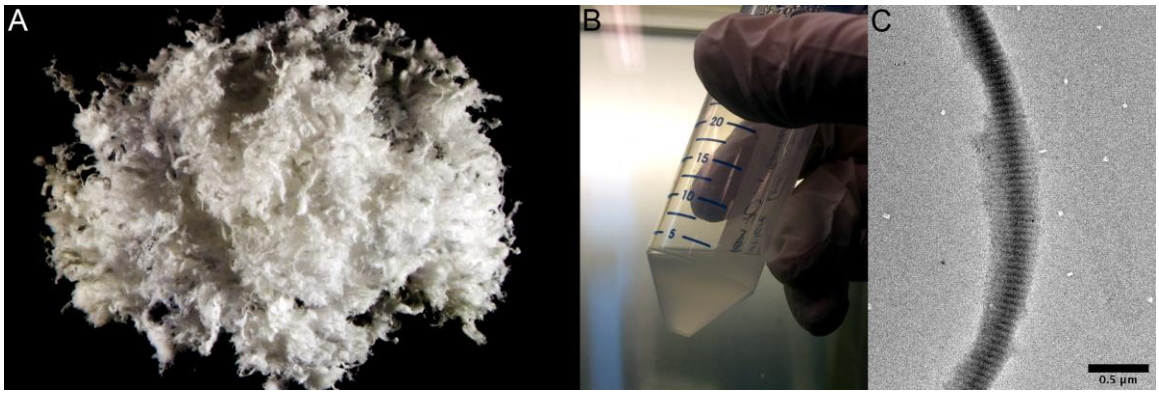

Fig. 2.3. Avitene MCH Flour dry macroscopic appearance, suspension, and TEM characterization. (A) Dry, sterile, Avitene™ MCH Flour. (B) Avitene suspended in 0.25 M at 1 mg/mL following stirring at room temperature for 24 hr and filtering with a nylon 70 µm cell strainer. (C) TEM image of Avitene morphology, displaying characteristic periodicity natural collagen due to the triple-helix structure. Scale bar 0.5 µm. TEM image courtesy of Dr. Boi Hoa San in Dr. Michael Yu's lab at the University of Utah.

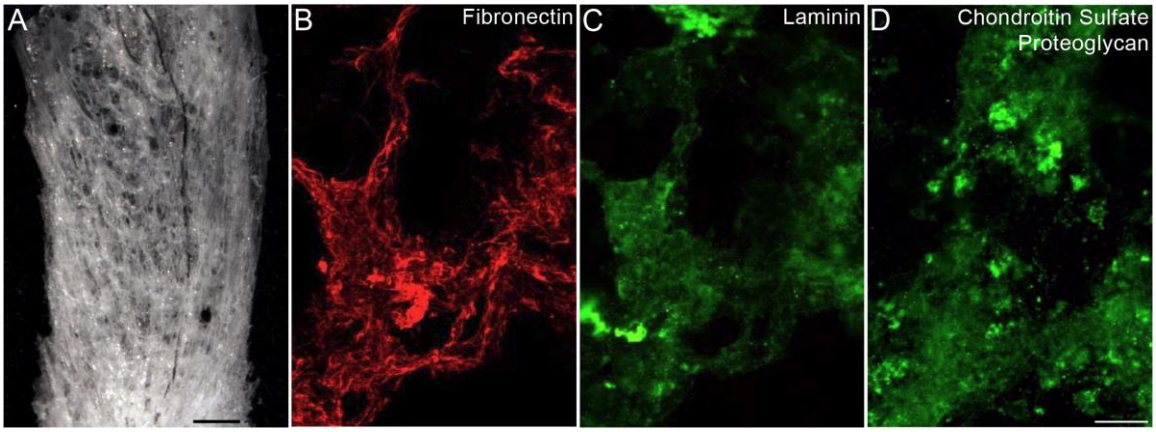

Fig. 2.4. Astrocyte-derived ECM scaffold and immunolabeled proteins. (A) Representative light micrograph of an astrocyte ECM scaffold after dissolution of the synthetic polyurethane foam and lyophilization. Scale bar 2 mm. Immunohistochemical labeling of astrocyte secreted ECM proteins (B) fibronectin, (C) laminin, and (D) chondroitin sulfate proteoglycan found in the astrocyte ECM. Scale bar 100 µm.

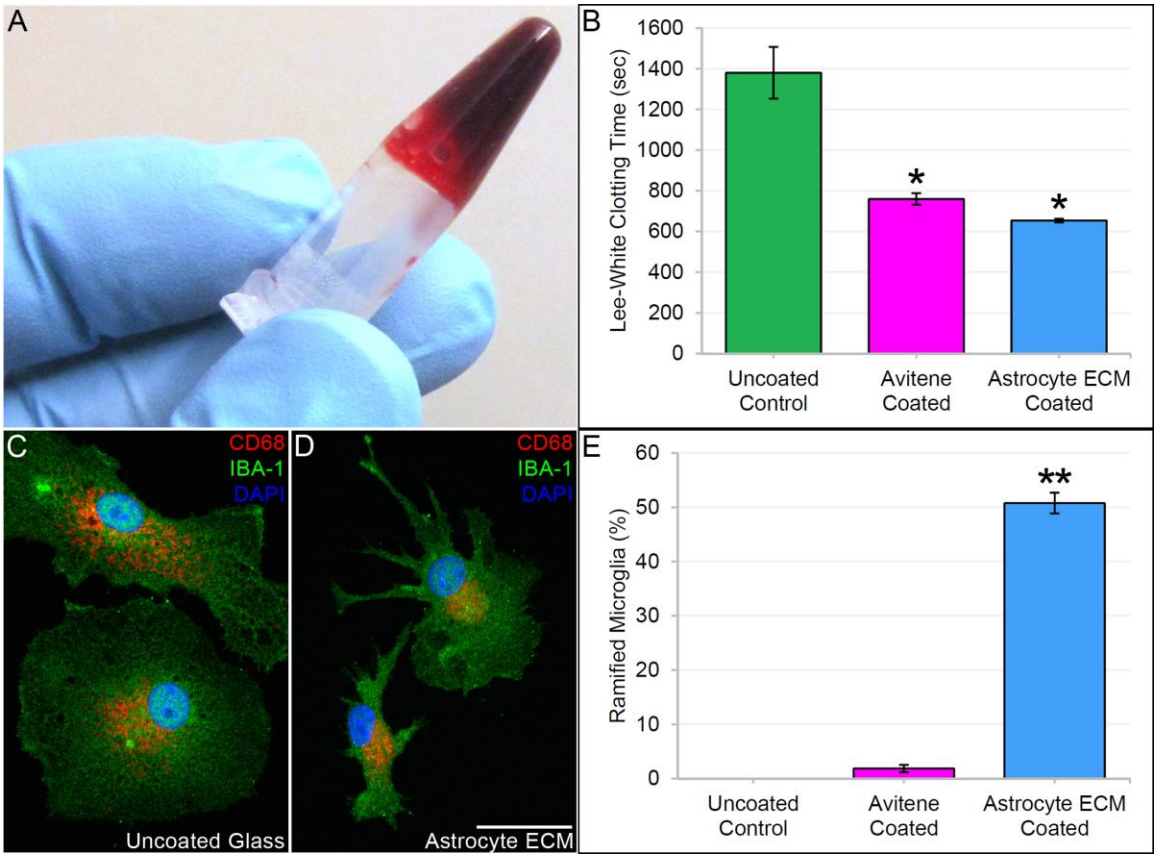

Fig. 2.5. ***In vitro*** **hemostatic and immunomodulatory characterization of ECM. Average Lee-White clotting time for (A) recalcified, citrated-whole blood placed in control centrifuge tubes or tubes coated with Avitene or astrocyte-derived ECM. (B) Both ECM coatings showed a similar ability to promote blood clotting compared to the uncoated control. (*) denotes significant difference with $p<0.05$, compared to uncoated control. Cytocompatibility studies showed the cell-derived material to be nontoxic to primary CNS cells. Representative P1 rat primary microglial morphology cultured on (C) uncoated glass or (D) an astrocyte-derived ECM coating. Scale bar 25 µm. (E) Quantification of microglia morphology on uncoated glass, Avitene and astrocyte-derived ECM coated coverslips, shown as percent ramified. Ramified cells had 2+ branches that were equal to at least 0.5 diameter of cell body. If only 2 branches were present then at least 1 branch had to be ramified. Coverslips coated with astrocyte-derived ECM had a significantly increased percentage of ramified microglia on the surface. (**) denotes significant difference with $p < 0.05$, compared to uncoated control and Avitene coated. Data shown as mean and standard error of the mean.**

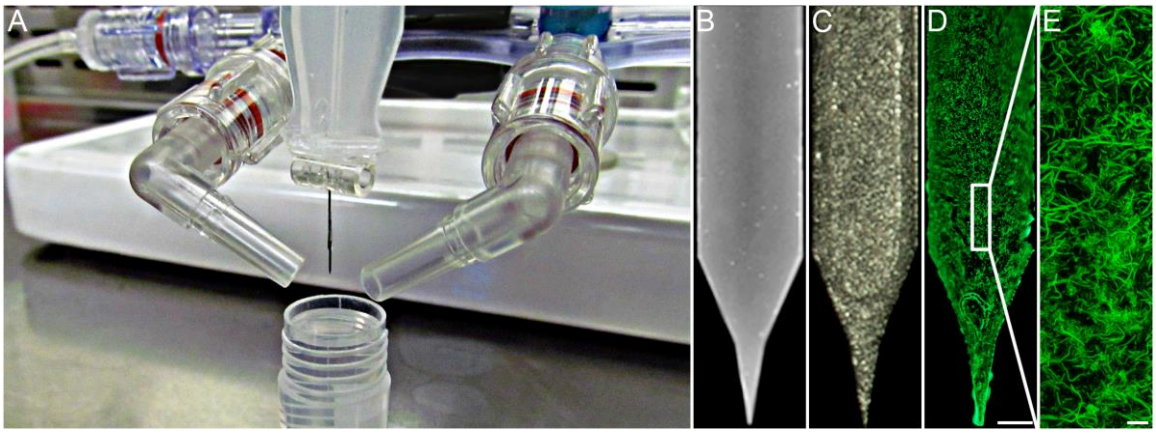

Fig. 2.6. Dip coating apparatus with astrocyte-derived ECM and Avitene coated MEAs. MEAs were dip coated in a (A) sterile environment containing a pneumatic dip coater, sterile filter nitrogen jets (to aid in layer adsorption and uniformity), and a protein suspension composed of Avitene Microfibrillar Collagen Hemostat or astrocyte-derived ECM. (B) A cleaned and sterilized silicon MEA. (C) Stereoscopic light micrograph of an astrocyte-derived ECM coated MEA. (D) Avitene coated MEA immunolabeled for collagen type I. Scale bar 100 µm. (E) A high magnification image of Avitene coated MEA immunolabeled for collagen type I. Scale bar 10 µm.

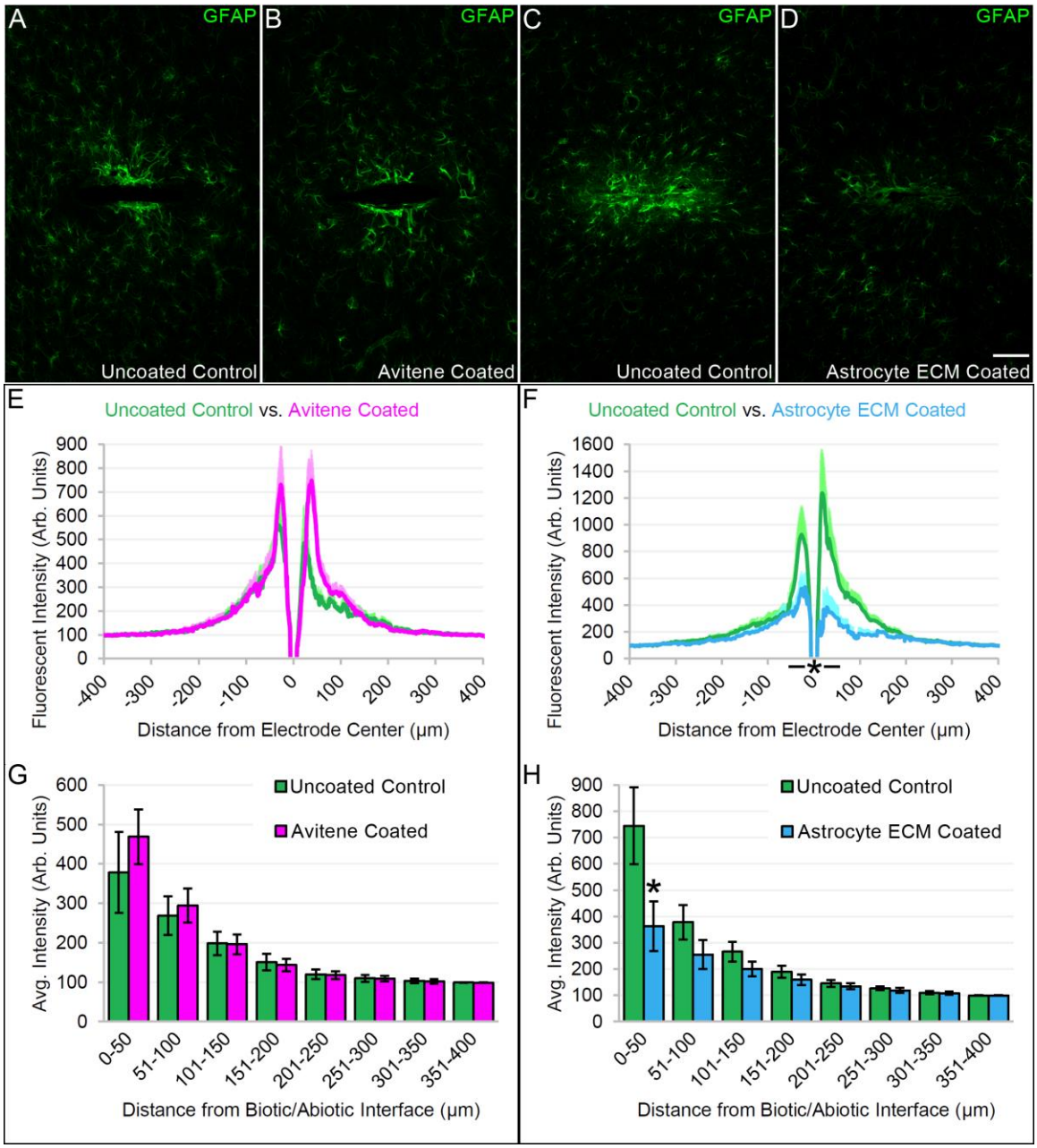

Fig. 2.7. Representative images of *in vivo* GFAP immunoreactivity and quantification. (A and B) Representative images of horizontal sections showing immunoreactivity for GFAP (astrocytes) surrounding (A) uncoated MEAs as compared with (B) Avitene coated MEAs. (C and D) Representative GFAP immunoreactivity surrounding (C) uncoated MEAs as compared with (D) astrocyte-derived ECM coated MEAs. Scale bar 100 μm. (E and F) Average immunofluorescent profiles comparing uncoated and coated cohorts. (G and H) GFAP immunofluorescence binned as a function of distance from the biotic/abiotic interface in 50 μm bins from 0 to 400 μm. (G) No significant differences were observed between uncoated controls and Avitene coated MEAs. 8-week time point, n = 6. (H) Compared to uncoated controls, MEAs coated with astrocyte-derived ECM had significantly reduced GFAP immunoreactivity within the presumptive recording zone (first 50 μm from the interface). 8-week time point, n = 5. (*) denotes significant difference with $p < 0.05$. Data shown as mean and standard error of the mean.

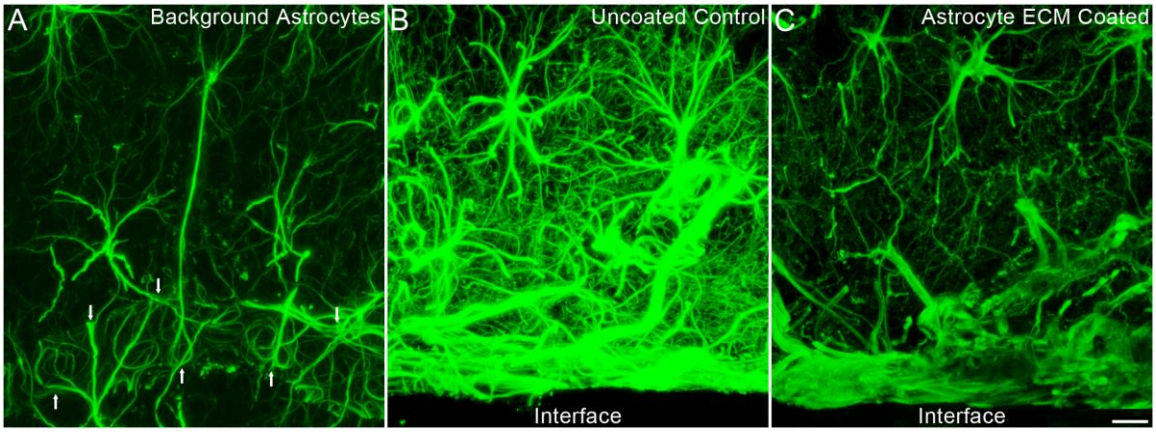

Fig. 2.8. Representative GFAP immunoreactivity at high magnification. GFAP immunolabeling observed in (A) background tissue (contralateral to implant), (B) at an uncoated interface, and (C) at an astrocyte ECM coated interface. (A) GFAP immunolabeling of a background astrocyte. Astrocyte end feet (white arrows) wrapping a blood vessel in the bottom portion of the image. (B) The intensity of GFAP immunoreactivity adjacent to an uncoated control interface is exponentially higher than background levels. (C) The intensity of GFAP immunoreactivity adjacent to an astrocyte ECM coated interface is higher than background but significantly lower than uncoated controls. All sections were batch stained, imaged and processed with identical settings and were from animals that arithmetically represented the mean cohort response (8-week time point). Scale bar 10 μm.

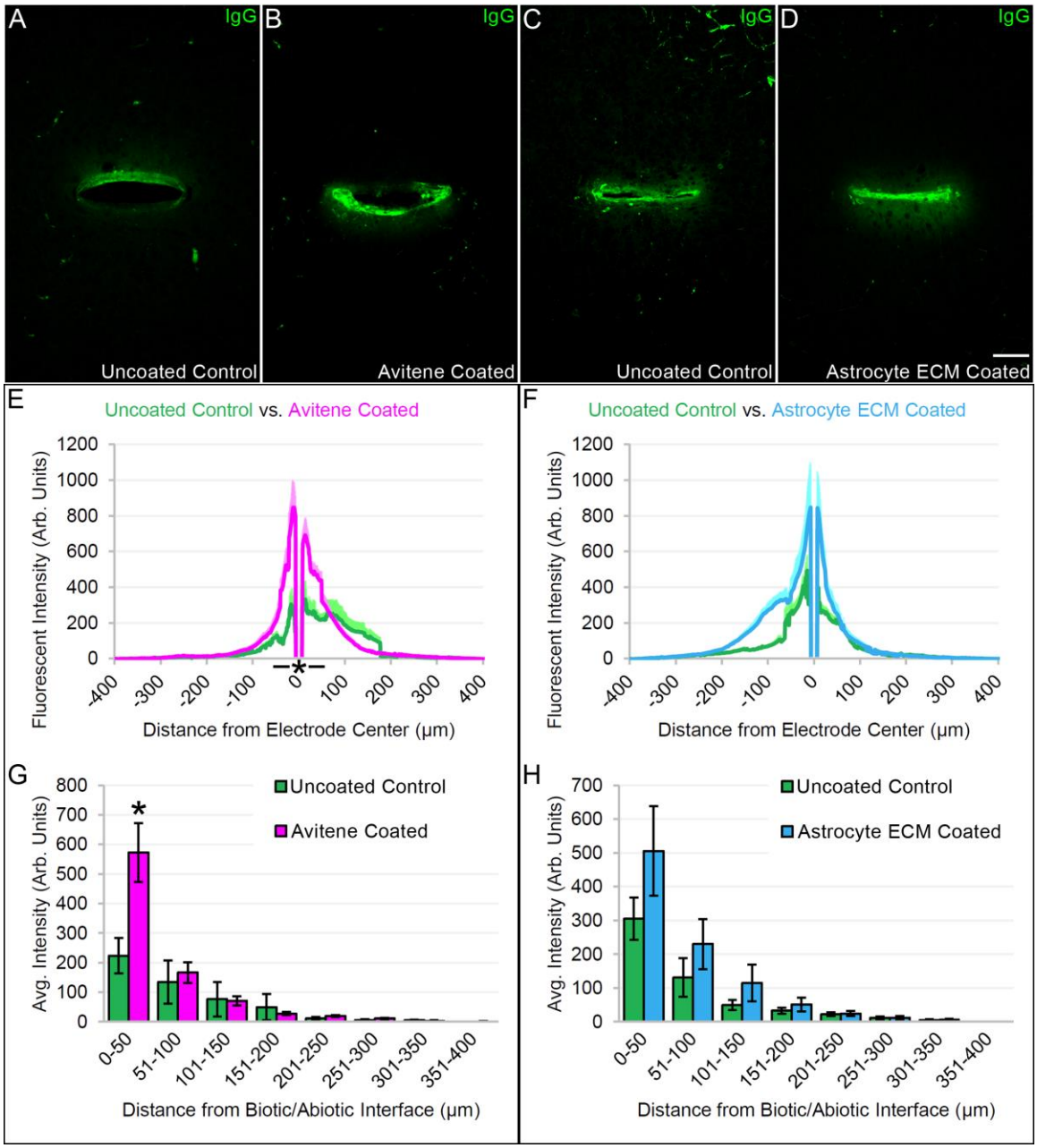

Fig. 2.9. Representative images of *in vivo* IgG immunoreactivity and quantification. (A and B) Representative images of horizontal sections showing immunoreactivity for IgG (blood products in brain parenchyma) surrounding (A) uncoated MEAs as compared with (B) Avitene coated. (C and D) Representative IgG immunoreactivity surrounding (C) uncoated MEAs as compared with (D) astrocyte-derived ECM coated MEAs. Scale bar 100 μm. (E and F) Average immunofluorescent profiles comparing uncoated and coated cohorts. (G and H) IgG immunofluorescence binned as a function of distance from the biotic/abiotic interface in 50 μm bins from 0 to 400 μm. (G) Compared to uncoated controls, MEAs coated with Avitene had significantly increased IgG immunoreactivity within the presumptive recording zone (first 50 μm from the interface). 8-week time point, n = 6. (H) No significant differences were observed between uncoated controls and astrocyte ECM coated MEAs. 8-week time point, n = 5. (*) denotes significant difference with $p < 0.005$. Data shown as mean and standard error of the mean.

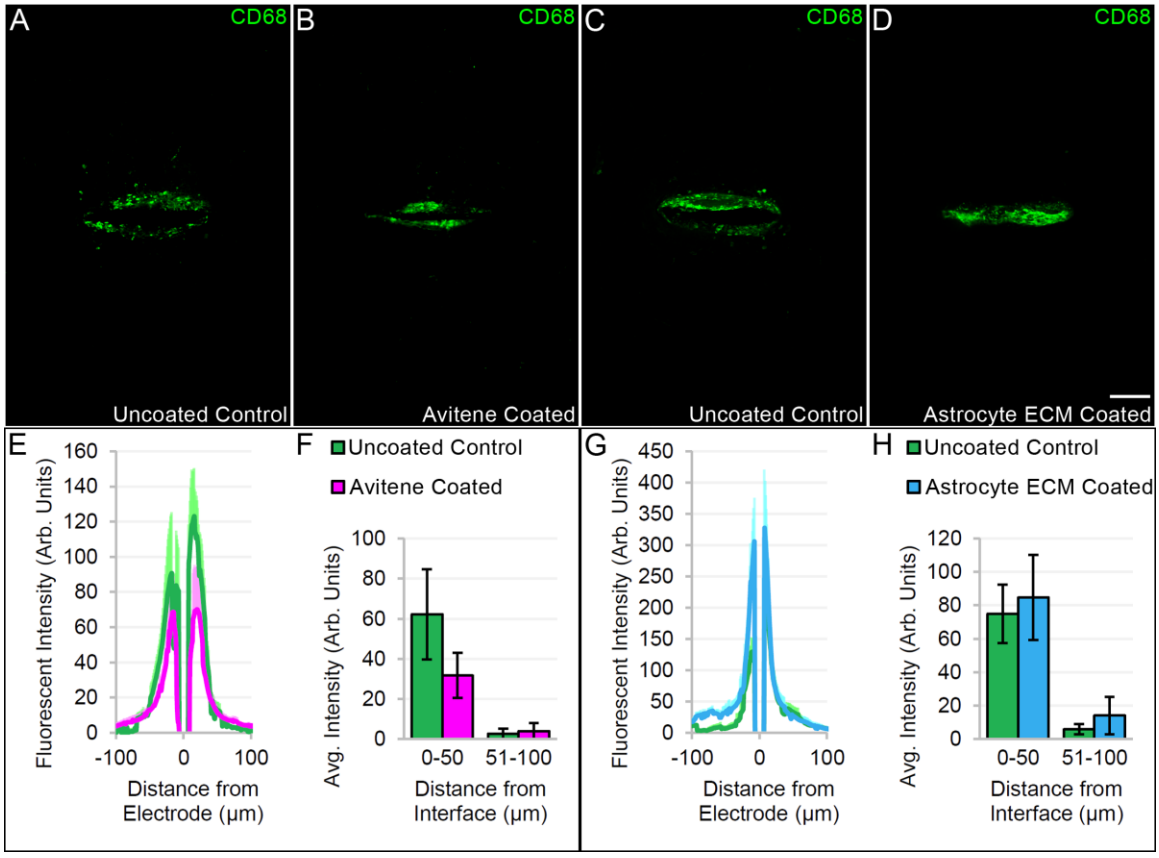

Fig. 2.10. Representative images of *in vivo* CD68 immunoreactivity and quantification. (A and B) Representative images of horizontal sections showing immunoreactivity for CD68 (activated macrophages) surrounding (A) uncoated MEAs as compared with (B) Avitene coated MEAs. (C and D) Representative CD68 immunoreactivity surrounding (C) uncoated MEAs as compared with (D) astrocyte-derived ECM coated MEAs. Scale bar 100 µm. (E and H) CD68 average immunofluorescent profiles for each cohort and immunofluorescence binned as a function of distance from the biotic/abiotic interface in 50 µm bins from 0 to 100 µm. No significant differences were observed between uncoated controls and astrocyte ECM or Avitene coated microelectrodes. 8-week time point, n = 5 for all cohorts. Data shown as mean and standard error of the mean.

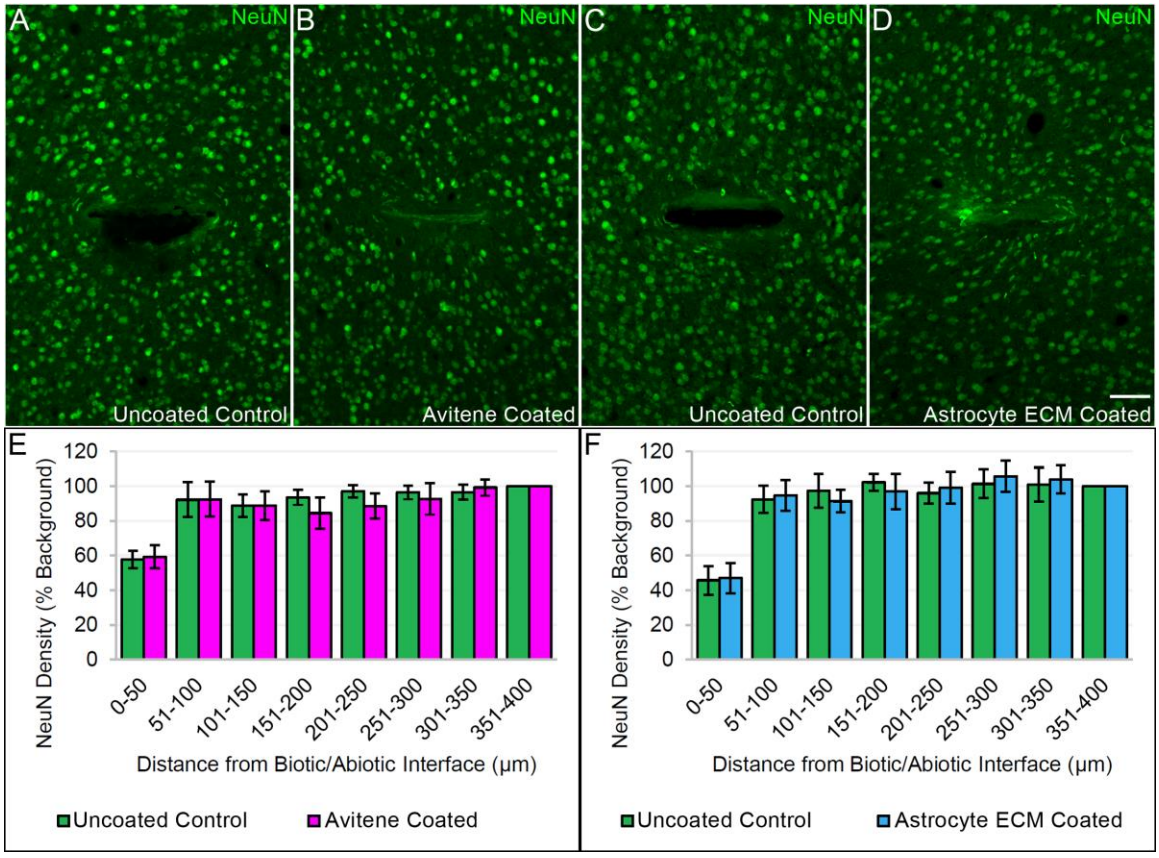

Fig. 2.11. Representative images of *in vivo* NeuN immunoreactivity and quantification. (A and B) Representative images of horizontal sections showing immunoreactivity for NeuN (neuronal nuclei) surrounding (A) uncoated MEAs as compared with (B) Avitene coated. (C and D) Representative NeuN immunoreactivity surrounding (C) uncoated MEAs as compared with (D) astrocyte-derived ECM coated MEAs. Scale bar 100 μm. (E-F) NeuN density for each cohort binned as a function of distance from the biotic/abiotic interface in 50 μm bins from 0 to 400 μm. No significant differences were observed between uncoated controls and (E) astrocyte coated MEAs. Similarly, no significant differences were observed between uncoated controls and astrocyte-derived ECM coated MEAs. 8-week time point, n = 5 for all cohorts. Data shown as mean and standard error of the mean.

Table 2.1. Example proteins found in astrocyte-derived ECM with MS/MS in addition to those identified with IHC (Fig. 2.4).

Component	Description and Role(s) In Wound Healing	Refs
Collagen VI	A beaded filament forming collagen that promotes platelet adhesion and thrombosis under low shear conditions. Binding site for Von Willebrand factor.	[180, 252, 253]
Collagen XII	A fibril associated proteoglycan important for proper matrix assembly and mechanotransduction. Also promotes platelet adhesion and thrombosis under low shear conditions.	[180, 254]
Tenascin N and W	Promotes neurite outgrowth and pathfinding. Regulates inflammatory cell migration and activity. Promotes glial proliferation and differentiation.	[255, 256]
Perlecan	A basement membrane-specific heparan sulfate proteoglycan participating in the blood brain barrier. Also promotes tissue regeneration by activating various growth factors.	[257-259]
Thromobospondin-1	An adhesive glycoprotein that promotes platelet adhesion. Binds to fibrinogen, fibronectin, laminin, and various collagens. Inhibiting neoangiogenesis. Major activator of TGFβ-1.	[260-262]
Fetuin-A	Plasma-binding protein that is heavily expressed during early brain development. Plays anti-inflammatory and neuroprotective roles in a variety of neurodegenerative disease and injury models. Fetuin can bind TGF-β1 and prevent TGF-β1-mediated signaling and fibrosis.	[250, 263, 264]
Neural Cell Adhesion Molecule (NCAM) 1	Cell-cell and Cell-matrix adhesion protein involved in CNS development, synaptic plasticity, and regeneration following ischemic injury.	[265-268]

CHAPTER 3

THE FOREIGN BODY RESPONSE TO HEADSTAGE COMPONENTS USED FOR DEVICE FIXATION IN CHRONIC CNS STUDIES IN RATS

The format of this chapter is based on the Biomaterials journal. Authors of the prepared manuscript include Robert S. Oakes, Dr. Michael B. Christensen, and Dr. Patrick A. Tresco.

3.1 Introduction

Neural recording devices that utilize cortically-implanted microelectrode arrays (MEAs) have become an invaluable tool for extending the understanding of neural circuitry [134, 269, 270]. In clinically relevant applications, cortically-implanted recording MEAs enable volitional control of various brain-machine interfaces (i.e., computer or robotic limb) with high resolution [43, 271]. However, variable functional reliability and inconsistent longevity are major hurdles that have limited the clinical translation of this promising technology [49, 60, 144, 272]. These shortcomings have, at least in part, been attributed to the foreign body response (FBR) at the electrode-brain tissue interface. The primary characteristics of which include persistent macrophage activation, astrogliosis, decreases in neuronal density, and BBB leakiness [76, 124, 132, 199]. To improve the biocompatibility of this type of device it is necessary to understand the causes of the FBR and to minimize its influence on recording performance [124, 136, 137].

While significant attention has been directed towards studying the FBR to different types of MEAs [70, 73], little attention has been directed to studying the FBR associated with the components used to secure such devices to the skull during chronic use, which include adhesives, acrylic cements and bone screws [58, 70, 197, 198]. Bone screws are of particular interest as they can penetrate the skull and make contact with the meninges and/or brain tissue.

In this study, using immunohistochemical approaches the FBR to various components used to

anchor recording devices to the rat skull was analyzed over a long indwelling period. The results indicate that headstage components add to the neuroinflammatory burden of such devices and may affect brain function at sites millimeters away from the implanted electrode.

3.2 Methods

3.2.1 Microelectrodes and headstage components

Several types of MEA fixation approaches were analyzed. Two types were *in situ* fabricated, and consisted of stainless steel self-tapping bone screws (#19010-00, 1.17 mm diameter, 18/8 grade SS, Fine Science Tools (FST), Foster City, CA), Kwik-Cast silicon elastomer (World Precision Instruments, Sarasota, FL), and either a medical-grade solvent-free ultraviolet-light (UV) curable acrylated urethane adhesive (MD-1187-M, Dymax, Torrington, CT) or a traditional two part acrylic cement. Another headstage type used a shear-resistant precast polyurethane elastomer (ST-1085 A/B, BJB Enterprises, Inc., Tustin, CA), Kwik-Cast silicon elastomer, and larger stainless steel screws (#B-MX-172-3, 1.85 mm diameter, 18/8 grade SS, Small Parts Inc., Miami Lakes, FL). All components were cleaned and sterilized with 70% isopropyl alcohol prior to implantation. Two types of recording devices were used including a 4 x 4 Utah Electrode Array (Blackrock Microsystems, Salt Lake City, UT) consisting of sixteen boron-doped silicon tapered shanks (1000 μm length, ~80 μm base thickness, 400 μm interelectrode spacing) or a lattice style or solid style Michigan planar array, also made of silicon. The recording devices were sterilized with ethylene oxide (EtO) by the University Hospital Surgical Processing Department and were allowed to outgas for at least 48 hr prior to implantation. Sterile packets containing the recording devices remained sealed until the time of implantation.

3.2.2 Animal surgery

All procedures involving animals were conducted in accordance with the University of Utah Institutional Animal Care and Use Committee (IACUC). Adult male Sprague Dawley rats (young: 10 weeks old ± 2 weeks and 325g ± 75g, n = 19; and older adult: 75 weeks old ± 2 weeks and 850g ± 75g, n = 19) were anesthetized via inhalation of vaporized 5% isoflurane/oxygen to induce anesthesia and then maintained at 2.5% isoflurane/oxygen during the

procedure. During the procedure, animal body temperature was regulated (ATC1000, World Precision Instruments, Sarasota, FL). After reaching a full level of anesthesia as assessed by lack of response to a tail/toe pinch, the animal's head was shaved, and the scalp was disinfected with 70% isopropanol and butadiene. Animals were then transferred to a stereotaxic frame, and a midline incision extending the length of the skull was made. The skin was retracted and the fascia was removed with a scalpel blade. The exposed skull was then thoroughly dried with cotton tipped applicators. Pilot holes for screws were made using a pneumatically-driven diamond micro burr. Screws are then turned into the skull with a handheld screw driver. For the *in situ* fabricated headstage (Fig. 3.1), four screws were placed in the parietal bone near the temporal ridge [198]. Two of the screws were placed contralateral to the electrode with the other two being placed ipsilateral, one anterior and one posterior to the planned electrode position. A craniotomy was then cut with a pneumatically-driven burr under sterile PBS irrigation, with the center of the hole positioned above the right hemisphere motor cortex at 0.2 mm forward of Bregma, and 3 mm lateral to Bregma. To measure skull thickness the bone that was removed was rinsed with PBS and measured with calipers. Using a stereomicroscope, the exposed Dura was then opened with a 25G needle and deflected to the side to expose the cortical surface. The electrode was stereotactically positioned over the craniotomy. The MEA was lowered into cortical tissue, Kwik-Cast was then applied to cover the implanted MEA and fill the craniotomy level with the skull surface. For the *in situ* fabricated headstage, UV-curable adhesive or traditional acrylic cement was used to encapsulate the electrical connector and screws. A UV lamp (50W, Dymax) was used to cure the UV curable adhesive during the deposition process, while the acrylic cement was allowed to air dry and cure. For the prefabricated headstage, MEA positioning and implantation was the same as described with the exception that only two screws were used to secure the headstage through pilot holes in the prefabricated polyurethane headstage. No UV-curable adhesive or cement solvent was used with these implants. The two screw locations were in the parietal bones contralateral and posterior to the electrode, respectively. Following these procedures, the skin was closed as needed around the headstage with suture, leaving the electrical connector percutaneously exposed. An antibiotic ointment, Neosporin (Johnson &

Johnson, New Brunswick, NJ), was applied around the headstage and sutures. The animals were allowed to recover in individual cages under observation. When sutures were required they were removed approximately a week after surgery [68].

3.2.3 Euthanasia and tissue preparation

Animals were deeply anesthetized with 5% isoflurane and transcardially perfused with PBS followed by 4% paraformaldehyde in PBS. Following perfusion fixation, intact neural interfaces (the headstage, bone screws, and wires attached to the skull) and brains were carefully dissected from tissue using microdissection forceps. Retrieved brains were postfixed with 4% paraformaldehyde for 24 hr at 4°C. Brains were then equilibrated in 30% sucrose. Following equilibration, brains were embedded in Tissue Freezing Medium (Triangle Biomedical Sciences, Durham, NC), serially sectioned in the horizontal or coronal plane at 30 µm thickness with a cryostat (Leica Microsystems, Bannockburn, IL).

3.2.4 Immunohistological explanted device surface analyses

Explanted tissue and components including the skull, headstage, bone screws, wires, and MEAs were imaged (SMZ800 stereoscope, Nikon Instruments Inc., Melville, NY; Coolsnap digital camera, Protometrics, Tucson, AZ; VHX-5000, Keyence, Itasca, IL) then immunolabeled with CD68 (ED-1, AbD Serotec, Raleigh, NC, 0.25 µg/mL) and IBA1 (WAKO, Richmond, VA, 0.5 µg/mL), then counterstained with DAPI (4',6-Diamidino-2-Phenylindole, Dihydrochloride, Life Technologies, Carlsbad, CA, 10 µM) to evaluate the presence of surface-adherent, activated macrophages as previously described [73]. In brief, antibodies were diluted in a blocking solution consisting of 4% (v/v) goat serum (Invitrogen, Carlsbad, CA), 0.5% (v/v) Triton-X 100, and 0.1% (w/v) sodium azide. Components were first incubated with blocking solution for 1 hr then with primary antibody for 18 hr at room temperature. They were then washed with PBS three times at room temperature to remove excess antibody (1 hr / wash). Then appropriate fluorescently labeled secondary antibodies were applied in block for 4 hr at room temperature, followed by three washes in PBS (1 hr / wash). Devices were imaged on a confocal microscope (Olympus Fluoview FV1000, Olympus America Inc., Center Valley, PA) using a 5x air or 40x water objective

then lightfield corrected [121].

3.2.5 Immunohistological tissue analyses

Prior to sectioning, photographs were taken of the cortical surface of whole perfused brains. Serial sections were processed using indirect immunohistochemistry for CD68 (ED-1, AbD Serotec, Raleigh, NC, 0.25 µg/mL) to assess activated microglia/macrophages; IBA1 (WAKO, Richmond, VA, 0.5 µg/mL) for microglial morphology and spatial distribution; GFAP (DAKO, Carpinteria, CA, 2.9 µg/mL) for astrocytes; NeuN (Chemicon/Millipore, Billerica, MA, 2.0 µg/mL) for neuronal nuclei; MAP-2 (AP20, Chemicon/Millipore, 1.0 µg/mL) for dendrites; NF200 (Sigma, St. Louis, MO, 8.0 µg/mL) for axons; RIP (NS-1, Chemicon/Millipore, 0.25 µg/mL) for myelination; rat IgG (Southern Biotech, Birmingham, AL, 0.5 µg/mL) for serum proteins in the brain parenchyma; and Lycopersicon Esculentum (Tomato) Lectin (Vector Laboratories, Burlingame, CA, 4.0 µg/mL), which labels vasculature and macrophages [72, 136, 190]. The same blocking solution used for explant analysis was used to dilute antibodies for tissue analysis. Free-floating (0.5 mL solution in 24-well plates) tissue sections were batch treated for 1 hr in blocking solution at room temperature, followed by incubation with primary antibodies for 18 hr at room temperature. After three washes in PBS at room temperature to remove excess antibody (1 hr / wash), appropriate fluorescently labeled secondary antibodies were applied in block for 18 hr at room temperature, followed by three washes in PBS (1 hr / wash). All sections were also counterstained with DAPI (4',6-Diamidino-2-Phenylindole, Dihydroch loride, Life Technologies, Carlsbad, CA, 10 µM) to identify cell nuclei. Tissue sections were mounted on microscope slides with Fluormount-G (Southern Biotech, Birmingham, AL) and cover-slipped. Fluorescent images of tissue sections from the cortex were imaged on a confocal microscope using a 20x air objective, lightfield corrected, then stitched together in Photoshop to create a larger field of view [72]. Select sections were analyzed on a phase contrast microscope (Nikon Eclipse E600) using a 40x oil objective to identify hemosiderin-laden macrophages.

3.3 Results

3.3.1 Retrieved device components were covered with adherent phagocytic macrophages

A representative MEA recording headstage and bone screw are shown in Fig. 3.1. Under light microscopy retrieved device components, headstage adhesive and screws, contained an adherent layer of material of cellular origin indicated by DAPI+ staining of cell nuclei. The adherent cells were almost exclusively immunopositive for CD68 and IBA1 (Fig. 3.2 and Fig. 3.3), indicating that they were activated macrophages. A large difference in skull thickness was observed between young (10 weeks old, 325 g) and older (75 weeks old, 850 g) adult rats in the bone located above the motor cortex. The younger adult rodent's skull measured 560 μm and the older adult rodent's skull measured 1170 μm. In all animals the area of skull identified as the temporal ridge, which is prominent in laboratory rats, was observed as the thickest area of skull suitable for screw fixation.

3.3.2 The foreign body response to screws in adjacent cortical tissue

3.3.2.1 Macroscopic analysis and correlation of response to screw position

Every animal (n = 38) exhibited at least one area of the cortex, which showed a response associated with an implanted screw (Fig. 3.4A). These cortical surface responses were visible in the perfused whole brain without magnification (Fig. 3.4). The response was noticeable underneath 98 of the 114 (86%) screws and was circular and often concave in appearance. Unlike the rest of the perfused brain, the cortical surface underneath screws was darker and brownish in color, presumably due to blood products that were not cleared following perfusion and fixation. These darker areas were evident over the entire indwelling period. Following tissue processing and sectioning, light microscopy confirmed that these areas were associated with hemosiderin-laden macrophages and inflammation associated angiogenesis (data not shown). Regardless of headstage type, screw type, or animal age there was no apparent difference in the occurrence of such cortical responses underneath screws that penetrated the rat skull.

3.3.2.2 Analysis of cortical tissue response

Horizontal and coronal tissue sections showed increased CD68+ and IBA1+ immunoreactivity in cortical tissue underneath bone screws (Fig. 3.5B-C and 3.6B-C). CD68+ macrophages adjacent to the interface had an amoeboid morphology, as compared to tissue further away. Surrounding the area of CD68+ / IBA1+ cells was an enhanced immunolabeling of GFAP (Fig. 3.6E). Coronal sections showed that increased GFAP immunolabeling could extend, in some cases, through the entire depth of the cortex (Fig. 3.6A). Sections immunolabeled for IgG showed a gradient of intensity that declined as a function of distance from the center of mass of the adjacent screw (Fig. 3.5B-C and 3.6C). Immunolabeled horizontal sections showed loss of neural tissue, which included a loss of neuronal nuclei (NeuN) and disruption of neural architecture (MAP-2, NF200 and RIP) (Fig. 3.7). Immunolabeling with Tomato Lectin (TL) showed a disrupted vascular network, associated with the area of neural tissue loss (data not shown).

3.4 Discussion

The results of this study show that various components commonly used to anchor recording and other biomedical devices to the rat skull for basic neuroscience and preclinical translational studies result in a FBR in adjacent brain tissue. These components are collectively referred to as the headstage. Results showed that any component, below the rat skull, was covered with a layer of CD68+ / IBA1+ macrophages. This included the adhesives and cements, regardless of whether they were fabricated *in situ* or precast prior to implantation, as well as bone screws, irrespective of their design. Furthermore, bone screws that penetrated the skull resulted in a FBR in the underlying cortical tissue, which had all of the FBR hallmarks as described for MEAs implanted in cortical tissue regardless of the depth of penetration.

Persistent macrophage activation was similar to that observed adjacent to penetrating cortical MEAs with the largest amount of CD68+ immunoreactivity residing immediately underneath the screw that was distributed in a pattern that reflected the overlying device geometry [76]. The extent of astrogliosis also appeared similar in spatial distribution and intensity to previous reports for penetrating MEAs, where astrocyte hypertrophy surrounded areas of

CD68+ immunoreactivity [73, 273, 274]. Similar to previous studies on penetrating MEAs, there were cells located within the area of the FBR that were DAPI+ but did not possess either macrophage or astrocyte biomarkers [73, 163]. Due to the proximity of the screws to meningeal tissue, it is plausible that these cells were meningeal fibroblasts, which may contribute to device encapsulation through extracellular matrix deposition [72, 75, 275]. Alternatively, they may have been neural progenitors attracted by soluble factor secretion from the activated macrophages [276].

Evidence of larger scale neuroinflammation and neural tissue loss including elimination of neuronal cell bodies, processes, and myelination were also observed [76]. The response was similar to that described after focal brain injury or in multiple sclerosis, which have been shown to disrupt neuronal circuitry and lead to neural damage of varying scale [230, 277, 278]. These focal areas of neuroinflammatory-related damage were generally circular in appearance as viewed in horizontal sections and varied in both size and depth. It is possible they resulted either from the initial injury associated with the drilling of pilot holes or screw insertion. However, the presence of macrophages and inflammatory biomarkers weeks to months after screw insertion suggests that at least part of the observed response was due to the FBR associated neuroinflammatory sequela, as its resolution would have been expected if it was only associated with the initial injury [230, 277].

We also observed BBB leakiness, which appeared as a gradient of IgG immunoreactivity that dissipated with increasing distance from the screw center of mass [124, 125, 279-281]. It is important to note that the figures provided in this study generally only show the tissue response to a single screw. However, the collective inflammatory response to multiple screws and the other headstage components likely added to the neuroinflammatory burden of the implanted MEA, and may influence recording performance and/or brain function at sites other than the site of the penetrating MEA.

These results strongly suggest that headstage components are contributing factors to the overall neuroinflammatory burden of chronic recording devices, or other skull affixed biomedical devices, which has implications for mental health beyond the electrode-brain tissue interface.

This idea is supported by a broader set of studies that show the negative impact of regional and systemic inflammation on neurogenesis and cognitive function.

For example, it has been shown that proinflammatory cytokines released from macrophages can have neurophysiological effects at sites distant from the site of their release [282]. In a recent study, autoradiography was used to map macrophage and glial activation in the rat brain accompanying a deep brain stimulator (DBS) fixed to the skull with multiple screws and acrylic dental cement. The results showed widespread and persistent neuroinflammation over an 8-week indwelling period that was accompanied by cognitive deficits, as determined by an object recognition test [203].

Direct comparisons may be made with the contralateral hemisphere, which is a common imaging control for background and normal tissue immunofluorescent intensity in CNS studies [59-61, 68, 76, 86, 141, 144, 151, 178, 192, 214, 283-288]. A more stringent control would use sections from age-matched uninjured rat brains to establish the innate biomarker distribution in the utilized model system. Some important anatomical features that are typically labelled by the biomarker panel at a heightened intensity in uninjured tissue include the glia limitans (GFAP, IgG) at the cortical surface, the corpus callosum where white matter tracts cross the midline (GFAP), and poorly perfused vasculature (IgG) [89, 289-291]. The IHC quantification process uses sections from the cortical regions V and VI as they are the thickest layers and have a fairly uniform cellular distribution [292].

Other groups have established the connection between inflammation, neurogenesis, and changes in cognition. One group employed a cortically-implanted electrode and cannula to directly stimulate neuroinflammation via lipopolysaccharide (LPS) infusion, and showed that the treatment decreased hippocampal neurogenesis [208]. Moreover, other groups have shown that inflammatory stimulation outside the CNS has detrimental effects on neurogenesis [207, 209, 210] as well as on neural connectivity [211]. Together such studies support the notion that inflammation either located within the brain or systemically can impact neurogenesis and impair cognition.

In support of this work's findings and their importance to larger and more clinically

relevant animal models, a recent publication identified headstage failure as a concern in nonhuman primate models, an experimental approach, which utilizes higher quality titanium mounts and bone screws in an animal that has a thicker skull [49]. In the current study, screw penetration depth was not controlled. A review of the literature suggests that this is a variable that is not specifically controlled by any means in any study. Moreover, screws are often used as electrical grounds or reference points for implanted recording devices, in which case they are intentionally implanted in cortical tissue [60]. Regardless of penetration depth, a high percentage of the screws used in this study (86%) elicited a FBR response in cortical tissue that resulted in loss of neural tissue and persistent inflammation. Together, the results indicate that headstage components, especially bone screws, can contribute to the overall neuroinflammatory burden of biomedical devices that are anchored to the skull.

One suggestion for improved fixation would be the use of older adult rats that have thicker skulls, which facilitates better screw fixation. A difference in skull thickness was observed across the two age groups with the skull thickness varying from 560 μm for the younger cohort of adult rodents to 1170 μm for the older animals, which is supported by the published results of an earlier study [293]. The thread spacing or pitch of a commonly used self-tapping bone screw for MEA headstage fixation measures approximately 400 μm (Fig. 3.8A). If placed perpendicular to the skull bone of a young, 325g adult rat, only 1.4 screw threads would interface with the bone (Fig. 3.8B). In contrast, 2.9 screw threads would interface with the bone of an older adult rat skull if placed in the same manner (Fig. 3.8C). The common self-tapping bone screw has a tapered tip, which measures approximately 580 μm in length that does not provide any anchorage benefit. Thus, when used in either case it is impossible to obtain adequate fixation without the bone screw tip penetrating beneath the skull bone if the screw is placed in the flat part of the skull (Fig. 3.8B-C). An additional concern for headstage fixation is the consequence of skull growth and expansion resulting from normal development during chronic studies. This issue is similar to clinical concerns regarding the use of metal plates for pediatric craniofacial surgery [294].

Another suggestion for improvement is to ensure that the screws are located in the temporal ridge, the thickest area of the skull, and placed at an angle as shown in Fig. 3.8D. The

temporal ridges are a prominent feature on the margins of the rat skull, which may facilitate better fixation and bury the tapered tip inside the skull bone, thus limiting contact with cortical tissue [295, 296].

The broader impact of these findings can be extended to a number of other implantable research tools and medical devices for CNS applications. These include not only neural recording devices, but deep brain stimulators, hydrocephalic shunts, optogenetic fiber optic probes, microdialysis probes, push-pull cannulas, tubing for drug infusion, and cranial windows used in advanced microscopy studies. Many of these approaches rely on screws and adhesives to anchor such devices to the skull [198]. These results suggest that innovative approaches for device fixation to the skull could be broadly beneficial to several research and medical fields.

3.5 Conclusions

Through an immunohistological analysis of headstage components and adjacent cortical tissue from 38 implanted rats, it was found that headstage components used to anchor neural recording devices elicit a FBR in adjacent brain tissue, characterized by neural tissue loss, persistent inflammation, astrogliosis, and BBB leakinesss, which adds to the neuroinflammatory burden beyond the electrode-brain tissue interface. The broader impact of such device related persistent neuroinflammation is a possible influence on neural plasticity, neurogenesis, and cognition that should be considered as the use of these devices is contemplated for clinical application. Future neural interface designs would benefit from a more holistic perspective that seeks to reduce neuroinflammatory footprint of the entire biomedical device.

Acknowledgements

This work was supported by the Defense Advanced Research Projects Agency (DARPA) MTO through the Space and Naval Warfare Systems Center, Pacific Grant/Contract Numbers N66001-11-1-4120 and N66001-12-C-4002. The authors would like to thank Dr. John Skousen, Nicolas Nolta, and Nikole Rhodes for assistance during imaging and tissue processing.

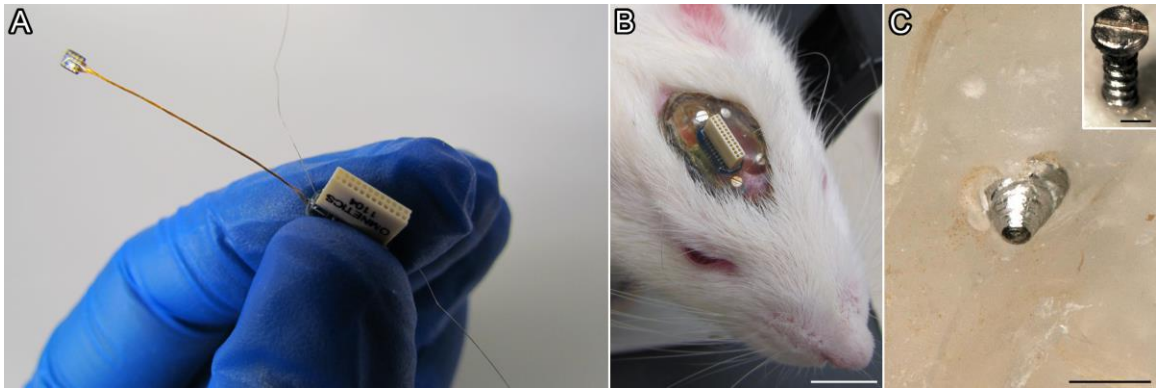

Fig. 3.1. MEA headstage and self-tapping fixation screw skull penetration. (A) 16 channel Omnetics wired UEA anchored to the skull with an *in situ* fabricated headstage for chronic neural recording. (B) Top view on headstage with bone screws visible through the polymer headstage used to anchor the implant and encapsulate the electrical connector and wires. (C) Underside and top view (inset) of a bone screw implanted in the skull along the temporal ridge. The conically shaped screw tip generally penetrates the skull as the threads do not begin until the screw diameter becomes constant, as seen in the inset. Scale bar for A is 10mm. Scale bars for B are 1mm, respectively.

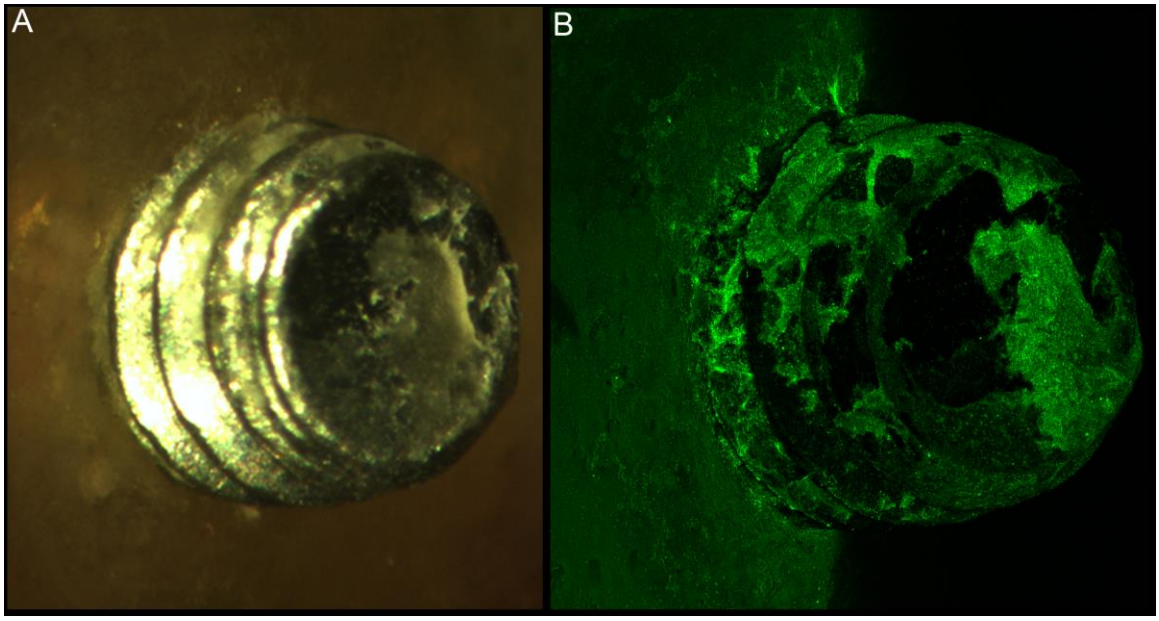

Fig. 3.2. Immunohistological surface analysis of blunt machine screw showed that all implanted surfaces were covered in (A) a layer of biological material that was (B) immunopositive for activated surface adherent macrophages (CD68).

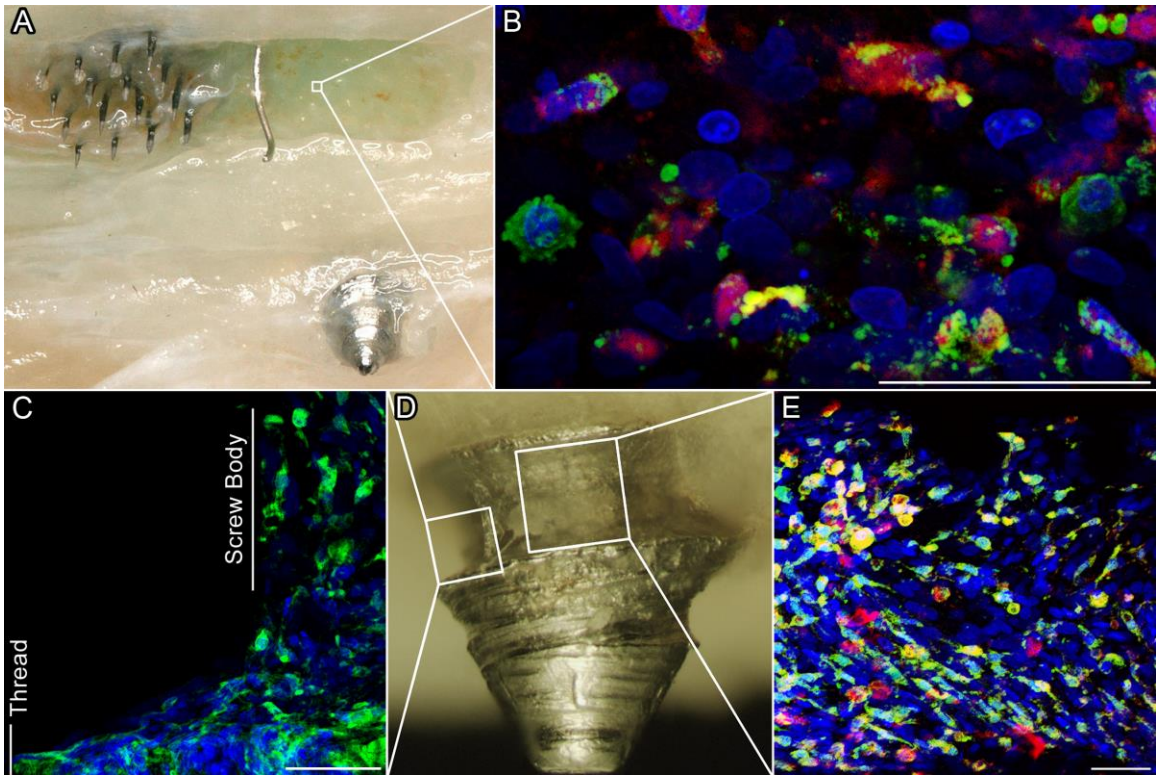

Fig. 3.3. Explanted device immunohistological surface analysis. Representative *in situ* fabricated headstage used for chronic neural recordings. (A) Top view on headstage with bone screws visible through the polymer headstage used to anchor the implant and encapsulate the electrical connector and wires. (B) Underside and top view (inset) of a bone screw implanted in the skull along the temporal ridge. The conically shaped screw tip generally penetrates the skull as the threads do not begin until the scre0w diameter becomes constant, as seen in the inset. Scale bar for A is 10mm. Scale bars for B are 1mm, respectively.

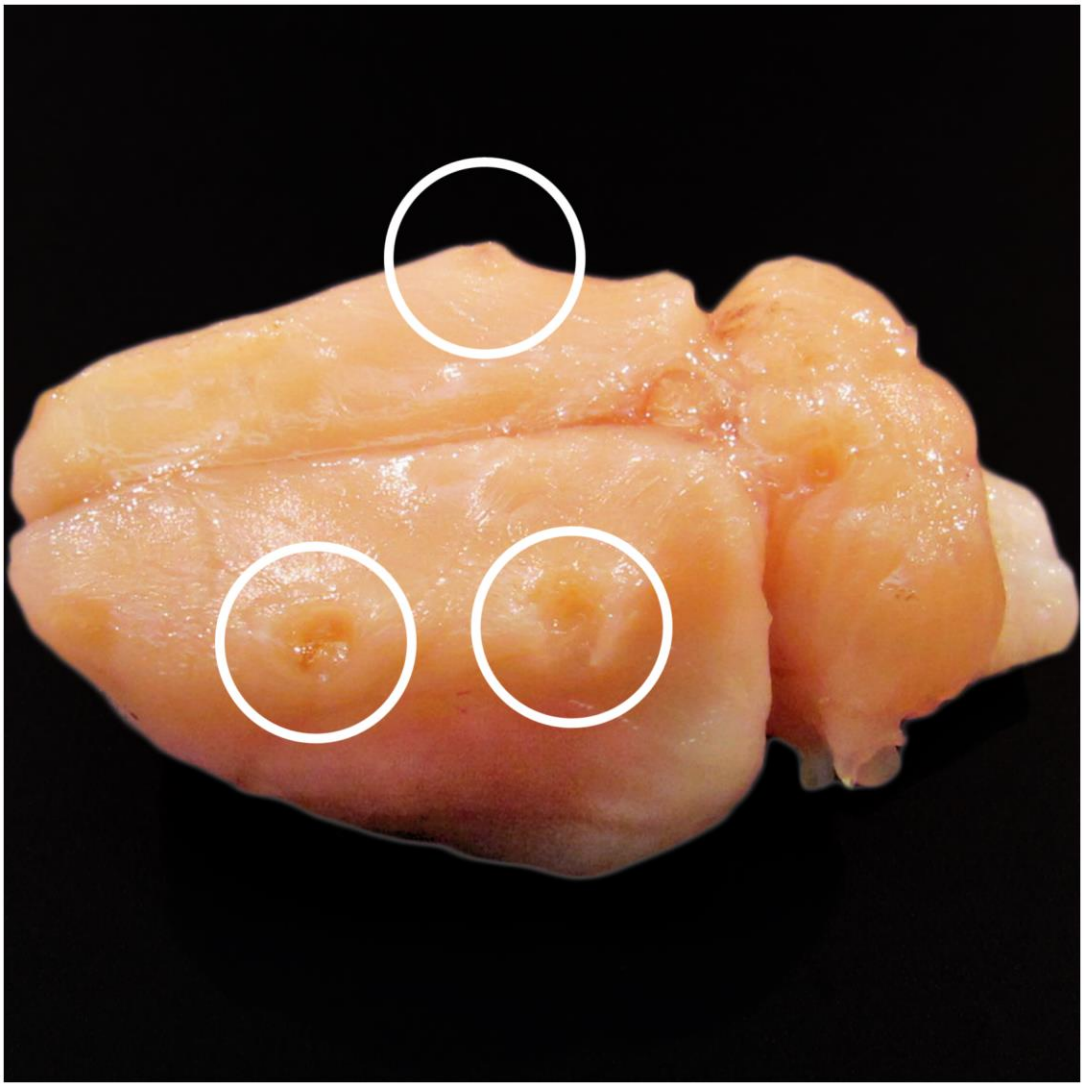

Fig. 3.4. Macroscopic remodeling (circled) of the cortex adjacent to fixation screws. These areas were crater-like in appearance and mimic the screw tip geometry. The occurrence of macroscopic remodeling was equally associated with self-tapping and blunt machine screws, with an overall occurrence of 86%.

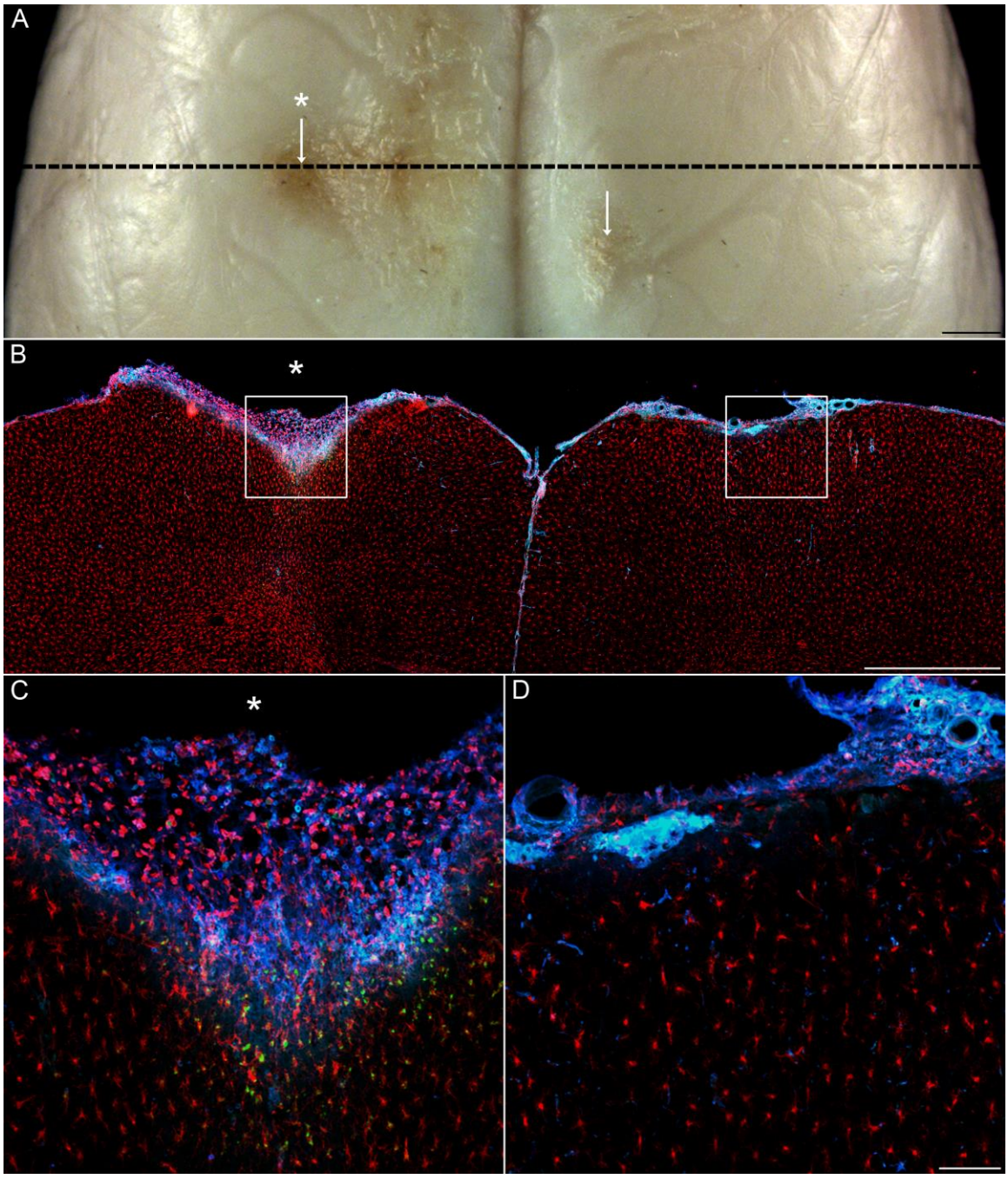

Fig. 3.5 Immunolabeling of inflammatory biomarkers in cortical tissue adjacent to screw location (coronal plane). Representative images of cortical tissue response 12 weeks after implantation. (A) Surface view of perfused rat brain showing two screw locations (white arrows) and the sectioning plane (dashed line) of the tissue section shown in (B) and (C), which shows immunoreactivity against IgG (serum proteins; blue) showing BBB leakiness, CD68+ immunoreactivity (green) showing activated macrophages, and IBA1+ (red) showing macrophages. (C) Magnified area in left hemisphere of B indicated with an asterisk showing magnified IgG immunoreactivity and activated macrophages (CD68+ / IBA1+) where the screw penetrated the skull. (D) Magnified area in right hemisphere of B showing absence of CD68 immunoreactivity in the contralateral hemisphere equidistance from other screw location. Scale bars for A-B, 1mm. Scale bars for C-D, 100 µm.

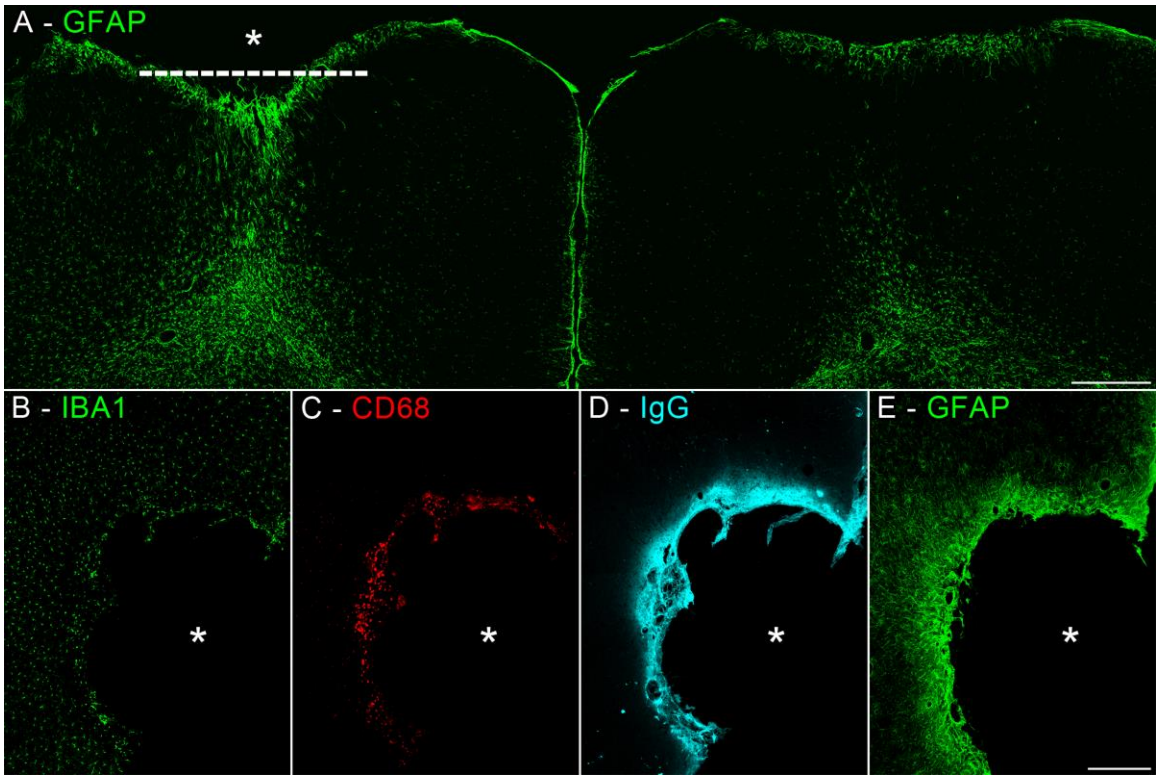

Fig. 3.6. Astrogliosis in cortical tissue adjacent to screw location (coronal plane) and upregulation of inflammatory biomarkers (horizontal plane). Representative sections showing FBR biomarker distribution under a bone screw 12 weeks after implantation. (A) A coronal tissue section taken adjacent to the section indicated in Fig. 3 showing increased GFAP+ immunoreactivity in the cortical column under the center of a bone screw in the left hemisphere. Note the absence of GFAP in the contralateral hemisphere indicating that the reactivity dissipates as one moves away from the inflammatory stimulus. Scale bar is 500 µm. (Lower panels) Representative horizontal sections in cortex approximately at level indicated by dashed line in A showing the distribution of FBR biomarkers adjacent to a bone screw 12 weeks after implantation. In all sections (B-E), one can observe a circular area of neural tissue loss. At the margin of the cavity there is an increase in IBA1+ immunoreactivity (B, green) that overlaps with a region of CD68+ immunoreactivity (C, red) and IgG+ immunoreactivity (C, blue) indicating the relationship between persistent inflammation and BBB leakiness. At the margin of tissue loss and surrounding the activated macrophages was an area of enhanced GFAP+ immunoreactivity (D, green) indicating glial scar formation in the underlying cortex. Scale bar is 500 µm.

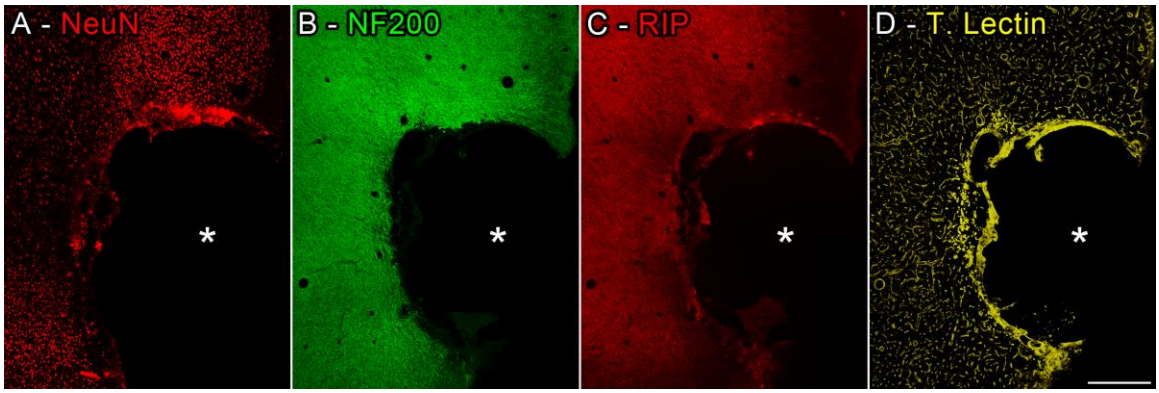

Fig. 3.7. Loss of cytoarchitectural and neurovascular networks (NeuN, NF200, RIP and TL) in cortical tissue adjacent to screw positon (horizontal). Representative immunolabeling of various cellular and molecular FBR biomarkers adjacent to a bone screw 12 weeks after implantation. Within the area of tissue loss there is an elimination of E) NeuN+ bodies, F-G) NF200+/RIP+ myelinated axons, and H) TL+ vasculature. TL also stains macrophages, exemplified by an increase in immunoreactivity at the tissue loss margin. Scale bar is 500 µm.

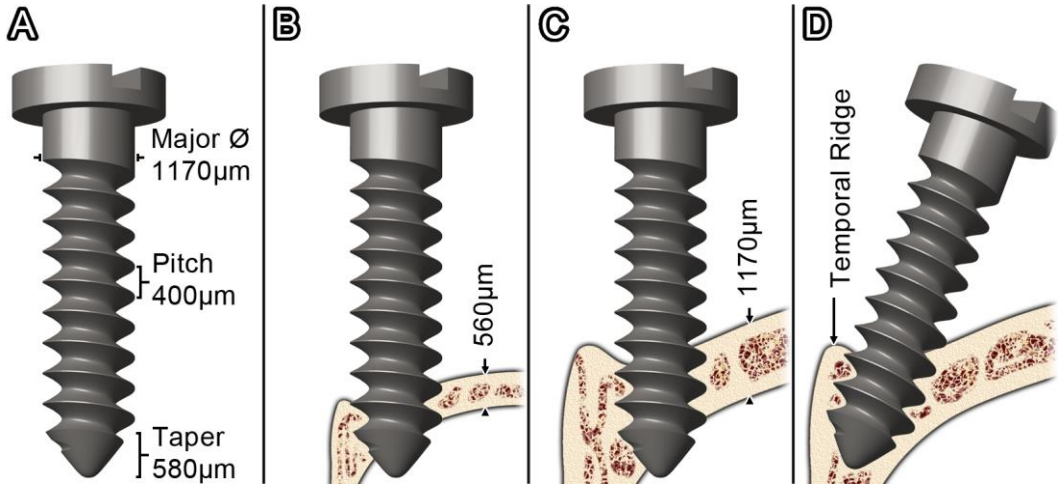

Fig. 3.8. Scaled drawing of a self-tapping bone screw penetrating the skull of young (10 week old) and aged (75 week old) adult rats. Screw dimensions which may influence fixation and the amount of screw penetration include the major diameter (Ø), pitch, taper length, screw angle and location. An additional factor is skull thickness, which is influenced by age and location. The thickness of the young adult rat skull (outlined in black, 560 µm) is less than half of the older adult rat skull (outlined in red, 1170 µm), based on craniotomy measurements. The thickest area of skull suitable for screw fixation is the temporal ridge, a prominent anatomical feature found in laboratory rats, regardless of age. Drawing perspective is normal to the coronal plane.

CHAPTER 4

CONCLUSIONS AND FUTURE WORK

4.1 Conclusions

The list below encompass the conclusions from this dissertation in its entirety and lays the foundation for the future directions and approaches addressed in section 4.2.

4.1.1 ECM protein coatings

- We hypothesized that ECM coatings which target initial hemorrhage should decrease aspects of the FBR by limiting the amount of hemorrhage, which is the initial trigger for inflammation and is neurotoxic.
- Collectively, the results in Chapter 2 show that ECM coatings with different genetic backgrounds and compositions are able to differentially affect specific aspects of the FBR surrounding single-shank, silicon MEAs.
- Silicon MEAs were coated with ECM through an adsorption dip-coating technique with either xenogeneic Avitene Microfibrillar Collagen Hemostat or allogeneic astrocyte ECM derived from an *in vitro* process.
- *In vitro* hemostatic assays showed that the Avitene and astrocyte-derived ECM were both equally able to promote coagulation. Furthermore, *in vitro* immunomodulatory assays showed that only the astrocyte-derived ECM coating had an influence on microglia phenotype, when compared to bare glass.
- Using GFAP as an indicator, the astrocyte-derived ECM coatings decreased the degree of astrogliosis within the recording zone as compared to uncoated controls. Conversely, there was no difference in GFAP surrounding the Avitene coated MEAs and uncoated controls. This differential is most likely due to an immunomodulatory influence given the

equivalent hemostatic ability of both xenogenic Avitene and the allogeneic astrocyte-derived ECM.

- Using IgG as an indicator, the Avitene coated microelectrodes significantly increased the amount of blood products within the recording zone as compared to uncoated controls. This indicates a potential increase late phase neuroinflammatory sequela surrounding Avitene coated MEAs. Conversely, there was no difference between the astrocyte-derived ECM and uncoated controls.
- Using CD68 and NeuN as indicators, neither the Avitene nor the astrocyte ECM coated microelectrodes had an influence on the intensity or spatial distribution of macrophage activation and neuronal density, respectively.

From these studies on ECM coatings there are a number of outstanding questions. Results showed that there was no beneficial influence of the hemostatic ECM coatings on CD68, IgG, and NeuN when using a single-shank MEA model, the most common for FBR studies. However, the influence of hemostatic ECM coatings on a different model system, such as a multi-shank MEA, with larger amount of injury and initial vascular damage is unknown. A surprising discovery was the increase in IgG adjacent to the Avitene coating. This result raises questions about the fate of ECM coatings following 8 weeks in vivo. In section 2.4 it was discussed that the existence of these coatings at 8 weeks would be unlikely, but the ultimate fate of the ECM coatings is unknown and worthy of future investigation. One remaining question about the astrocyte-derived ECM coating is the decrease in GFAP, which may have been promoted by modulated macrophage activation. However, it is unknown if this difference is attributed to allogeneic nature, tissue-specificity, cell-specificity, or derivation process used for the ECM harvest. Finally, while the focus of this work was centered on biomaterial development and the FBR, for this work to influence the clinical translation of recording MEAs the influence on recording ability would need to be assessed. Based on the results, a cell-derived ECM coating would be the best candidate for this purpose if using a single-shank recording MEA.

4.1.2 FBR to headstage components

- We found that the FBR to fixation screws and fixation anchoring adhesive illicit a chronic FBR that has all of the hallmarks described for MEAs implanted in brain tissue.
- Screws which penetrated the cranium could elicit increases in astrogliosis throughout the depth of the cerebral cortex. This increase in GFAP is evident when compared with the contralateral hemisphere.
- We found evidence of persistent neuroinflammation below a variety of fixation screws including chronic macrophage activation, demyelination, and neural tissue loss. Both self-tapping and blunt machine screws exhibited this reaction.
- The FBR of fixation techniques, which is common to a wide variety of CNS devices, may improve the biocompatibility of existing devices and provide a reference for future biologically-informed device designs.

From these studies on the headstage FBR there are a number of outstanding questions. Based on studies in the literature a relationship can be developed between the FBR and the widespread neuroinflammatory burden. However, a direct correlation of IHC biomarkers and autoradiography markers, such as PK11195, or other indicators of systemic inflammation may be useful for directing the biomaterials and device design fields. From a design perspective a strategy such as decreasing the surface area of the headstage may lower its neuroinflammatory burden, but a comprehensive design and evaluation process that identifies and tests strategies to maximize device fixation while minimizing the neuroinflammatory burden is lacking in the literature. For proper evaluation, both of these outstanding questions would most likely require a dedicated study that allows for exclusion of the cortically implanted device and a sole focus on headstage development.

4.2 Future Directions and Approaches

A number of future directions and approaches can be based on the results and conclusions presented in this dissertation. Sections 4.2.1-4.2.6 focus on the ECM coatings presented in Chapter 2 and sections 4.2.7-4.2.8 focus on device fixation presented in Chapter 3.

4.2.1 In vitro mechanistic studies of ECM coatings

The first rational direction to develop a better understanding of the ECM coatings influence on the FBR is through *in vitro* mechanistic studies. These studies would provide insights on specific cellular interactions with the ECM coated interfaces in a controlled in vitro setting.

To advance knowledge on the hemostatic potential of ECM a number of strategies could be used to better understand platelet interactions as they are an important moderator of coagulation. One of the most powerful techniques is parallel plate perfusion, which allows for the perfusion of whole blood or platelet rich plasma at a controlled perfusion speed and associated shear force. The level of shear may prove important for future studies given the composition of the astrocyte-derived ECM, which contained collagen type VI and type XII. These collagen types facilitate platelet adhesion at low shear rates, but not high shear rates. Conversely, collagen type I-III are able to facilitate platelet adhesion and activation at higher shear rates [180]. A potential experimental design for a first study on platelet interactions would be to flow platelet rich plasma over uncoated controls, Avitene coated, and astrocyte-derived ECM coated with a range of shear rates (i.e., 300, 800, and 2000 s^{-1}) [182, 297]. The dynamic platelet interactions with the surface may be viewed in real-time with differential interference contrast microscopy or post processed with Giemsa staining following glutaraldehyde fixation and methanol dehydration. Other techniques to analyze platelet activation include the quantification of soluble factor release. For example, adenosine triphosphate release is quantifiable through surface-immobilization of firefly luciferase or β-thromboglobulin release is quantifiable through an enzyme-linked immunosorbent assay (ELISA) [179, 298, 299].

Results from Chapter 2 show that ECM coatings derived from astrocytes *in vitro* is able to modulate macrophage activation *in vitro*. This result is based on a single test, additional assays which build on this and provide a better understanding of the ECM's influence on inflammation may provide insights on the differential response seen in the GFAP (Fig. 2.7 and 2.8) and IgG (Fig. 2.9) results surrounding ECM coatings. While the influence of the Avitene and astrocyte-derived ECM coatings on macrophage phenotype *in vitro* was assessed, the macrophages'

secretion profiles are unknown on these coatings. The use of an ELISA or mass spectroscopy on macrophage secreted media and quantitative reverse transcription polymerase chain reaction (qRT-PCR) on cell lysate would inform us on which proteins, cytokines, and chemokines are being secreted or genetically upregulated, respectively [121, 300]. Additionally, derivation of macrophages from other tissue sources, such as bone marrow, may prove useful for comparative analysis with our previous results on microglia harvested from rat pup cerebral cortices. Findings from this comparison would contribute to the growing body of research seeking to understand microglia's role in the CNS injury [102, 103, 301].

4.2.2 In Vivo mechanistic studies of ECM coatings

The second rational path to direct the understanding of the ECM protein coatings is *in vivo* mechanistic studies. These studies would build on knowledge acquired during the *in vitro* studies and the *in vivo* results from Chapter 2 to provide insights on the ECM coatings influence on the acute tissue response and the longevity of the ECM coatings.

Shorter time points would be the first *in vivo* study to build on the results presented in this dissertation. Two specific time points of interest would be 48 hr and 2 weeks. These time points, especially 48 hr, are commonly used in the fields of TBI and stroke to assess hemorrhage formation, and thus would provide a better understanding of the ECM coatings *in vivo* hemostatic performance [302, 303]. Also, it is known from previous studies that the glial scar surrounding a similar device does not change after 2 weeks [73]. Therefore, analysis of inflammatory and astrocyte biomarkers surrounding astrocyte-derived ECM may answer if the decrease in GFAP at 8 weeks is attributed to acute immunomodulation or a specific interaction with astrocytes.

A second *in vivo* study would be the prelabeling of coated proteins with a marker which can be later detected in tissue. This could provide insights on the activity of surface adherent macrophages (Fig. 4.1) and possibly be used to track their migration following interaction with the device interface. Care must be taken in this step to minimize the alterations to the protein function. Potential labeling techniques would include fluorophore conjugation to the proteins, which would be the simplest through an amine-fluorophore conjugation with either the Avitene or the astrocyte-derived ECM coating. This step could be integrated prior or during the coating

deposition. However, fluorophores are hydrophobic which could have influence on the FBR as the adsorption of labelled proteins would be affected, thus requiring a fluorophore only coating for control [304]. A different labeling technique which has been previously used to assess ECM scaffold degradation would be the radiolabeling of the proteins [245]. An advantage of this technique is the limited influence on the natural ECM architecture. One experimental approach involves supplementing the source animal with ^{14}C-proline, which integrates within the native triple helix of fibrous collagen. This would be unfeasible for ECMs where there is no control the development, such as Avitene, but may be possible for the cell-derived ECMs developed *in vitro*. A potential path for post developmental radiolabeling of ECM could use an amine conjugation to integrate the radiolabeled element [305, 306]. If radiolabeling is accomplished, the quantity of material in tissue sections could be quantified at various time points with liquid scintillation counting (LSC) [307, 308]. To better determine the spatial distribution it may be possible to isolate micrometer size regions of tissue with laser capture microdissection (LCM) [309]. LCM and radio-iodination have not been previously combined in this manner, but similar approaches indicate that labeled protein sensitivity would be adequate for quantification [310].

Lastly, gene delivery techniques could enable a number of studies on *in vivo* mechanisms. First, it could enable labeling of cells at the interface through viral transduction of GFP [311]. Along with these GFP, other genes encoding the knock-in of anti-inflammatory molecules or knockdown of proinflammatory molecules could be delivered [312, 313]. One example showed transduction of IL-10 in cells (mostly macrophages) surrounding an implanted polymer scaffold which decreased leukocyte trafficking by 50% relative to controls at 7 days post-implantation [314]. This would be a powerful way to interrogate inflammation's influence on the chronic FBR surrounding CNS implants. One of the most important parts of this approach is to ensure efficient cellular transduction. Techniques where delivery of the vector is rapid (e.g., injection) have experienced poor gene transduction. However, prolonged delivery via immobilizing the viral vectors within a degradable substrate, such as PLGA, improves the efficacy of gene delivery [315]. For MEAs, this could be done by linking PLGA to the surface either as a coating or as an aggregate of nanoparticles. While the translatable nature of genetic engineering

is uncertain, these techniques may allow the field to ask the next phase of questions that will improve clinical efficacy of CNS devices.

4.2.3 Investigate new FBR biomarkers and quantification approaches

To better understand the FBR surrounding brain implanted devices, it may prove beneficial to expanded immunohistochemical quantification in the future with novel biomarkers, higher magnification quantification, and emerging techniques.

Various studies indicate a heterogeneity of macrophage phenotypes. Within this dogma, macrophages have mostly been classified as M1 (proinflammatory) or M2 (proregenerative). However, it is well-recognized now that this view is incomplete as the phenotypes of macrophages *in vivo* are much more variable than the induced phenotypes observed *in vitro* due to supplementation of LPS and various interleukins [316, 317]. Still, these techniques have pushed the field to recognize new biomarkers for quantifying cell phenotype. Two differential biomarkers that seem promising from these macrophage phenotypic studies are arginase and iNOS which may be detected through immunolabeling, similar to the protocols used in Chapters 2 and 3 [190]. These two markers are promising because they originate from a diverging pathway which is based on competitive metabolization of the same substrate, L-arginine. The products of iNOS metabolism of L-arginine are inflammation and tissue damage (NO and L-citrulline). Conversely, arginase metabolism of L-arginine results in ECM production and cell proliferation (L-proline and polyamines) [317, 318].

Laser capture microdissection of tissue could also be combined with qRT-PCR to map the genetic upregulation of various biomarkers surrounding the uncoated and ECM coated interfaces. This could be a beneficial supplement to quantitative IHC used to describe the FBR. This technique has been used to profile sections from multiple intracortical MEA studies [120, 124], which indicated an increase in various matrix metalloproteases (MMP), including gelatinases MMP-2 and MMP-9, which are potent drives of inflammation and are associated with BBB permeability [319]. Adoption of this approach may be especially useful for comparing the neuroinflammatory profile of the FBR surrounding uncoated controls and ECM coated MEAs. However, a number of pitfalls have been identified with qRT-PCR, including poor correlation

between mRNA and protein abundance, which should to be considered prior to technique adoption [320].

4.2.4 Influence ECM derivation process and cell/species origin of the ECM protein coatings

For the derivation of ECM *in vitro* an area of improvement is the design and need for sacrificial scaffolds. An alternate scaffold fabrication technique, electrospinning of polymer nanofibers, would provide a higher degree of tortuosity within the scaffold than the porous PU scaffolds and may further promote the degree of molecular crowding and ECM accumulation (Fig. 4.2A-B) [321]. However, a better route may be to eliminate the sacrificial scaffold all together. One means to do this would be electrospinning of a nanofiber protein scaffold, similar to those fabricated with solubilized collagen suspended in 1,1,1,3,3,3-hexafluoro-2-propanol [322, 323]. This initial electrospun protein scaffold could then serve as the substrate and be enriched by *in vitro* cell proliferation and ECM accumulation. Furthermore, it was shown in our lab that derivation of ECM is possible from decellularized cell sheets (Fig. 4.2C) [324]. These alternate cell-derived harvesting techniques may be useful for delineating what influence the harvesting technique has on differences observed surrounding the ECM coatings.

The results within Chapter 2 are the first FBR response to an allogeneic cell-type specific ECM coating, and indicate that ECM origin and composition have an influence on the FBR. A next step is to use ECM proteins derived from different cellular origins or with more specific protein composition to delineate the role of cell-, tissue-, and species-specificity.

One advantage of the cell-derived ECM is that it originates from a specific cell type in a controlled environment. This has proven useful for deriving ECM from cells of various potential such as mesenchymal stem cells and from different tissues such as the dermis [234, 236]. In relation to its influence on the FBR, it limits the ability to isolate the effect of a specific protein on the FBR. Although, isolating a single protein for the coating would obscure the possibility that a heterogeneous protein composition may be required for the observed benefit or deficit. Some single proteins that may prove useful, but have not been investigated *in vivo*, are biglycan, decorin, lumican, or homologous proteins, which have been shown to modulate TGFβ1 signaling and may have more influence on the FBR.

A potentially interesting experiment would be the assessment of a proinflammatory protein coating, using proteins such as IL-1β, IL-6, MCP-1, or RANTES. The inflammatory chemoattractant protein RANTES could be one option and has been investigated *in vivo* through subdermal injections and showed upregulation in the activation of eosinophils, mast cells, lymphocytes, macrophages, and basophils [325]. Given that attempts to decrease the chronic inflammation at the electrode-tissue interface have had limited influence, the rationale for this experiment would be to better understand the influence of acute inflammation on the other aspects of the FBR, and to ask if an increased acute inflammatory response leads to an elevated or equivalent chronic inflammatory response and FBR, when compared to uncoated controls. The approach for this experimental concept would most likely require analysis of several coatings with various concentrations of the proinflammatory stimulus to understand the thresholds of proinflammatory delivery.

4.2.5 Determine ECM coating's influence on a clinical device with an increased FBR

The model device for the presented work, a silicon single-shank MEA, was chosen based on its use historically to understand the FBR. A potential path forward to address multiple facets of the FBR would include coating a lattice designed MEA as indicated in our previous work [163]. Surrounding the lattice, there was a decrease in inflammation (CD68), BBB permeability (IgG), and an increase in neuronal density (NeuN). However, the lattice architecture did not decrease the level of astrogliosis (GFAP). The allogeneic astrocyte-derived ECM coating, on the other hand, was able to influence the level of astrogliosis while not having an influence on the other aspects of the FBR. Thus, combining the lattice architecture and ECM coating may prove synergistic and minimize multiple aspects of the FBR (Fig. 4.3).

Yet, as indicated to in section 1.3.2, these single-shank silicon MEAs create a fairly small degree of damage in comparison to multi-shank MEAs, such as the UEA. From one perspective, a multi-shank model may provide a different result as it is essentially increasing the signal-to-noise ratio of the IHC quantification, with the signal being the level of biomarker immunoreactivity adjacent to the interface and the noise being the level in background tissue. Furthermore, this larger injury is characterized by a prominent lesion and tissue loss occurring below the base (Fig

4.4). This larger injury may originate from the loss of vasculature perfusion redundancy in the brain, which is relatively robust when a focal area of vascular is ruptured. However, more widespread instances of damage may result in loss of this redundant vascular perfusion and a larger area of damage [35]. Thus, it is reasonable to believe that a hemostatic coating maybe have a different response in this model system due to increased biological interactions. This larger injury has been quantified in terms of cavity volume as defined by a prismoidal formula and immunofluorescence of biomarkers within the first 100 μm of the outermost electrodes [27]. Due to the lesion this quantification approach, unlike the one used for single-shank MEAs, is unable to assess the reaction around each shank of the UEA due to the irregularities of the cavity. Given that the only influence on the FBR was observed within 50 μm of the single-shank MEAs, it may be necessary to revise these previous quantification approaches to more specifically analyze the reaction to the individual electrode shanks.

4.2.6 Incorporate recording techniques to assess functional correlations

Ultimately one of the most important future experiments for the presented work and any technique that alters the FBR is the integration of a functional assessment. This could be done with a functionalized single-shank MEA. However, given that the UEA is one of the most utilized recording devices, it would be logical to integrate recording into the section 4.2.5. A majority of the recording data with UEAs originates from primates. However, its adoption in rats may grow with use of smaller 4 x 4 UEAs as detailed in a recent report from our lab [68]. The metrics most often associated with recording performance are signal-to-noise ratio (how high is the recording signal compared to background noise), driven channels (how many electrode sites are able to detect single unit APs), electrode impedance (the ability of current to flow under a driving voltage, typically 1 kHz), and recording longevity (for what length of time are single unit APs detectable) [49, 58, 61, 68, 70, 326]. The experimental protocol for recording would follow similar studies [68], and employ a Cerebus or Cereplex recording data acquisition system supplied by Blackrock Technologies Inc. and equipped with Plexon Offline Sorter software to quantify the signal-to-noise ratio, driven channels, and recording longevity as described above. Additionally, with the compatible Cereplex A amplifier the impedance of each electrode in the UEA can be quantified

and would add to the results from previous work which did not assess impedance. Impedance has been suggested as a correlate to cell reactivity and astrogliosis surrounding the MEA interface, thus it is believed that the allogeneic astrocyte-derived ECM coating would improve this recording metric [327, 328].

4.2.7 Influence of headstage on systemic inflammation and neurogenesis

A few techniques which would be interesting to expand our understanding of the headstage FBR include the cytokine analysis from blood draws at acute and chronic time points, assessment of neurogenesis, cognitive function, and other techniques to assess neuroinflammation. Ideally these experiments would be done with the headstage alone as a control. One potential technique uses autoradiography of [3H]PK11195, which labels a benzodiazepine receptor, to quantify microglia and astrocyte reactivity [329]. One study which used this technique to show the neuroinflammatory burden of DBS implants in rats controlled for the influence of the surgery with a surgical sham, however, failed to assess the influence of the screws and dental acrylic used to affix the DBS to the skull by implanting only a headstage [203].

Assessment of neurogenesis and cognitive ability could be performed in tandem with other techniques through hippocampal evaluation determined by the proportion of Bromodeoxyuridine-positive (BrdU+) proliferative cells that co-express the early neuronal marker doublecortin (Dcx) and an animal memory exercise such as object recognition test [207]. Using this technique with a number of different headstage designs, and the absence of an intracortical implant for control, it would be possible to better determine the neuroinflammatory burden of the headstage alone and guide the field on which approach might least influence brain health.

Incorporation of a device development and commercialization phases in a NIH SBIR/STTR or technology development grant (such as those distributed at the state level for technology commercialization) would strengthen the funding potential and ultimate impact of the work by providing for a more comprehensive analysis and development phases, with analyses from Chapter 3 partially serving as developmental design parameters. In this way, understanding the FBR to headstage components plays into the larger issue of improved headstage components and improved surgical methods for small animal studies.

4.2.8 Design of universal small animal skull fixation device or technique

A purpose of Chapter 3 is to serve as a stepping stone for biologically-informed device design. Design of a novel fixation techniques for rodents and other small animals would benefit a number of fields. Some criteria that need to be considered for this new fixation technique are detailed below.

- Fixation strength is a primary concern as any new methodology needs to ensure that it will not compromise the study. Furthermore, it should endeavor to provide a level of fixation that decreases the fixation failures of current designs. This strong fixation is needed to compensate for animals manipulation of transcutaneous components as well as their natural grooming patterns. Headstage designs for larger animals use titanium components to promote osseointegration due to the titanium oxide-bone interactions [330]. The use of these materials have yet to translate to rodent CNS experiments as the common materials still used are stainless steel screws and dental acrylic.
- Size and surface area of the headstage should be minimized without compromising anchorage. Eliminating the screws and management of skull penetration is one of the largest challenges in regard to fixation. Additionally, a new device or technique would need to account for the innate variability of skull shape and thickness within species, as well as interspecies (rat, mouse, guinea pig). Since the skull size and shape changes over the lifespan of animals, another consideration would need to be the age of the animals at implant and the intended study length.
- Modularity of the technique or headstage device would be needed for adoption by multiple fields. In rodents the most common craniotomy location for access to the cranial vault is in the parietal plate, thus the design would need to maintain this area of accessibility.
- Ease of use and cost would also play a large role in the adoption of the techniques or fixation device. Most importantly the ease of use would help promote repeatable fixation and limit surgeon related variability.

  From these criteria and considering the headstages used in larger animal models, the

most direct path forward would be a titanium plate and screw headstage designed for the rodent skull (Fig. 4.5 and 4.6). An added benefit of titanium would be the possibility of sintering or creating pores on the baseplate surface (Fig. 4.5B) to further promote osseointegration. Levering the osseointegration advantage may allow for a decrease in the screws required and the total implanted surface area. Fabrication of such devices would be feasible within the laboratory setting through the use of laser etching techniques which could be used for developing the baseplate profile as well as creating the porous surface on the base of the plate. Laser etching has shown an ability for high tolerance cutting of titanium within an inert gas environment [331], and studies indicate a laser textured pore size of 200 μm would be optimal for promoting osseointegration of the baseplate with the rodent skull [332].

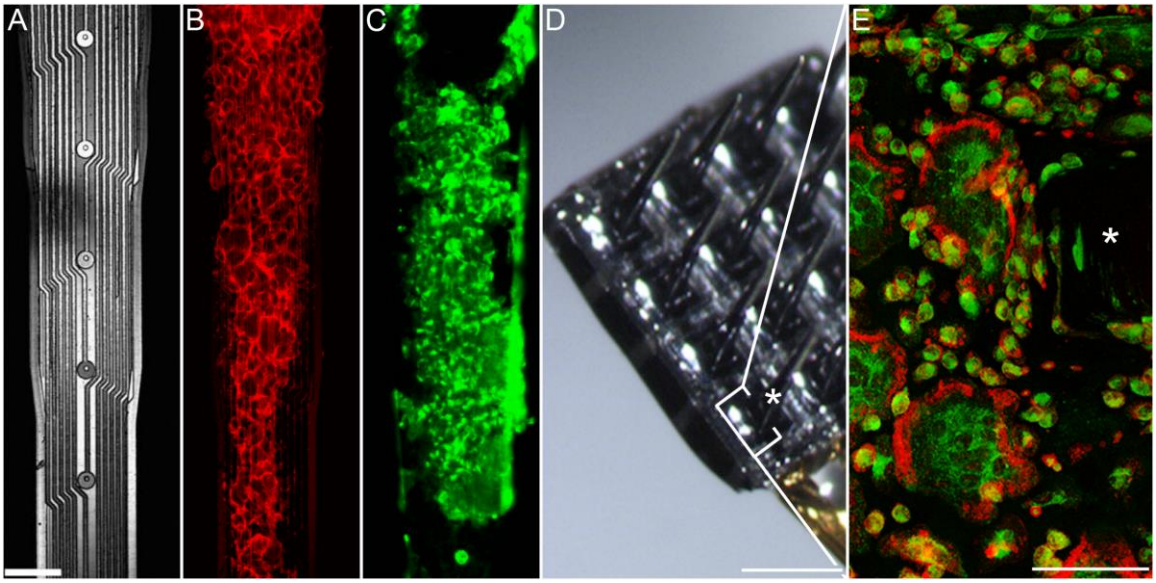

Fig. 4.1. Surface adherent macrophages on single-shank and multi-shank MEAs. (A) Single-shank planar MEA under lightfield illumination. Scale bar 50 µm. (B-C) The same location on an explanted single-shank MEA showing a layer of activated macrophages (MAC-1+ / CD68+). (D) Multi-shank MEA (16-channel UEA) under lightfield illumination. Zoom box indicates similar location from (E) an explanted MEA showing a layer of activated macrophages (IBA-1+ / CD68+).

(A-C) Adapted by permission from Elsevier: Biomaterials, R. Biran, D. C. Martin, P. A. Tresco, Neuronal cell loss accompanies the brain tissue response to chronically implanted silicon microelectrode arrays, Exp. Neurol. 195 (2005) 115-126. http://dx.doi.org/10.1016/j.expneurol.2005.04.020. [76], Copyright 2005. (D-E) Adapted by permission from Elsevier: Biomaterials, N. F. Nolta, M. B. Christensen, P. D. Crane, J. L. Skousen, P. A. Tresco, BBB leakage, astrogliosis, and tissue loss correlate with silicon microelectrode array recording performance, Biomaterials 53 (2015) 753-762. http://dx.doi.org/10.1016/j.biomaterials.2015.02.081. [68], Copyright 2015.

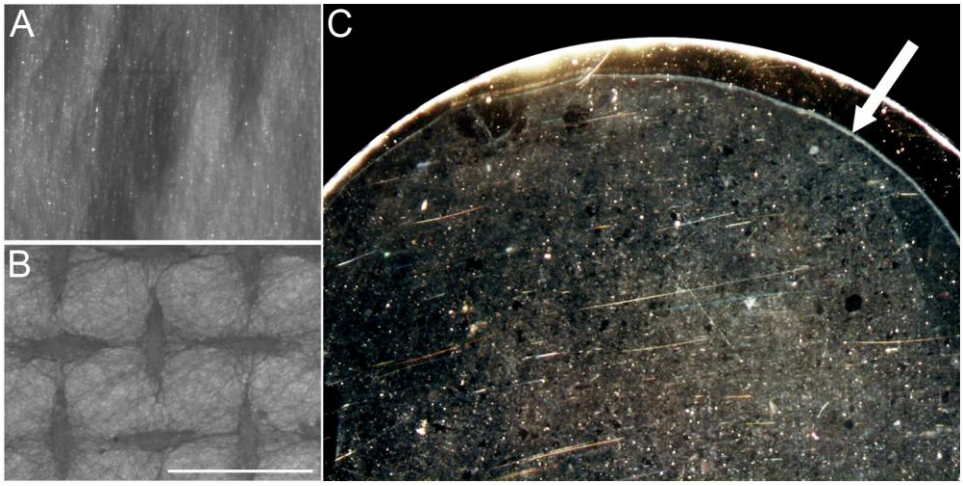

Fig. 4.2. Electrospun polyurethane scaffolds and astrocyte-derived ECM cell sheet. (A) An anisotropic PU scaffold deposited on a conductive spinning mandrel. (B) A grid patterned PU scaffold deposited on a stationary conductive wire mesh. (C) Decellularized astrocyte-derived ECM sheet similar to those fabricated by Meng et al. [324]. The picture sheet (white arrow) retracted from the edge but remained adherent to the coverslip during detergent and enzymatic decellularization steps. These sheets were robust enough to wrap a single-shank planar MEA. However, the innate tension of the sheet caused the silicon MEAs to bend upon drying.

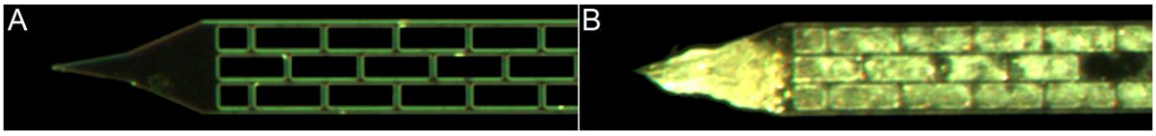

Fig. 4.3. Single-shank lattice geometry silicon MEA coated with astrocyte-derived ECM. (A) Uncoated control lattice MEA compared with (B) an astrocyte-derived ECM coated MEA. In previous studies the lattice geometry showed a lower level of inflammation and BBB permeability, however did not decrease the level of astrocyte reactivity [163]. Combining this approach of device geometry modification and the ECM coating, may prove synergistic for decreasing multiple aspects of the FBR.

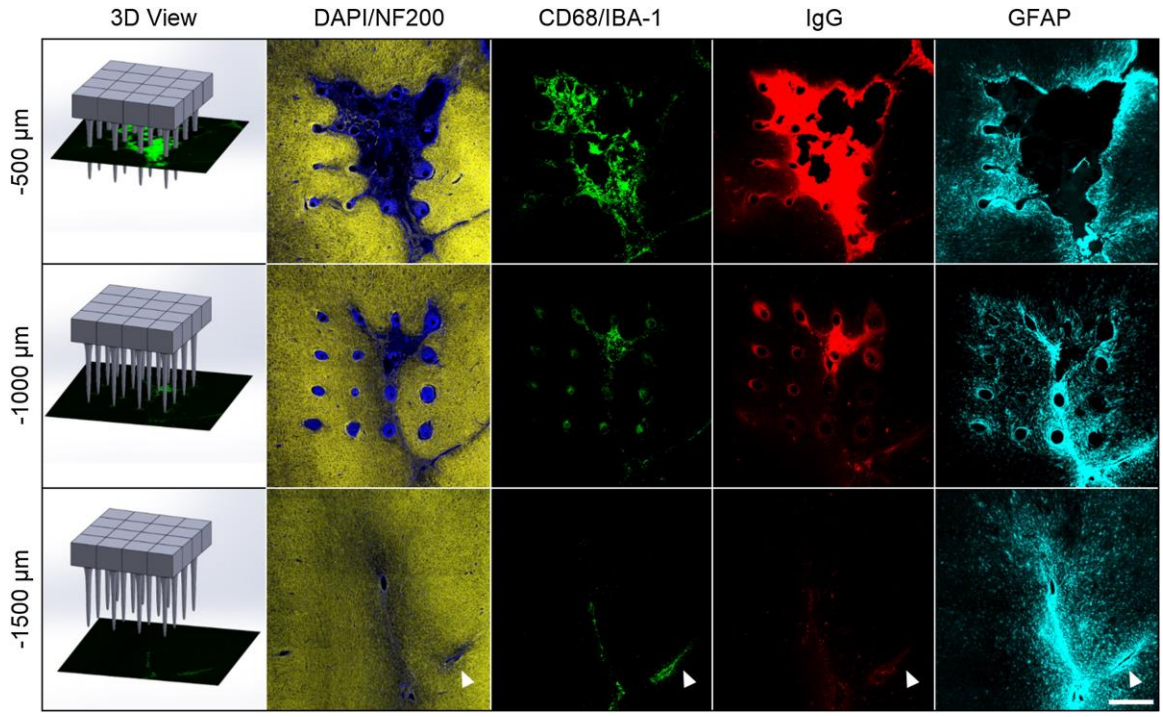

Fig. 4.4. Lesion size at various cortical depths resulting from multi-shank MEA implantation. Representative horizontal sections from an animal sacrificed at 4 weeks showing cell nuclei (DAPI, blue), axons (NF200, yellow), activated macrophages (CD68/IBA-1 colocalization, green), BBB leakage (IgG, red), and astrocyte cytoskeleton (GFAP, cyan). Sections from three different depths are shown including -500 µm, -1000 µm, and -1500 µm. Hypercellular, CD68+, IBA-1+, IgG+, NF200- areas of damaged neural tissue were most evident superficial cortex(-500 µm), while microelectrodes apart from the tissue loss areas had an FBR typical of single-shank MEAs. In deeper cortex (-1000 µm and -1500 µm), the tissue loss area was smaller. Scale bar 500 µm.
Reprinted by permission from Elsevier: Biomaterials, N. F. Nolta, M. B. Christensen, P. D. Crane, J. L. Skousen, P. A. Tresco, BBB leakage, astrogliosis, and tissue loss correlate with silicon microelectrode array recording performance, Biomaterials 53 (2015) 753-762. http://dx.doi.org/10.1016/j.biomaterials.2015.02.081. [68], Copyright 2015.

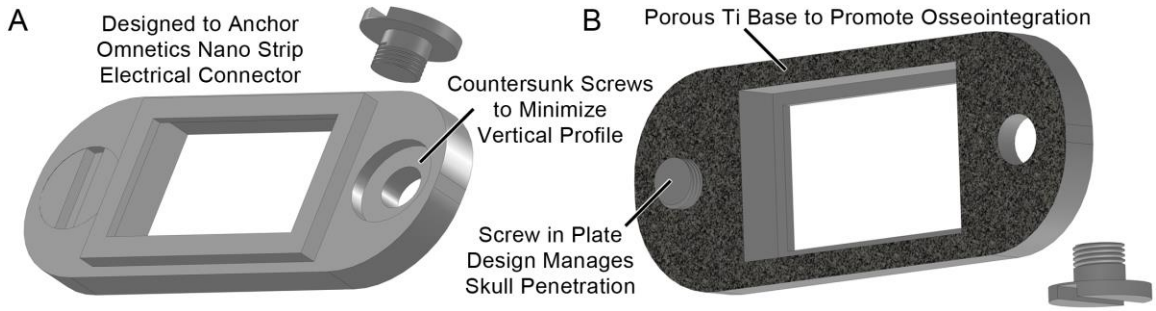

Fig. 4.5. Theoretical titanium headstage mount for fixation of electrical connector in rodents. (A) Top view of headstage securement design showing the integration of countersunk screw holes to minimize the vertical profile. Inner edge has been designed to retain a single Omnetics electrical connector, however may be easily adapted to integrate a cannula or cranial window. (B) Bottom view of possible design showing a porous titanium base to support osseointegration and mechanical interlocking with the skull bone, similar to protocols used for orthopedic devices [333]. Additionally, one of the most important aspects would be the screw in plate design which limits the potential skull penetration. The proposed design has a 600 μm penetration limit, detailed in Fig. 4.6, which corresponds to the approximate skull thickness of a 10 week old Sprague-Dawley rat.

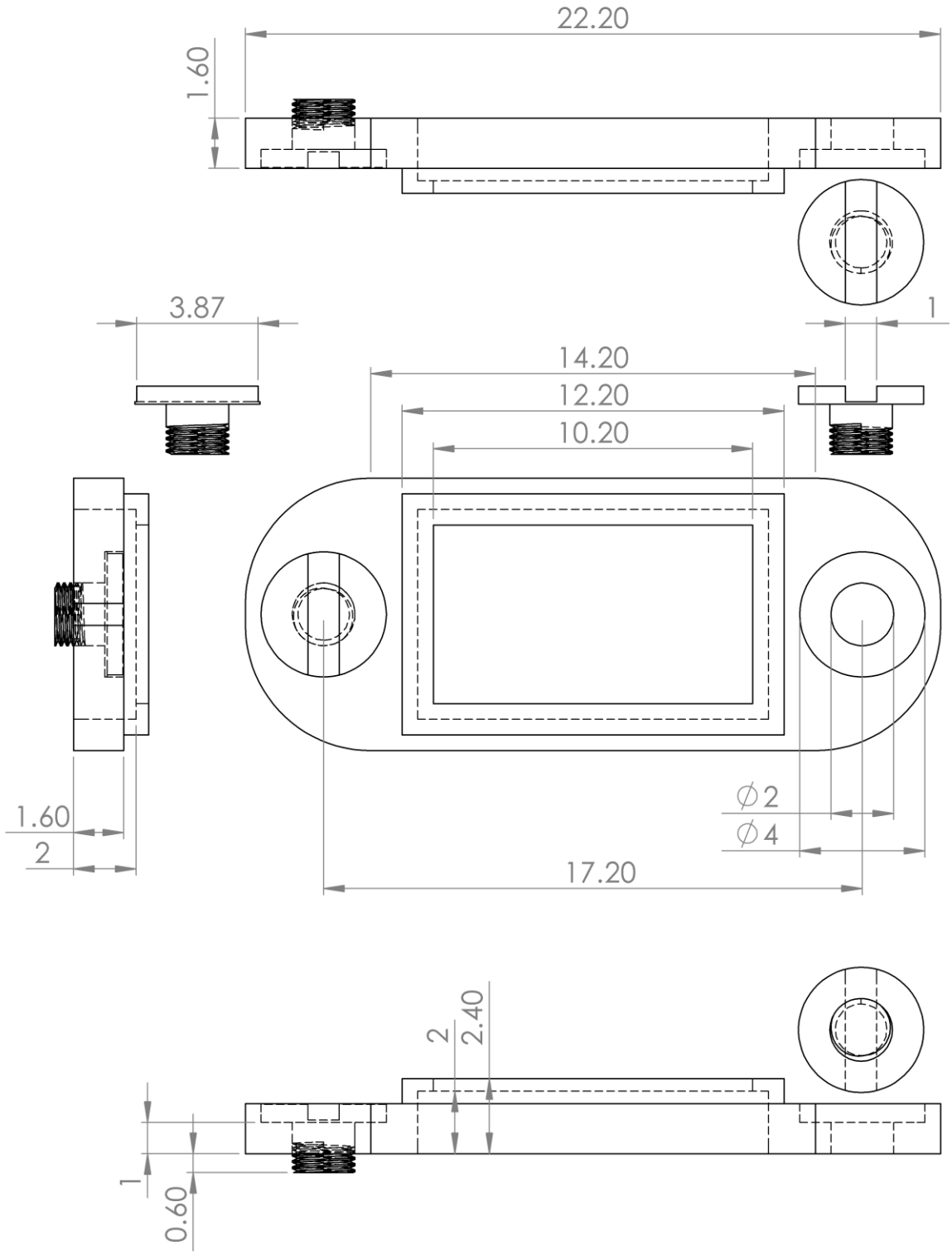

Fig. 4.6. Dimensions of theoretical titanium headstage mount pictured in Fig. 4.5. CAD and drawing output was performed in Solidworks.

REFERENCES

[1] C. Ballard, S. Gauthier, A. Corbett, C. Brayne, D. Aarsland, E. Jones, Alzheimer's disease, Lancet 377 (2011) 1019-1031. http://dx.doi.org/10.1016/s0140-6736(10)61349-9

[2] 2015 Alzheimer's disease facts and figures, Alzheimers Dement. 11 (2015) 332-384. http://dx.doi.org/10.1016/j.jalz.2015.02.003

[3] J. M. Fearnley, A. J. Lees, Ageing and Parkinson's disease: substantia nigra regional selectivity, Brain 114 (Pt 5) (1991) 2283-2301.

[4] S. L. Kowal, T. M. Dall, R. Chakrabarti, M. V. Storm, A. Jain, The current and projected economic burden of Parkinson's disease in the United States, Mov. Disord. 28 (2013) 311-318. http://dx.doi.org/10.1002/mds.25292

[5] W. Robberecht, T. Philips, The changing scene of amyotrophic lateral sclerosis, Nat. Rev. Neurosci. 14 (2013) 248-264. http://dx.doi.org/10.1038/nrn3430

[6] P. Mehta, V. Antao, W. Kaye, M. Sanchez, D. Williamson, L. Bryan, et al., Prevalence of amyotrophic lateral sclerosis - United States, 2010-2011, MMWR Surveill. Summ. Suppl. 7 (2014) 1-14.

[7] S. L. Colby, J. M. Ortman. The baby boom cohort in the United States: 2012 to 2060. Current Population Reports. U. S. Census Bureau, Washington DC. Online. 2014. Available from URL: https://www.census.gov/prod/2014pubs/p25-1141.pdf

[8] H. L. Rekate, The definition and classification of hydrocephalus: a personal recommendation to stimulate debate, Cerebrospinal Fluid. Res. 5 (2008) 2. http://dx.doi.org/10.1186/1743-8454-5-2

[9] T. D. Simon, J. Riva-Cambrin, R. Srivastava, S. L. Bratton, J. M. Dean, J. R. Kestle, et al., Hospital care for children with hydrocephalus in the United States: utilization, charges, comorbidities, and deaths, J. Neurosurg. Pediatr. 1 (2008) 131-137. http://dx.doi.org/10.3171/PED/2008/1/2/131

[10] D. Mozaffarian, E. J. Benjamin, A. S. Go, D. K. Arnett, M. J. Blaha, M. Cushman, et al., Heart disease and stroke statistics--2015 update: a report from the American Heart Association, Circulation 131 (2015) e29-e322. http://dx.doi.org/10.1161/CIR.0000000000000152

[11] K. M. Fargen, M. Rahman, D. Neal, B. L. Hoh, Prevalence of patient safety indicators and hospital-acquired conditions in those treated for unruptured cerebral aneurysms: establishing standard performance measures using the Nationwide Inpatient Sample database, J. Neurosurg. 119 (2013) 966-973. http://dx.doi.org/10.3171/2013.5.JNS122378

[12] V. Y. Ma, L. Chan, K. J. Carruthers, Incidence, prevalence, costs, and impact on disability of common conditions requiring rehabilitation in the United States: stroke, spinal cord injury, traumatic brain injury, multiple sclerosis, osteoarthritis, rheumatoid arthritis, limb loss, and back pain, Arch. Phys. Med. Rehabil. 95 (2014) 986-995. http://dx.doi.org/10.1016/j.apmr.2013.10.032

[13] M. J. Devivo, Epidemiology of traumatic spinal cord injury: trends and future implications, Spinal Cord 50 (2012) 365-372. http://dx.doi.org/10.1038/sc.2011.178

[14] K. Nowak, E. Mix, J. Gimsa, U. Strauss, K. K. Sriperumbudur, R. Benecke, et al., Optimizing a rodent model of Parkinson's disease for exploring the effects and mechanisms of deep brain stimulation, Parkinsons Dis. 2011 (2011) 1-19. http://dx.doi.org/10.4061/2011/414682

[15] M. Han, D. B. McCreery, Microelectrode Technologies for Deep Brain Stimulation, in: D. D. Zhou, E. Greenbaum (Eds.), Implantable Neural Protheses 1, Springer-Verlag, New York, 2009, pp. 195-219. http://dx.doi.org/10.1007/978-0-387-77261-5_6

[16] S. F. Cogan, Neural stimulation and recording electrodes, Annu. Rev. Biomed. Eng. 10 (2008) 275-309. http://dx.doi.org/10.1146/annurev.bioeng.10.061807.160518

[17] D. D. Zhou, E. Greenbaum. Implantable Neural Prostheses 1, Springer-Verlag, New York, 2009. http://dx.doi.org/10.1007/978-0-387-77261-5.

[18] C. Magarinos-Ascone, J. H. Pazo, O. Macadar, W. Buno, High-frequency stimulation of the subthalamic nucleus silences subthalamic neurons: a possible cellular mechanism in Parkinson's disease, Neurosci. 115 (2002) 1109-1117.

[19] Transparency Market Research, Deep Brain Stimulation Devices Market for Parkinson’s Disease – Global Industry Analysis, Size, Share, Growth, Trends and Forecast, 2014 – 2020, http://www.transparencymarketresearch.com/deep-brain-stimulator-market.html, 2014, (accessed 10.03.2015)

[20] S. R. Winn, P. A. Tresco, B. Zielinski, L. A. Greene, C. B. Jaeger, P. Aebischer, Behavioral recovery following intrastriatal implantation of microencapsulated PC12 cells, Exp. Neurol. 113 (1991) 322-329. http://dx.doi.org/10.1016/0014-4886(91)90022-5

[21] P. A. Tresco, S. R. Winn, P. Aebischer, Polymer encapsulated neurotransmitter secreting cells. Potential treatment for Parkinson's disease, ASAIO J. 38 (1992) 17-23.

[22] D. F. Emerich, G. Orive, C. Thanos, J. Tornoe, L. U. Wahlberg, Encapsulated cell therapy for neurodegenerative diseases: from promise to product, Adv. Drug. Deliv. Rev. 67-68 (2014) 131-141. http://dx.doi.org/10.1016/j.addr.2013.07.008

[23] N. Popovic, P. Brundin, Therapeutic potential of controlled drug delivery systems in neurodegenerative diseases, Int. J. Pharm. 314 (2006) 120-126. http://dx.doi.org/10.1016/j.ijpharm.2005.09.040

[24] D. A. Bota, A. Desjardins, J. A. Quinn, M. L. Affronti, H. S. Friedman, Interstitial chemotherapy with biodegradable BCNU (Gliadel®) wafers in the treatment of malignant gliomas, Ther. Clin. Risk. Manag. 3 (2007) 707-715. http://dx.doi.org/10.1.1.275.1682

[25] A. Chari, M. Czosnyka, H. K. Richards, J. D. Pickard, Z. H. Czosnyka, Hydrocephalus shunt technology: 20 years of experience from the Cambridge Shunt Evaluation Laboratory, J. Neurosurg. 120 (2014) 697-707. http://dx.doi.org/10.3171/2013.11.JNS121895

[26] Y. Murayama, S. Tateshima, N. R. Gonzalez, F. Vinuela, Matrix and bioabsorbable polymeric coils accelerate healing of intracranial aneurysms: long-term experimental study, Stroke 34 (2003) 2031-2037. http://dx.doi.org/10.1161/01.STR.0000083394.33633.C2

[27] J. M. Abrahams, S. L. Diamond, R. W. Hurst, E. L. Zager, M. S. Grady, Topic review: surface modifications enhancing biological activity of guglielmi detachable coils in treating intracranial aneurysms, Surg. Neurol. 54 (2000) 34-41. http://dx.doi.org/10.1016/s0090-3019(00)00269-x

[28] I. van der Schaaf, A. Algra, M. Wermer, A. Molyneux, M. Clarke, J. van Gijn, et al., Endovascular coiling versus neurosurgical clipping for patients with aneurysmal subarachnoid haemorrhage, Cochrane Database Syst. Rev. (2005) 1-29. http://dx.doi.org/10.1002/14651858.CD003085.pub2

[29] A. B. Schwartz, X. T. Cui, D. J. Weber, D. W. Moran, Brain-controlled interfaces: movement restoration with neural prosthetics, Neuron 52 (2006) 205-220. http://dx.doi.org/10.1016/j.neuron.2006.09.019

[30] B. Lee, C. Y. Liu, M. L. Apuzzo, A primer on brain-machine interfaces, concepts, and technology: a key element in the future of functional neurorestoration, World Neurosurg. 79 (2013) 457-471. http://dx.doi.org/10.1016/j.wneu.2013.01.078

[31] B. I. Morshed, A. Khan, A Brief Review of Brain Signal Monitoring Technologies for BCI Applications: Challenges and Prospects, J. Bioeng. Biomed. Sci. 4 (2014) 1-10. http://dx.doi.org/10.4172/2155-9538.1000141

[32] M. A. Lebedev, R. Crist, M. A. Nicolelis, Building Brain–Machine Interfaces to Restore Neurological Functions, in: M. A. L. Nicolelis (Eds.), Methods for Neural Ensemble Recordings, 2nd ed., CRC Press, Boca Raton (FL), 2008, pp. 1-15, NCBI Bookshelf, Web (accessed 04.27.2014)

[33] A. Branner, Micro-Wires, Enc. Comp. Neurosci. (2014) 1-4. http://dx.doi.org/10.1007/978-1-4614-7320-6_597-1

[34] G. Lehew, M. A. Nicolelis, State-of-the-Art Microwire Array Design for Chronic Neural Recordings in Behaving Animals, in: M. A. L. Nicolelis (Eds.), Methods for Neural Ensemble Recordings, 2nd ed., CRC Press, Boca Raton (FL), 2008, pp. 1-31, NCBI Bookshelf, Web (accessed 04.27.2014)

[35] Tucker-Davis Technologies. Cortical Array Designer. http://www.tdt.com/cortical-array-designer.html. (accessed 09.30.2015)

[36] K. D. Wise, D. J. Anderson, J. F. Hetke, D. R. Kipke, K. Najafi, Wireless Implantable Microsystems: High-Density Electronic Interfaces to the Nervous System, Proc. IEEE 92 (2004) 76-97. http://dx.doi.org/10.1109/jproc.2003.820544

[37] J.-M. Yoo, A. Sharma, P. Tathireddy, L. W. Rieth, F. Solzbacher, J.-I. Song, Excimer-laser deinsulation of Parylene-C coated Utah electrode array tips, Sens. Actuators B Chem. 166-167 (2012) 777-786. http://dx.doi.org/10.1016/j.snb.2012.03.073

[38] P. K. Campbell, K. E. Jones, R. A. Normann, A 100 electrode intracortical array: structural variability, Biomed. Sci. Instrum. 26 (1990) 161-165.

[39] P. K. Campbell, K. E. Jones, R. J. Huber, K. W. Horch, R. A. Normann, A silicon-based, three-dimensional neural interface: manufacturing processes for an intracortical electrode array, IEEE Trans. Biomed. Eng. 38 (1991) 758-768. http://dx.doi.org/10.1109/10.83588

[40] A. Sharma, L. Rieth, P. Tathireddy, R. Harrison, H. Oppermann, M. Klein, et al., Evaluation of the packaging and encapsulation reliability in fully integrated, fully wireless 100 channel Utah Slant Electrode Array (USEA): Implications for long term functionality, Sens. Actuators A Phys. 188 (2012) 167-172. http://dx.doi.org/10.1016/j.sna.2011.11.015

[41] D. C. Bradley, P. R. Troyk, J. A. Berg, M. Bak, S. Cogan, R. Erickson, et al., Visuotopic mapping through a multichannel stimulating implant in primate V1, J. Neurophysiol. 93 (2005) 1659-1670. http://dx.doi.org/10.1152/jn.01213.2003

[42] C. I. Baker, E. Peli, N. Knouf, N. G. Kanwisher, Reorganization of visual processing in macular degeneration, J. Neurosci. 25 (2005) 614-618. http://dx.doi.org/10.1523/JNEUROSCI.3476-04.2005

[43] L. R. Hochberg, M. D. Serruya, G. M. Friehs, J. A. Mukand, M. Saleh, A. H. Caplan, et al., Neuronal ensemble control of prosthetic devices by a human with tetraplegia, Nature 442 (2006) 164-171. http://dx.doi.org/10.1038/nature04970

[44] J. Moss, T. Ryder, T. Z. Aziz, M. B. Graeber, P. G. Bain, Electron microscopy of tissue adherent to explanted electrodes in dystonia and Parkinson's disease, Brain 127 (2004) 2755-2763. http://dx.doi.org/10.1093/brain/awh292

[45] C. A. Sarkiss, R. Sarkar, W. Yong, J. A. Lazareff, Time dependent pattern of cellular characteristics causing ventriculoperitoneal shunt failure in children, Clin. Neurol. Neurosurg. 127 (2014) 30-32. http://dx.doi.org/10.1016/j.clineuro.2014.09.029

[46] M. Killer, A. S. Arthur, J. D. Barr, B. Richling, G. M. Cruise, Histomorphology of thrombus organization, neointima formation, and foreign body response in retrieved human aneurysms treated with hydrocoil devices, J. Biomed. Mat. Res. B Appl. Biomater. 94 (2010) 486-492. http://dx.doi.org/10.1002/jbm.b.31660

[47] T. D. Y. Kozai, K. Catt, X. Li, Z. V. Gugel, V. T. Olafsson, A. L. Vazquez, et al., Mechanical failure modes of chronically implanted planar silicon-based neural probes for laminar recording, Biomaterials 37 (2015) 25-39. http://dx.doi.org/10.1016/j.biomaterials.2014.10.040

[48] R. A. Miranda, W. D. Casebeer, A. M. Hein, J. W. Judy, E. P. Krotkov, T. L. Laabs, et al., DARPA-funded efforts in the development of novel brain-computer interface technologies, J. Neurosci. Methods 244 (2015) 52-67. http://dx.doi.org/10.1016/j.jneumeth.2014.07.019

[49] J. C. Barrese, N. Rao, K. Paroo, C. Triebwasser, C. Vargas-Irwin, L. Franquemont, et al., Failure mode analysis of silicon-based intracortical microelectrode arrays in non-human primates, J. Neural. Eng. 10 (2013) 066014. http://dx.doi.org/10.1088/1741-2560/10/6/066014

[50] A. J. Mangram, T. C. Horan, M. L. Pearson, L. C. Silver, W. R. Jarvis, Publication of Guideline for Prevention of Surgical Site Infection, 1999, JAMA 281 (1999) 97-134. http://dx.doi.org/10.1001/jama.281.20.1884-JWR0526-2-1

[51] A. M. Korinek, T. Baugnon, J. L. Golmard, R. van Effenterre, P. Coriat, L. Puybasset, Risk factors for adult nosocomial meningitis after craniotomy: role of antibiotic prophylaxis, Neurosurgery 59 (2006) 126-133. http://dx.doi.org/10.1227/01.NEU.0000220477.47323.92

[52] R. Thomas, S. Lee, S. Patole, S. Rao, Antibiotic-impregnated catheters for the prevention of CSF shunt infections: a systematic review and meta-analysis, Br. J. Neurosurg. 26 (2012) 175-184. http://dx.doi.org/10.3109/02688697.2011.603856

[53] J. J. Stone, C. T. Walker, M. Jacobson, V. Phillips, H. J. Silberstein, Revision rate of pediatric ventriculoperitoneal shunts after 15 years, J. Neurosurg. Pediatr. 11 (2013) 15-19. http://dx.doi.org/10.3171/2012.9.PEDS1298

[54] J. Kast, D. Duong, F. Nowzari, W. M. Chadduck, S. J. Schiff, Time-related patterns of ventricular shunt failure, Childs Nerv. Sys. 10 (1994) 524-528. http://dx.doi.org/10.1007/bf00335075

[55] M. R. Del Bigio, Biological reactions to cerebrospinal fluid shunt devices: a review of the cellular pathology, Neurosurgery 42 (1998) 319-325.

[56] E. Fernandez, B. Greger, P. A. House, I. Aranda, C. Botella, J. Albisua, et al., Acute human brain responses to intracortical microelectrode arrays: challenges and future prospects, Front. Neuroeng. 7 (2014) 1-6. http://dx.doi.org/10.3389/fneng.2014.00024

[57] X. Liu, D. B. McCreery, L. A. Bullara, W. F. Agnew, Evaluation of the stability of intracortical microelectrode arrays, IEEE Trans. Neural. Syst. Rehabil. Eng. 14 (2006) 91-100. http://dx.doi.org/10.1109/TNSRE.2006.870495

[58] R. J. Vetter, J. C. Williams, J. F. Hetke, E. A. Nunamaker, D. R. Kipke, Chronic neural recording using silicon-substrate microelectrode arrays implanted in cerebral cortex, IEEE Trans. Biomed. Eng. 51 (2004) 896-904. http://dx.doi.org/10.1109/TBME.2004.826680

[59] M. A. Freire, E. Morya, J. Faber, J. R. Santos, J. S. Guimaraes, N. A. Lemos, et al., Comprehensive analysis of tissue preservation and recording quality from chronic multielectrode implants, PloS One 6 (2011) e27554. http://dx.doi.org/10.1371/journal.pone.0027554

[60] A. Prasad, Q. S. Xue, V. Sankar, T. Nishida, G. Shaw, W. J. Streit, et al., Comprehensive characterization and failure modes of tungsten microwire arrays in chronic neural implants, J. Neural Eng. 9 (2012) 056015. http://dx.doi.org/10.1088/1741-2560/9/5/056015

[61] A. Prasad, Q. S. Xue, R. Dieme, V. Sankar, R. C. Mayrand, T. Nishida, et al., Abiotic-biotic characterization of Pt/Ir microelectrode arrays in chronic implants, Front. Neuroeng. 7 (2014) 1-15. http://dx.doi.org/10.3389/fneng.2014.00002

[62] J. C. Williams, R. L. Rennaker, D. R. Kipke, Long-term neural recording characteristics of wire microelectrode arrays implanted in cerebral cortex, Brain Res. Brain. Res. Protoc. 4 (1999) 303-313. http://dx.doi.org/10.1016/s1385-299x(99)00034-3

[63] P. J. Rousche, R. A. Normann, Chronic recording capability of the Utah Intracortical Electrode Array in cat sensory cortex, J. Neurosci. Methods 82 (1998) 1-15.

[64] L. Xindong, D. B. McCreery, R. R. Carter, L. A. Bullara, T. G. H. Yuen, W. F. Agnew, Stability of the interface between neural tissue and chronically implanted intracortical microelectrodes, IEEE Trans. Rehab. Eng. 7 (1999) 315-326. http://dx.doi.org/10.1109/86.788468

[65] J. A. Perge, M. L. Homer, W. Q. Malik, S. Cash, E. Eskandar, G. Friehs, et al., Intra-day signal instabilities affect decoding performance in an intracortical neural interface system, J. Neural Eng. 10 (2013) 036004. http://dx.doi.org/10.1088/1741-2560/10/3/036004

[66] E. M. Schmidt, J. S. McIntosh, M. J. Bak, Long-term implants of Parylene-C coated microelectrodes, Med. Biol. Eng. Comput. 26 (1988) 96-101. http://dx.doi.org/10.1007/bf02441836

[67] C. A. Chestek, V. Gilja, P. Nuyujukian, J. D. Foster, J. M. Fan, M. T. Kaufman, et al., Long-term stability of neural prosthetic control signals from silicon cortical arrays in rhesus macaque motor cortex, J. Neural Eng. 8 (2011) 045005. http://dx.doi.org/10.1088/1741-2560/8/4/045005

[68] N. F. Nolta, M. B. Christensen, P. D. Crane, J. L. Skousen, P. A. Tresco, BBB leakage, astrogliosis, and tissue loss correlate with silicon microelectrode array recording performance, Biomaterials 53 (2015) 753-762. http://dx.doi.org/10.1016/j.biomaterials.2015.02.081

[69] R. R. Nelson, On the uneven evolution of human know-how, Res. Policy 32 (2003) 909-922. http://dx.doi.org/10.1016/s0048-7333(02)00093-8

[70] M. P. Ward, P. Rajdev, C. Ellison, P. P. Irazoqui, Toward a comparison of microelectrodes for acute and chronic recordings, Brain Res. 1282 (2009) 183-200. http://dx.doi.org/10.1016/j.brainres.2009.05.052

[71] A. J. Woolley, H. A. Desai, K. J. Otto, Chronic intracortical microelectrode arrays induce non-uniform, depth-related tissue responses, J. Neural Eng. 10 (2013) 026007. http://dx.doi.org/10.1088/1741-2560/10/2/026007

[72] B. D. Winslow, P. A. Tresco, Quantitative analysis of the tissue response to chronically implanted microwire electrodes in rat cortex, Biomaterials 31 (2010) 1558-1567. http://dx.doi.org/10.1016/j.biomaterials.2009.11.049

[73] B. D. Winslow, M. B. Christensen, W. K. Yang, F. Solzbacher, P. A. Tresco, A comparison of the tissue response to chronically implanted Parylene-C-coated and uncoated planar silicon microelectrode arrays in rat cortex, Biomaterials 31 (2010) 9163-9172. http://dx.doi.org/10.1016/j.biomaterials.2010.05.050

[74] V. S. Polikov, P. A. Tresco, W. M. Reichert, Response of brain tissue to chronically implanted neural electrodes, J. Neurosci. Methods 148 (2005) 1-18. http://dx.doi.org/10.1016/j.jneumeth.2005.08.015

[75] R. Biran, D. C. Martin, P. A. Tresco, The brain tissue response to implanted silicon microelectrode arrays is increased when the device is tethered to the skull, J. Biomed. Mater. Res. A 82 (2007) 169-178. http://dx.doi.org/10.1002/jbm.a.31138

[76] R. Biran, D. C. Martin, P. A. Tresco, Neuronal cell loss accompanies the brain tissue response to chronically implanted silicon microelectrode arrays, Exp. Neurol. 195 (2005) 115-126. http://dx.doi.org/10.1016/j.expneurol.2005.04.020

[77] K. A. Potter, A. C. Buck, W. K. Self, J. R. Capadona, Stab injury and device implantation within the brain results in inversely multiphasic neuroinflammatory and neurodegenerative responses, J. Neural Eng. 9 (2012) 046020. http://dx.doi.org/10.1088/1741-2560/9/4/046020

[78] R. Shechter, M. Schwartz, CNS sterile injury: just another wound healing?, Trends Mol. Med. 19 (2013) 135-143. http://dx.doi.org/10.1016/j.molmed.2012.11.007

[79] J. D. Stroncek, W. M. Reichert, Overview of Wound Healing in Different Tissue Types, in: Reichert WM, (Eds.), Indwelling Neural Implants: Strategies for Contending with the In Vivo Environment., CRC Press/Taylor & Francis, Boca Raton (FL), 2008, pp. 3-38, NCBI Bookshelf, Web (accessed 09.27.2015)

[80] A. S. Brunswick, B. Y. Hwang, G. Appelboom, R. Y. Hwang, M. A. Piazza, E. S. Connolly, Jr., Serum biomarkers of spontaneous intracerebral hemorrhage induced secondary brain injury, J. Neurol. Sci. 321 (2012) 1-10. http://dx.doi.org/10.1016/j.jns.2012.06.008

[81] A. Szymanska, J. Biernaskie, D. Laidley, S. Granter-Button, D. Corbett, Minocycline and intracerebral hemorrhage: influence of injury severity and delay to treatment, Exp. Neurol. 197 (2006) 189-196. http://dx.doi.org/10.1016/j.expneurol.2005.09.011

[82] J. Lok, W. Leung, S. Murphy, W. Butler, N. Noviski, E. H. Lo, Intracranial hemorrhage: mechanisms of secondary brain injury, Acta Neurochir. Suppl. 111 (2011) 63-69. http://dx.doi.org/10.1007/978-3-7091-0693-8_11

[83] G. Xi, R. F. Keep, J. T. Hoff, Mechanisms of brain injury after intracerebral haemorrhage, Lancet Neurol. 5 (2006) 53-63. http://dx.doi.org/10.1016/s1474-4422(05)70283-0

[84] S. Hirsch, J. Reichold, M. Schneider, G. Szekely, B. Weber, Topology and hemodynamics of the cortical cerebrovascular system, J. Cereb. Blood Flow Metab. 32 (2012) 952-967. http://dx.doi.org/10.1038/jcbfm.2012.39

[85] S. Beriault, A. F. Sadikot, F. Alsubaie, S. Drouin, D. L. Collins, G. B. Pike, Neuronavigation using susceptibility-weighted venography: application to deep brain stimulation and comparison with gadolinium contrast, J. Neurosurg. 121 (2014) 131-141. http://dx.doi.org/10.3171/2014.3.JNS131860

[86] M. Welkenhuysen, A. Andrei, L. Ameye, W. Eberle, B. Nuttin, Effect of insertion speed on tissue response and insertion mechanics of a chronically implanted silicon-based neural probe, IEEE Trans. Biomed. Eng. 58 (2011) 3250-3259. http://dx.doi.org/10.1109/TBME.2011.2166963

[87] T. D. Kozai, T. C. Marzullo, F. Hooi, N. B. Langhals, A. K. Majewska, E. B. Brown, et al., Reduction of neurovascular damage resulting from microelectrode insertion into the cerebral cortex using in vivo two-photon mapping, J. Neural Eng. 7 (2010) 046011. http://dx.doi.org/10.1088/1741-2560/7/4/046011

[88] P. A. House, J. D. MacDonald, P. A. Tresco, R. A. Normann, Acute microelectrode array implantation into human neocortex: preliminary technique and histological considerations, Neurosurg. Focus 20 (2006) 1-4. http://dx.doi.org/10.3171/foc.2006.20.5.5

[89] C. S. Bjornsson, S. J. Oh, Y. A. Al-Kofahi, Y. J. Lim, K. L. Smith, J. N. Turner, et al., Effects of insertion conditions on tissue strain and vascular damage during neuroprosthetic device insertion, J. Neural Eng. 3 (2006) 196-207. http://dx.doi.org/10.1088/1741-2560/3/3/002

[90] A. Kumar, D. J. Loane, Neuroinflammation after traumatic brain injury: opportunities for therapeutic intervention, Brain Behav. Immun. 26 (2012) 1191-1201. http://dx.doi.org/10.1016/j.bbi.2012.06.008

[91] D. J. McCabe, P. Harrison, I. J. Mackie, P. S. Sidhu, G. Purdy, A. S. Lawrie, et al., Platelet degranulation and monocyte-platelet complex formation are increased in the acute and convalescent phases after ischaemic stroke or transient ischaemic attack, Br. J. Haematol. 125 (2004) 777-787. http://dx.doi.org/10.1111/j.1365-2141.2004.04983.x

[92] S. David, A. Kroner, Repertoire of microglial and macrophage responses after spinal cord injury, Nat. Rev. Neuro. 12 (2011) 388-399. http://dx.doi.org/10.1038/nrn3053

[93] C. Power, S. Henry, M. R. Del Bigio, P. H. Larsen, D. Corbett, Y. Imai, et al., Intracerebral hemorrhage induces macrophage activation and matrix metalloproteinases, Ann. Neurol. 53 (2003) 731-742. http://dx.doi.org/10.1002/ana.10553

[94] A. Lee, M. K. Whyte, C. Haslett, Inhibition of apoptosis and prolongation of neutrophil functional longevity by inflammatory mediators, J. Leukoc. Biol. 54 (1993) 283-288.

[95] P. G. Ren, Z. Huang, T. Ma, S. Biswal, R. L. Smith, S. B. Goodman, Surveillance of systemic trafficking of macrophages induced by UHMWPE particles in nude mice by noninvasive imaging, J. Biomed. Mater. Res. A 94 (2010) 706-711. http://dx.doi.org/10.1002/jbm.a.32744

[96] W. F. Hickey, Basic principles of immunological surveillance of the normal central nervous system, Glia 36 (2001) 118-124.

[97] A. K. Abbas, A. H. H. Lichtman, S. Pillai, Cellular and Molecular Immunology: with STUDENT CONSULT Online Access. 7th ed., Saunders, Philadelphia (PA), 2011.

[98] K. Lhotta, R. Wurzner, F. Kronenberg, M. Oppermann, P. Konig, Rapid activation of the complement system by cuprophane depends on complement component C4, Kidney Int. 53 (1998) 1044-1051. http://dx.doi.org/10.1111/j.1523-1755.1998.00836.x

[99] B. Nilsson, K. N. Ekdahl, T. E. Mollnes, J. D. Lambris, The role of complement in biomaterial-induced inflammation, Mol. Immunol. 44 (2007) 82-94. http://dx.doi.org/10.1016/j.molimm.2006.06.020

[100] B. R. Tambuyzer, P. Ponsaerts, E. J. Nouwen, Microglia: gatekeepers of central nervous system immunology, J. Leukoc. Biol. 85 (2009) 352-370. http://dx.doi.org/10.1189/jlb.0608385

[101] F. Ginhoux, M. Greter, M. Leboeuf, S. Nandi, P. See, S. Gokhan, et al., Fate mapping analysis reveals that adult microglia derive from primitive macrophages, Science 330 (2010) 841-845. http://dx.doi.org/10.1126/science.1194637

[102] M. Schilling, M. Besselmann, M. Muller, J. K. Strecker, E. B. Ringelstein, R. Kiefer, Predominant phagocytic activity of resident microglia over hematogenous macrophages following transient focal cerebral ischemia: an investigation using green fluorescent protein transgenic bone marrow chimeric mice, Exp. Neurol. 196 (2005) 290-297. http://dx.doi.org/10.1016/j.expneurol.2005.08.004

[103] M. Ravikumar, S. Sunil, J. Black, D. S. Barkauskas, A. Y. Haung, R. H. Miller, et al., The roles of blood-derived macrophages and resident microglia in the neuroinflammatory response to implanted Intracortical microelectrodes, Biomaterials 35 (2014) 8049-8064. http://dx.doi.org/10.1016/j.biomaterials.2014.05.084

[104] S. K. Chen, P. Tvrdik, E. Peden, S. Cho, S. Wu, G. Spangrude, et al., Hematopoietic origin of pathological grooming in Hoxb8 mutant mice, Cell 141 (2010) 775-785. http://dx.doi.org/10.1016/j.cell.2010.03.055

[105] P. J. Lindsberg, D. Strbian, M. L. Karjalainen-Lindsberg, Mast cells as early responders in the regulation of acute blood-brain barrier changes after cerebral ischemia and hemorrhage, J. Cereb. Blood Flow Metab. 30 (2010) 689-702. http://dx.doi.org/10.1038/jcbfm.2009.282

[106] Y. Dong, E. N. Benveniste, Immune function of astrocytes, Glia 36 (2001) 180-190. http://dx.doi.org/10.1002/glia.1107

[107] D. M. Mosser, J. P. Edwards, Exploring the full spectrum of macrophage activation, Nat. Rev. Immunol. 8 (2008) 958-969. http://dx.doi.org/10.1038/nri2448

[108] J. Silver, J. H. Miller, Regeneration beyond the glial scar, Nat. Rev. Neuro. 5 (2004) 146-156. http://dx.doi.org/10.1038/nrn1326

[109] R. J. Gilbert, R. J. McKeon, A. Darr, A. Calabro, V. C. Hascall, R. V. Bellamkonda, CS-4,6 is differentially upregulated in glial scar and is a potent inhibitor of neurite extension, Mol. Cell. Neurosci. 29 (2005) 545-558. http://dx.doi.org/10.1016/j.mcn.2005.04.006

[110] J. R. Faulkner, J. E. Herrmann, M. J. Woo, K. E. Tansey, N. B. Doan, M. V. Sofroniew, Reactive astrocytes protect tissue and preserve function after spinal cord injury, J. Neurosci. 24 (2004) 2143-2155. http://dx.doi.org/10.1523/JNEUROSCI.3547-03.2004

[111] M. L. Block, L. Zecca, J. S. Hong, Microglia-mediated neurotoxicity: uncovering the molecular mechanisms, Nat. Rev. Neurosci. 8 (2007) 57-69. http://dx.doi.org/10.1038/nrn2038

[112] E. Polazzi, A. Contestabile, Reciprocal Interactions Between Microglia and Neurons: From Survival to Neuropathology, Rev. Neurosci. 13 (2002) 221-242. http://dx.doi.org/10.1515/revneuro.2002.13.3.221

[113] K. I. Park, Y. D. Teng, E. Y. Snyder, The injured brain interacts reciprocally with neural stem cells supported by scaffolds to reconstitute lost tissue, Nat. Biotechnol. 20 (2002) 1111-1117. http://dx.doi.org/10.1038/nbt751

[114] F. Yin, C. Meng, R. Lu, L. Li, Y. Zhang, H. Chen, et al., Bone marrow mesenchymal stem cells repair spinal cord ischemia/reperfusion injury by promoting axonal growth and anti-autophagy, Neural Regen. Res. 9 (2014) 1665-1671. http://dx.doi.org/10.4103/1673-5374.141801

[115] Y. T. Kim, M. J. Bridge, P. A. Tresco, The influence of the foreign body response evoked by fibroblast transplantation on soluble factor diffusion in surrounding brain tissue, J. Control. Release 118 (2007) 340-347. http://dx.doi.org/10.1016/j.jconrel.2007.01.002

[116] J. M. Anderson, A. Rodriguez, D. T. Chang, Foreign body reaction to biomaterials, Semin. Immunol. 20 (2008) 86-100. http://dx.doi.org/10.1016/j.smim.2007.11.004

[117] J. M. Anderson, Biological responses to materials, Ann. Rev. Mater. Res. 31 (2001) 81-110. http://dx.doi.org/10.1146/annurev.matsci.31.1.81

[118] J. A. Jones, D. T. Chang, H. Meyerson, E. Colton, I. K. Kwon, T. Matsuda, et al., Proteomic analysis and quantification of cytokines and chemokines from biomaterial surface-adherent macrophages and foreign body giant cells, J. Biomed. Mater. Res. A 83 (2007) 585-596. http://dx.doi.org/10.1002/jbm.a.31221

[119] M. N. Woodroofe, G. S. Sarna, M. Wadhwa, G. M. Hayes, A. J. Loughlin, A. Tinker, et al., Detection of interleukin-1 and interleukin-6 in adult rat brain, following mechanical injury, by in vivo microdialysis: evidence of a role for microglia in cytokine production, J. Neuroimmunol. 33 (1991) 227-236. http://dx.doi.org/10.1016/0165-5728(91)90110-s

[120] L. Karumbaiah, S. E. Norman, N. B. Rajan, S. Anand, T. Saxena, M. Betancur, et al., The upregulation of specific interleukin (IL) receptor antagonists and paradoxical enhancement of neuronal apoptosis due to electrode induced strain and brain micromotion, Biomaterials 33 (2012) 5983-5996. http://dx.doi.org/10.1016/j.biomaterials.2012.05.021

[121] B. K. Leung, R. Biran, C. J. Underwood, P. A. Tresco, Characterization of microglial attachment and cytokine release on biomaterials of differing surface chemistry, Biomaterials 29 (2008) 3289-3297. http://dx.doi.org/10.1016/j.biomaterials.2008.03.045

[122] U. K. Hanisch, Microglia as a source and target of cytokines, Glia 40 (2002) 140-155. http://dx.doi.org/10.1002/glia.10161

[123] R. W. Griffith, D. R. Humphrey, Long-term gliosis around chronically implanted platinum electrodes in the Rhesus macaque motor cortex, Neurosci. Lett. 406 (2006) 81-86. http://dx.doi.org/10.1016/j.neulet.2006.07.018

[124] T. Saxena, L. Karumbaiah, E. A. Gaupp, R. Patkar, K. Patil, M. Betancur, et al., The impact of chronic blood-brain barrier breach on intracortical electrode function, Biomaterials 34 (2013) 4703-4713. http://dx.doi.org/10.1016/j.biomaterials.2013.03.007

[125] A. J. Sawyer, T. R. Kyriakides, Nanoparticle-based evaluation of blood-brain barrier leakage during the foreign body response, J. Neural Eng. 10 (2013) 016013. http://dx.doi.org/10.1088/1741-2560/10/1/016013

[126] N. J. Abbott, A. A. Patabendige, D. E. Dolman, S. R. Yusof, D. J. Begley, Structure and function of the blood-brain barrier, Neurobiol. Dis. 37 (2010) 13-25. http://dx.doi.org/10.1016/j.nbd.2009.07.030

[127] D. Davalos, K. Akassoglou, Fibrinogen as a key regulator of inflammation in disease, Semin. Immunopathol. 34 (2012) 43-62. http://dx.doi.org/10.1007/s00281-011-0290-8

[128] D. Davalos, J. Grutzendler, G. Yang, J. V. Kim, Y. Zuo, S. Jung, et al., ATP mediates rapid microglial response to local brain injury in vivo, Nat. Neurosci. 8 (2005) 752-758. http://dx.doi.org/10.1038/nn1472

[129] D. Davalos, J. K. Ryu, M. Merlini, K. M. Baeten, N. Le Moan, M. A. Petersen, et al., Fibrinogen-induced perivascular microglial clustering is required for the development of axonal damage in neuroinflammation, Nat. Commun. 3 (2012) 1227. http://dx.doi.org/10.1038/ncomms2230

[130] P. A. Schwartzkroin, S. C. Baraban, D. W. Hochman, Osmolarity, ionic flux, and changes in brain excitability, Epilepsy Res. 32 (1998) 275-285.

[131] C. Nicholson, J. M. Phillips, Ion diffusion modified by tortuosity and volume fraction in the extracellular microenvironment of the rat cerebellum, J. Physiol. 321 (1981) 225-257.

[132] G. C. McConnell, H. D. Rees, A. I. Levey, C. A. Gutekunst, R. E. Gross, R. V. Bellamkonda, Implanted neural electrodes cause chronic, local inflammation that is correlated with local neurodegeneration, J. Neural Eng. 6 (2009) 056003. http://dx.doi.org/10.1088/1741-2560/6/5/056003

[133] T. C. Chiganos, Jr., W. Jensen, P. J. Rousche, Electrophysiological response dynamics during focal cortical infarction, J. Neural Eng. 3 (2006) L15-22. http://dx.doi.org/10.1088/1741-2560/3/4/L01

[134] G. Buzsaki, Large-scale recording of neuronal ensembles, Nat. Neurosci. 7 (2004) 446-451. http://dx.doi.org/10.1038/nn1233

[135] F. Mechler, J. D. Victor, I. Ohiorhenuan, A. M. Schmid, Q. Hu, Three-dimensional localization of neurons in cortical tetrode recordings, J. Neurophysiol. 106 (2011) 828-848. http://dx.doi.org/10.1152/jn.00515.2010

[136] J. L. Skousen, M. J. Bridge, P. A. Tresco, A strategy to passively reduce neuroinflammation surrounding devices implanted chronically in brain tissue by manipulating device surface permeability, Biomaterials 36 (2015) 33-43. http://dx.doi.org/10.1016/j.biomaterials.2014.08.039

[137] T. D. Kozai, X. Li, L. M. Bodily, E. M. Caparosa, G. A. Zenonos, D. L. Carlisle, et al., Effects of caspase-1 knockout on chronic neural recording quality and longevity: Insight into cellular and molecular mechanisms of the reactive tissue response, Biomaterials 35 (2014) 9620-9634. http://dx.doi.org/10.1016/j.biomaterials.2014.08.006

[138] M. Protasoni, S. Sangiorgi, A. Cividini, G. T. Culuvaris, G. Tomei, C. Dell'Orbo, et al., The collagenic architecture of human dura mater, J. Neurosurg. 114 (2011) 1723-1730. http://dx.doi.org/10.3171/2010.12.JNS101732

[139] A. A. Schendel, M. W. Nonte, C. Vokoun, T. J. Richner, S. K. Brodnick, F. Atry, et al., The effect of micro-ECoG substrate footprint on the meningeal tissue response, J. Neural Eng. 11 (2014) 046011. http://dx.doi.org/10.1088/1741-2560/11/4/046011

[140] E. M. Maynard, E. Fernandez, R. A. Normann, A technique to prevent dural adhesions to chronically implanted microelectrode arrays, J. Neurosci. Methods 97 (2000) 93-101. http://dx.doi.org/10.1016/s0165-0270(00)00159-x

[141] L. Spataro, J. Dilgen, S. Retterer, A. J. Spence, M. Isaacson, J. N. Turner, et al., Dexamethasone treatment reduces astroglia responses to inserted neuroprosthetic devices in rat neocortex, Exp. Neurol. 194 (2005) 289-300. http://dx.doi.org/10.1016/j.expneurol.2004.08.037

[142] K. A. Potter-Baker, W. G. Stewart, W. H. Tomaszewski, C. T. Wong, W. D. Meador, N. P. Ziats, et al., Implications of chronic daily anti-oxidant administration on the inflammatory response to intracortical microelectrodes, J. Neural Eng. 12 (2015) 046002. http://dx.doi.org/10.1088/1741-2560/12/4/046002

[143] T. Tikka, B. Biebich, G. Gundars, R. Keinanen, J. Koistinaho, Minocycline, a tetracycline derivative, is neuroprotective against excitotoxicity by inhibiting activation and proliferation of microglia, J Neurosci 21 (2001) 2580-2588.

[144] R. L. Rennaker, J. Miller, H. Tang, D. A. Wilson, Minocycline increases quality and longevity of chronic neural recordings, J. Neural Eng. 4 (2007) L1-5. http://dx.doi.org/10.1088/1741-2560/4/2/L01

[145] A. Mercanzini, S. T. Reddy, D. Velluto, P. Colin, A. Maillard, J. C. Bensadoun, et al., Controlled release nanoparticle-embedded coatings reduce the tissue reaction to neuroprostheses, J. Control. Release 145 (2010) 196-202. http://dx.doi.org/10.1016/j.jconrel.2010.04.025

[146] R. Wadhwa, C. F. Lagenaur, X. T. Cui, Electrochemically controlled release of dexamethasone from conducting polymer polypyrrole coated electrode, J. Control. Release 110 (2006) 531-541. http://dx.doi.org/10.1016/j.jconrel.2005.10.027

[147] H. Schacke, Mechanisms involved in the side effects of glucocorticoids, Pharmacol. Ther. 96 (2002) 23-43. http://dx.doi.org/10.1016/s0163-7258(02)00297-8

[148] Y. Zhong, R. V. Bellamkonda, Dexamethasone-coated neural probes elicit attenuated inflammatory response and neuronal loss compared to uncoated neural probes, Brain Res. 1148 (2007) 15-27. http://dx.doi.org/10.1016/j.brainres.2007.02.024

[149] D. H. Kim, D. C. Martin, Sustained release of dexamethasone from hydrophilic matrices using PLGA nanoparticles for neural drug delivery, Biomaterials 27 (2006) 3031-3037. http://dx.doi.org/10.1016/j.biomaterials.2005.12.021

[150] Y. Zhong, R. V. Bellamkonda, Controlled release of anti-inflammatory agent alpha-MSH from neural implants, J. Control. Release 106 (2005) 309-318. http://dx.doi.org/10.1016/j.jconrel.2005.05.012

[151] S. M. Gutowski, J. T. Shoemaker, K. L. Templeman, Y. Wei, R. A. Latour, Jr., R. V. Bellamkonda, et al., Protease-degradable PEG-maleimide coating with on-demand release of IL-1Ra to improve tissue response to neural electrodes, Biomaterials 44 (2015) 55-70. http://dx.doi.org/10.1016/j.biomaterials.2014.12.009

[152] J. C. Williams, M. M. Holecko, 2nd, S. P. Massia, P. Rousche, D. R. Kipke, Multi-site incorporation of bioactive matrices into MEMS-based neural probes, J. Neural Eng. 2 (2005) L23-L28. http://dx.doi.org/10.1088/1741-2560/2/4/L03

[153] P. Rohatgi, N. B. Langhals, D. R. Kipke, P. G. Patil, In vivo performance of a microelectrode neural probe with integrated drug delivery, Neurosurg. Focus 27 (2009) E8. http://dx.doi.org/10.3171/2009.4.FOCUS0983

[154] R. Grill, K. Murai, A. Blesch, F. H. Gage, M. H. Tuszynski, Cellular delivery of neurotrophin-3 promotes corticospinal axonal growth and partial functional recovery after spinal cord injury, J. Neurosci. 17 (1997) 5560-5572.

[155] E. J. Bradbury, L. D. Moon, R. J. Popat, V. R. King, G. S. Bennett, P. N. Patel, et al., Chondroitinase ABC promotes functional recovery after spinal cord injury, Nature 416 (2002) 636-640. http://dx.doi.org/10.1038/416636a

[156] P. Lu, L. L. Jones, E. Y. Snyder, M. H. Tuszynski, Neural stem cells constitutively secrete neurotrophic factors and promote extensive host axonal growth after spinal cord injury, Exp. Neurol. 181 (2003) 115-129. http://dx.doi.org/10.1016/s0014-4886(03)00037-2

[157] A. J. Hyatt, D. Wang, J. C. Kwok, J. W. Fawcett, K. R. Martin, Controlled release of chondroitinase ABC from fibrin gel reduces the level of inhibitory glycosaminoglycan chains in lesioned spinal cord, J. Control. Release 147 (2010) 24-29. http://dx.doi.org/10.1016/j.jconrel.2010.06.026

[158] K. Moore, M. MacSween, M. Shoichet, Immobilized concentration gradients of neurotrophic factors guide neurite outgrowth of primary neurons in macroporous scaffolds, Tissue Eng 12 (2006) 267-278. http://dx.doi.org/10.1089/ten.2006.12.267

[159] H. M. Tuinstra, D. J. Margul, A. G. Goodman, R. M. Boehler, S. J. Holland, M. L. Zelivyanskaya, et al., Long-term characterization of axon regeneration and matrix changes using multiple channel bridges for spinal cord regeneration, Tissue Eng. A 20 (2014) 1027-1037. http://dx.doi.org/10.1089/ten.TEA.2013.0111

[160] F. Wu, M. Im, E. Yoon. A flexible fish-bone-shaped neural probe strengthened by biodegradable silk coating for enhanced biocompatibility, TRANSDUCERS 16th International Conference, Beijing, China, 2011, pp. 966-969. http://dx.doi.org/10.1109/TRANSDUCERS.2011.5969356

[161] D. Y. Lewitus, K. L. Smith, W. Shain, D. Bolikal, J. Kohn, The fate of ultrafast degrading polymeric implants in the brain, Biomaterials 32 (2011) 5543-5550. http://dx.doi.org/10.1016/j.biomaterials.2011.04.052

[162] T. Kim, A. Branner, T. Gulati, S. F. Giszter, Braided multi-electrode probes: mechanical compliance characteristics and recordings from spinal cords, J. Neural Eng. 10 (2013) 045001. http://dx.doi.org/10.1088/1741-2560/10/4/045001

[163] J. L. Skousen, S. M. Merriam, O. Srivannavit, G. Perlin, K. D. Wise, P. A. Tresco, Reducing surface area while maintaining implant penetrating profile lowers the brain foreign body response to chronically implanted planar silicon microelectrode arrays, Prog. Brain Res. 194 (2011) 167-180. http://dx.doi.org/10.1016/B978-0-444-53815-4.00009-1

[164] J. K. Nguyen, D. J. Park, J. L. Skousen, A. E. Hess-Dunning, D. J. Tyler, S. J. Rowan, et al., Mechanically-compliant intracortical implants reduce the neuroinflammatory response, J. Neural Eng. 11 (2014) 056014. http://dx.doi.org/10.1088/1741-2560/11/5/056014

[165] S. R. Goldstein, M. Salcman, Mechanical factors in the design of chronic recording intracortical microelectrodes, IEEE Trans. Biomed. Eng. 20 (1973) 260-269. http://dx.doi.org/10.1109/TBME.1973.324190

[166] J. P. Harris, A. E. Hess, S. J. Rowan, C. Weder, C. A. Zorman, D. J. Tyler, et al., In vivo deployment of mechanically adaptive nanocomposites for intracortical microelectrodes, J. Neural Eng. 8 (2011) 046010. http://dx.doi.org/10.1088/1741-2560/8/4/046010

[167] C. A. Lopez, A. J. Fleischman, S. Roy, T. A. Desai, Evaluation of silicon nanoporous membranes and ECM-based microenvironments on neurosecretory cells, Biomaterials 27 (2006) 3075-3083. http://dx.doi.org/10.1016/j.biomaterials.2005.12.017

[168] C. A. Chapman, H. Chen, M. Stamou, J. Biener, M. M. Biener, P. Lein, et al., Nanoporous gold as a neural interface coating: effects of topography, surface chemistry, and feature size, ACS App. Mater. Interfaces 7 (2015) 7093–7100. http://dx.doi.org/10.1021/acsami.5b00410

[169] A. Misra, P. Kondaveeti, J. Nissanov, K. Barbee, P. Shewokis, L. Rioux, et al., Preventing neuronal damage and inflammation in vivo during cortical microelectrode implantation through the use of poloxamer P-188, J. Neural Eng. 10 (2013) 016011. http://dx.doi.org/10.1088/1741-2560/10/1/016011

[170] L. Rao, H. Zhou, T. Li, C. Li, Y. Y. Duan, Polyethylene glycol-containing polyurethane hydrogel coatings for improving the biocompatibility of neural electrodes, Acta Biomat. 8 (2012) 2233-2242. http://dx.doi.org/10.1016/j.actbio.2012.03.001

[171] T. D. Kozai, N. B. Langhals, P. R. Patel, X. Deng, H. Zhang, K. L. Smith, et al., Ultrasmall implantable composite microelectrodes with bioactive surfaces for chronic neural interfaces, Nat. Mater. 11 (2012) 1065-1073. http://dx.doi.org/10.1038/nmat3468

[172] X. Cui, J. Wiler, M. Dzaman, R. A. Altschuler, D. C. Martin, In vivo studies of polypyrrole/peptide coated neural probes, Biomaterials 24 (2003) 777-787.

[173] P. Kohler, A. Wolff, F. Ejserholm, L. Wallman, J. Schouenborg, C. E. Linsmeier, Influence of probe flexibility and gelatin embedding on neuronal density and glial responses to brain implants, PloS One 10 (2015) e0119340. http://dx.doi.org/10.1371/journal.pone.0119340

[174] E. Azemi, W. R. Stauffer, M. S. Gostock, C. F. Lagenaur, X. T. Cui, Surface immobilization of neural adhesion molecule L1 for improving the biocompatibility of chronic neural probes: In vitro characterization, Acta Biomater. 4 (2008) 1208-1217. http://dx.doi.org/10.1016/j.actbio.2008.02.028

[175] E. Azemi, C. F. Lagenaur, X. T. Cui, The surface immobilization of the neural adhesion molecule L1 on neural probes and its effect on neuronal density and gliosis at the probe/tissue interface, Biomaterials 32 (2011) 681-692. http://dx.doi.org/10.1016/j.biomaterials.2010.09.033

[176] A. H. Taub, R. Hogri, A. Magal, M. Mintz, Y. Shacham-Diamand, Bioactive anti-inflammatory coating for chronic neural electrodes, J. Biomed. Mater. Res. A 100 (2012) 1854-1858. http://dx.doi.org/10.1002/jbm.a.34152

[177] W. He, G. C. McConnell, R. V. Bellamkonda, Nanoscale laminin coating modulates cortical scarring response around implanted silicon microelectrode arrays, J. Neural Eng. 3 (2006) 316-326. http://dx.doi.org/10.1088/1741-2560/3/4/009

[178] D. H. Szarowski, M. D. Andersen, S. Retterer, A. J. Spence, M. Isaacson, H. G. Craighead, et al., Brain responses to micro-machined silicon devices, Brain Res. 983 (2003) 23-35. http://dx.doi.org/10.1016/s0006-8993(03)03023-3

[179] M. L. Rand, R. Leung, M. A. Packham, Platelet function assays, Transfusion and Apheresis Science 28 (2003) 307-317. http://dx.doi.org/10.1016/s1473-0502(03)00050-8

[180] R. W. Farndale, J. J. Sixma, M. J. Barnes, P. G. de Groot, The role of collagen in thrombosis and hemostasis, J. Thromb. Haemost. 2 (2004) 561-573. http://dx.doi.org/10.1111/j.1538-7836.2004.00665.x

[181] J. Emsley, C. G. Knight, R. W. Farndale, M. J. Barnes, R. C. Liddington, Structural Basis of Collagen Recognition by Integrin α2β1, Cell 101 (2000) 47-56. http://dx.doi.org/10.1016/s0092-8674(00)80622-4

[182] C. Knight, L. F. Morton, D. J. Onley, A. R. Peachey, T. Ichinohe, M. Okuma, et al., Collagen–platelet interaction: Gly-Pro-Hyp is uniquely specific for platelet Gp VI and mediates platelet activation by collagen, Cardiovasc. Res. 41 (1999) 450-457. http://dx.doi.org/10.1016/s0008-6363(98)00306-x

[183] O. Inoue, K. Suzuki-Inoue, O. J. McCarty, M. Moroi, Z. M. Ruggeri, T. J. Kunicki, et al., Laminin stimulates spreading of platelets through integrin alpha6beta1-dependent activation of GPVI, Blood 107 (2006) 1405-1412. http://dx.doi.org/10.1182/blood-2005-06-2406

[184] K. Jurk, B. E. Kehrel, Platelets: physiology and biochemistry, Semin. Thromb. Hemost. 31 (2005) 381-392. http://dx.doi.org/10.1055/s-2005-916671

[185] W. R. Wagner, J. M. Pachence, J. Ristich, P. C. Johnson, Comparative in vitro analysis of topical hemostatic agents, J. Surg. Res. 66 (1996) 100-108. http://dx.doi.org/10.1006/jsre.1996.0379

[186] B. N. Brown, R. Londono, S. Tottey, L. Zhang, K. A. Kukla, M. T. Wolf, et al., Macrophage phenotype as a predictor of constructive remodeling following the implantation of biologically derived surgical mesh materials, Acta Biomater. 8 (2012) 978-987. http://dx.doi.org/10.1016/j.actbio.2011.11.031

[187] B. N. Brown, J. E. Valentin, A. M. Stewart-Akers, G. P. McCabe, S. F. Badylak, Macrophage phenotype and remodeling outcomes in response to biologic scaffolds with and without a cellular component, Biomaterials 30 (2009) 1482-1491. http://dx.doi.org/10.1016/j.biomaterials.2008.11.040

[188] D. M. Faulk, R. Londono, M. T. Wolf, C. A. Ranallo, C. A. Carruthers, J. D. Wildemann, et al., ECM hydrogel coating mitigates the chronic inflammatory response to polypropylene mesh, Biomaterials 35 (2014) 8585-8595. http://dx.doi.org/10.1016/j.biomaterials.2014.06.057

[189] A. Mantovani, S. K. Biswas, M. R. Galdiero, A. Sica, M. Locati, Macrophage plasticity and polarization in tissue repair and remodelling, J. Pathol. 229 (2013) 176-185. http://dx.doi.org/10.1002/path.4133

[190] K. A. Kigerl, J. C. Gensel, D. P. Ankeny, J. K. Alexander, D. J. Donnelly, P. G. Popovich, Identification of two distinct macrophage subsets with divergent effects causing either neurotoxicity or regeneration in the injured mouse spinal cord, J. Neurosci. 29 (2009) 13435-13444. http://dx.doi.org/10.1523/JNEUROSCI.3257-09.2009

[191] D. P. Schafer, E. K. Lehrman, A. G. Kautzman, R. Koyama, A. R. Mardinly, R. Yamasaki, et al., Microglia sculpt postnatal neural circuits in an activity and complement-dependent manner, Neuron 74 (2012) 691-705. http://dx.doi.org/10.1016/j.neuron.2012.03.026

[192] L. Zhang, F. Zhang, Z. Weng, B. N. Brown, H. Yan, X. M. Ma, et al., Effect of an inductive hydrogel composed of urinary bladder matrix upon functional recovery following traumatic brain injury, Tissue Eng. A 19 (2013) 1909-1918. http://dx.doi.org/10.1089/ten.TEA.2012.0622

[193] J. Tanaka, K. Toku, M. Sakanaka, N. Maeda, Morphological differentiation of microglial cells in culture: involvement of insoluble factors derived from astrocytes, Neurosci. Res. 34 (1999) 207-215. http://dx.doi.org/10.1016/s0168-0102(99)00041-3

[194] J. Tanaka, K. Toku, S. Matsuda, S. Sudo, H. Fujita, M. Sakanaka, et al., Induction of resting microglia in culture medium devoid of glycine and serine, Glia 24 (1998) 198-215.

[195] J. Tanaka, N. Maeda, Microglial ramification requires nondiffusible factors derived from astrocytes, Exp. Neurol. 137 (1996) 367-375. http://dx.doi.org/10.1006/exnr.1996.0038

[196] G. Acevedo, N. K. Padala, L. Ni, G. M. Jonakait, Astrocytes inhibit microglial surface expression of dendritic cell-related co-stimulatory molecules through a contact-mediated process, J. Neurochem. 125 (2013) 575-587. http://dx.doi.org/10.1111/jnc.12221

[197] N. Jackson, A. Sridharan, S. Anand, M. Baker, M. Okandan, J. Muthuswamy, Long-Term Neural Recordings Using MEMS Based Movable Microelectrodes in the Brain, Front. Neuroeng. 3 (2010) 10. http://dx.doi.org/10.3389/fneng.2010.00010

[198] L. M. O. Oliveira, D. Dimitrov, Surgical Techniques for Chronic Implantation of Microwire Arrays in Rodents and Primates, in: M. A. L. Nicolelis (Eds.), Methods for Neural Ensemble Recordings, 2nd ed., CRC Press, Boca Raton (FL), 2008, pp. 1-25, NCBI Bookshelf, Web (accessed 04.27.2014) http://dx.doi.org/ 10.1201/9781420006414.ch2

[199] L. Karumbaiah, T. Saxena, D. Carlson, K. Patil, R. Patkar, E. A. Gaupp, et al., Relationship between intracortical electrode design and chronic recording function, Biomaterials 34 (2013) 8061-8074. http://dx.doi.org/10.1016/j.biomaterials.2013.07.016

[200] R. E. Hampson, V. Collins, S. A. Deadwyler, A wireless recording system that utilizes Bluetooth technology to transmit neural activity in freely moving animals, J. Neurosci. Methods 182 (2009) 195-204. http://dx.doi.org/10.1016/j.jneumeth.2009.06.007

[201] S. Venkatraman, X. Jin, R. M. Costa, J. M. Carmena, Investigating neural correlates of behavior in freely behaving rodents using inertial sensors, J. Neurophysiol. 104 (2010) 569-575. http://dx.doi.org/10.1152/jn.00121.2010

[202] T. W. Gardiner, L. A. Toth, Stereotactic Surgery and Long-Term Maintenance of Cranial Implants in Research Animals, Contemp. Top. Lab. Anim. Sci. 38 (1999) 56-63.

[203] Y. K. Hirshler, U. Polat, A. Biegon, Intracranial electrode implantation produces regional neuroinflammation and memory deficits in rats, Exp. Neurol. 222 (2010) 42-50. http://dx.doi.org/10.1016/j.expneurol.2009.12.006

[204] J. G. McCall, T. I. Kim, G. Shin, X. Huang, Y. H. Jung, R. Al-Hasani, et al., Fabrication and application of flexible, multimodal light-emitting devices for wireless optogenetics, Nat. Protoc. 8 (2013) 2413-2428. http://dx.doi.org/10.1038/nprot.2013.158

[205] D. R. Sparta, A. M. Stamatakis, J. L. Phillips, N. Hovelso, R. van Zessen, G. D. Stuber, Construction of implantable optical fibers for long-term optogenetic manipulation of neural circuits, Nat. Protoc. 7 (2012) 12-23. http://dx.doi.org/10.1038/nprot.2011.413

[206] A. Y. Shih, J. D. Driscoll, P. J. Drew, N. Nishimura, C. B. Schaffer, D. Kleinfeld, Two-photon microscopy as a tool to study blood flow and neurovascular coupling in the rodent brain, J. Cereb. Blood Flow Metab. 32 (2012) 1277-1309. http://dx.doi.org/10.1038/jcbfm.2011.196

[207] M. L. Monje, H. Toda, T. D. Palmer, Inflammatory blockade restores adult hippocampal neurogenesis, Science 302 (2003) 1760-1765. http://dx.doi.org/10.1126/science.1088417

[208] C. T. Ekdahl, J. H. Claasen, S. Bonde, Z. Kokaia, O. Lindvall, Inflammation is detrimental for neurogenesis in adult brain, Proc. Natl. Acad. Sci. U. S. A. 100 (2003) 13632-13637. http://dx.doi.org/10.1073/pnas.2234031100

[209] A. Borsini, P. A. Zunszain, S. Thuret, C. M. Pariante, The role of inflammatory cytokines as key modulators of neurogenesis, Trends Neurosci. 38 (2015) 145-157. http://dx.doi.org/10.1016/j.tins.2014.12.006

[210] N. P. Turrin, D. Gayle, S. E. Ilyin, M. C. Flynn, W. Langhans, G. J. Schwartz, et al., Pro-inflammatory and anti-inflammatory cytokine mRNA induction in the periphery and brain following intraperitoneal administration of bacterial lipopolysaccharide, Brain Res. Bull. 54 (2001) 443-453. http://dx.doi.org/10.1016/s0361-9230(01)00445-2

[211] K. Jakubs, S. Bonde, R. E. Iosif, C. T. Ekdahl, Z. Kokaia, M. Kokaia, et al., Inflammation regulates functional integration of neurons born in adult brain, J. Neurosci. 28 (2008) 12477-12488. http://dx.doi.org/10.1523/JNEUROSCI.3240-08.2008

[212] J. T. Cole, A. Yarnell, W. S. Kean, E. Gold, B. Lewis, M. Ren, et al., Craniotomy: true sham for traumatic brain injury, or a sham of a sham?, J. Neurotrauma 28 (2011) 359-369. http://dx.doi.org/10.1089/neu.2010.1427

[213] H. T. Xu, F. Pan, G. Yang, W. B. Gan, Choice of cranial window type for in vivo imaging affects dendritic spine turnover in the cortex, Nat. Neurosci. 10 (2007) 549-551. http://dx.doi.org/10.1038/nn1883

[214] S. M. Gutowski, K. L. Templeman, A. B. South, J. C. Gaulding, J. T. Shoemaker, M. C. LaPlaca, et al., Host response to microgel coatings on neural electrodes implanted in the brain, J. Biomed. Mater. Res. A 102 (2014) 1486-1499. http://dx.doi.org/10.1002/jbm.a.34799

[215] W. He, G. C. McConnell, T. M. Schneider, R. V. Bellamkonda, A Novel Anti-inflammatory Surface for Neural Electrodes, Adv. Mater. 19 (2007) 3529-3533. http://dx.doi.org/10.1002/adma.200700943

[216] S. De Faveri, E. Maggiolini, E. Miele, F. De Angelis, F. Cesca, F. Benfenati, et al., Bio-inspired hybrid microelectrodes: a hybrid solution to improve long-term performance of chronic intracortical implants, Front. Neuroeng. 7 (2014) 7. http://dx.doi.org/10.3389/fneng.2014.00007

[217] W. He, R. V. Bellamkonda, Nanoscale neuro-integrative coatings for neural implants, Biomaterials 26 (2005) 2983-2990. http://dx.doi.org/10.1016/j.biomaterials.2004.08.021

[218] T. D. Kozai, Z. Gugel, X. Li, P. J. Gilgunn, R. Khilwani, O. B. Ozdoganlar, et al., Chronic tissue response to carboxymethyl cellulose based dissolvable insertion needle for ultra-small neural probes, Biomaterials 35 (2014) 9255-9268. http://dx.doi.org/10.1016/j.biomaterials.2014.07.039

[219] J. Y. Lee, Z. Z. Khaing, J. J. Siegel, C. E. Schmidt, Surface modification of neural electrodes with a pyrrole-hyaluronic acid conjugate to attenuate reactive astrogliosis in vivo, RSC Adv. 5 (2015) 39228-39231. http://dx.doi.org/10.1039/c5ra03294f

[220] Y. Lu, T. Li, X. Zhao, M. Li, Y. Cao, H. Yang, et al., Electrodeposited polypyrrole/carbon nanotubes composite films electrodes for neural interfaces, Biomaterials 31 (2010) 5169-5181. http://dx.doi.org/10.1016/j.biomaterials.2010.03.022

[221] S. Sommakia, J. Gaire, J. L. Rickus, K. J. Otto, Resistive and reactive changes to the impedance of intracortical microelectrodes can be mitigated with polyethylene glycol under acute

in vitro and in vivo settings, Front. Neuroeng. 7 (2014) 1-8. http://dx.doi.org/10.3389/fneng.2014.00033

[222] H. Zhou, X. Cheng, L. Rao, T. Li, Y. Y. Duan, Poly(3,4-ethylenedioxythiophene)/multiwall carbon nanotube composite coatings for improving the stability of microelectrodes in neural prostheses applications, Acta Biomater. 9 (2013) 6439-6449. http://dx.doi.org/10.1016/j.actbio.2013.01.042

[223] T. Krucker, A. Lang, E. P. Meyer, New polyurethane-based material for vascular corrosion casting with improved physical and imaging characteristics, Microsc. Res. Tech. 69 (2006) 138-147. http://dx.doi.org/10.1002/jemt.20263

[224] P. Blinder, P. S. Tsai, J. P. Kaufhold, P. M. Knutsen, H. Suhl, D. Kleinfeld, The cortical angiome: an interconnected vascular network with noncolumnar patterns of blood flow, Nat. Neurosci. 16 (2013) 889-897. http://dx.doi.org/10.1038/nn.3426

[225] D. L. Coleman, R. N. King, J. D. Andrade, The foreign body reaction: a chronic inflammatory response, J. Biomed. Mater. Res. 8 (1974) 199-211. http://dx.doi.org/10.1002/jbm.820080503

[226] A. E. Wright, S. R. Douglas, An Experimental Investigation of the Role of the Blood Fluids in Connection with Phagocytosis, Proc. Royal Soc. Lond. 72 (1903) 357-370. http://dx.doi.org/10.1098/rspl.1903.0062

[227] J. V. Ravetch, S. Bolland, IgG Fc receptors, Annu. Rev. Immunol. 19 (2001) 275-290. http://dx.doi.org/10.1146/annurev.immunol.19.1.275

[228] E. Metchnikoff, F. G. Binnie, Immunity in infective diseases, University Press, Cambridge, 1905, Web, (accessed 10.20.2015) http://dx.doi.org/10.5962/bhl.title.29861

[229] C. Schachtrup, J. K. Ryu, M. J. Helmrick, E. Vagena, D. K. Galanakis, J. L. Degen, et al., Fibrinogen triggers astrocyte scar formation by promoting the availability of active TGF-beta after vascular damage, J. Neurosci. 30 (2010) 5843-5854. http://dx.doi.org/10.1523/JNEUROSCI.0137-10.2010

[230] A. Y. Shih, P. Blinder, P. S. Tsai, B. Friedman, G. Stanley, P. D. Lyden, et al., The smallest stroke: occlusion of one penetrating vessel leads to infarction and a cognitive deficit, Nat. Neurosci. 16 (2013) 55-63. http://dx.doi.org/10.1038/nn.3278

[231] M. B. Ariganello, D. T. Simionescu, R. S. Labow, J. M. Lee, Macrophage differentiation and polarization on a decellularized pericardial biomaterial, Biomaterials 32 (2011) 439-449. http://dx.doi.org/10.1016/j.biomaterials.2010.09.004

[232] N. Sadr, B. E. Pippenger, A. Scherberich, D. Wendt, S. Mantero, I. Martin, et al., Enhancing the biological performance of synthetic polymeric materials by decoration with engineered, decellularized extracellular matrix, Biomaterials 33 (2012) 5085-5093. http://dx.doi.org/10.1016/j.biomaterials.2012.03.082

[233] H. H. Yao, M. K. Hong, K. J. Drummond, Haemostasis in neurosurgery: what is the evidence for gelatin-thrombin matrix sealant?, J. Clin. Neurosci. 20 (2013) 349-356. http://dx.doi.org/10.1016/j.jocn.2012.09.005

[234] J. C. Wolchok, P. A. Tresco, The isolation of cell derived extracellular matrix constructs using sacrificial open-cell foams, Biomaterials 31 (2010) 9595-9603. http://dx.doi.org/10.1016/j.biomaterials.2010.08.072

[235] K. Webb, R. W. Hitchcock, R. M. Smeal, W. Li, S. D. Gray, P. A. Tresco, Cyclic strain increases fibroblast proliferation, matrix accumulation, and elastic modulus of fibroblast-seeded polyurethane constructs, J. Biomech. 39 (2006) 1136-1144. http://dx.doi.org/10.1016/j.jbiomech.2004.08.026

[236] J. C. Wolchok, P. A. Tresco, Using growth factor conditioning to modify the properties of human cell derived extracellular matrix, Biotechnol. Prog. 28 (2012) 1581-1587. http://dx.doi.org/10.1002/btpr.1625

[237] R. Biran, M. D. Noble, P. A. Tresco, Directed nerve outgrowth is enhanced by engineered glial substrates, Exp. Neurol. 184 (2003) 141-152. http://dx.doi.org/10.1016/s0014-4886(03)00253-x

[238] D. J. Rosario, G. C. Reilly, E. Ali Salah, M. Glover, A. J. Bullock, S. Macneil, Decellularization and sterilization of porcine urinary bladder matrix for tissue engineering in the lower urinary tract, Regen. Med. 3 (2008) 145-156. http://dx.doi.org/10.2217/17460751.3.2.145

[239] J. D. Rybock, D. M. Long, Use of microfibrillar collagen as a topical hemostatic agent in brain tissue, J. Neurosurg. 46 (1977) 501-505. http://dx.doi.org/10.3171/jns.1977.46.4.0501

[240] M. J. Bridge, P. Tresco, In Vivo Solute Diffusivity in Brain Tissue Surrounding Indwelling Neural Implants, in: Reichert WM, (Eds.), Indwelling Neural Implants: Strategies for Contending with the In Vivo Environment., CRC Press/Taylor & Francis, Boca Raton (FL), 2008, pp. 117-148, NCBI Bookshelf, Web (accessed 09.27.2015)

[241] A. Dietrich, M. Myers, S. Schneid, Collagen Powder, United States, Innocoll Technologies Limited, 2014.

[242] J. Nichols, I. Oneson, Purified Collagen Fibrils, United States, Ethicon Inc.; 1970.

[243] M. V. Sofroniew, Molecular dissection of reactive astrogliosis and glial scar formation, Trends Neurosci. 32 (2009) 638-647. http://dx.doi.org/10.1016/j.tins.2009.08.002

[244] A. J. Singer, R. A. Clark, Cutaneous wound healing, N. Engl. J. Med. 341 (1999) 738-746. http://dx.doi.org/10.1056/NEJM199909023411006

[245] L. E. Carey, C. L. Dearth, S. A. Johnson, R. Londono, C. J. Medberry, K. A. Daly, et al., In vivo degradation of 14C-labeled porcine dermis biologic scaffold, Biomaterials 35 (2014) 8297-8304. http://dx.doi.org/10.1016/j.biomaterials.2014.06.015

[246] E. Allaire, P. Bruneval, C. Mandet, J.-P. Becquemin, J.-B. Michel, The immunogenicity of the extracellular matrix in arterial xenografts, Surgery 122 (1997) 73-81. http://dx.doi.org/10.1016/s0039-6060(97)90267-1

[247] J. M. Singelyn, J. A. DeQuach, S. B. Seif-Naraghi, R. B. Littlefield, P. J. Schup-Magoffin, K. L. Christman, Naturally derived myocardial matrix as an injectable scaffold for cardiac tissue engineering, Biomaterials 30 (2009) 5409-5416. http://dx.doi.org/10.1016/j.biomaterials.2009.06.045

[248] S. D. Keene, T. M. Greco, I. Parastatidis, S. H. Lee, E. G. Hughes, R. J. Balice-Gordon, et al., Mass spectrometric and computational analysis of cytokine-induced alterations in the astrocyte secretome, Proteomics 9 (2009) 768-782. http://dx.doi.org/10.1002/pmic.200800385

[249] N. H. Moore, L. G. Costa, S. A. Shaffer, D. R. Goodlett, M. Guizzetti, Shotgun proteomics implicates extracellular matrix proteins and protease systems in neuronal development induced

by astrocyte cholinergic stimulation, J. Neurochem. 108 (2009) 891-908. http://dx.doi.org/10.1111/j.1471-4159.2008.05836.x

[250] J. Elsas, B. Sellhaus, M. Herrmann, A. Kinkeldey, J. Weis, W. Jahnen-Dechent, et al., Fetuin-a in the developing brain, Dev. Neurobiol. 73 (2013) 354-369. http://dx.doi.org/10.1002/dneu.22064

[251] K. Webb, W. Li, R. W. Hitchcock, R. M. Smeal, S. D. Gray, P. A. Tresco, Comparison of human fibroblast ECM-related gene expression on elastic three-dimensional substrates relative to two-dimensional films of the same material, Biomaterials 24 (2003) 4681-4690. http://dx.doi.org/10.1016/s0142-9612(03)00368-5

[252] J. H. Rand, N. D. Patel, E. Schwartz, S. L. Zhou, B. J. Potter, 150-kD von Willebrand factor binding protein extracted from human vascular subendothelium is type VI collagen, J. Clin. Invest. 88 (1991) 253-259. http://dx.doi.org/10.1172/JCI115285

[253] C. Denis, D. Baruch, C. M. Kielty, N. Ajzenberg, O. Christophe, D. Meyer, Localization of von Willebrand factor binding domains to endothelial extracellular matrix and to type VI collagen, Arterioscler. Thromb. 13 (1993) 398-406.

[254] M. Yamagata, K. M. Yamada, S. S. Yamada, S. Tamayaki, H. Tanaka, Y. Nishida, et al., The complete primary structure of type XII collagen shows a chimeric molecule with reiterated fibronectin type III motifs, von Willebrand factor A motifs, a domain homologous to a noncollagenous region of type IX collagen, and short collagenous domains with an Arg-Gly-Asp site, J. Cell Biol. 115 (1991) 209-221. http://dx.doi.org/10.1083/jcb.115.1.209

[255] N. A. DiProspero, S. Meiners, H. M. Geller, Inflammatory cytokines interact to modulate extracellular matrix and astrocytic support of neurite outgrowth, Exp. Neurol. 148 (1997) 628-639. http://dx.doi.org/10.1006/exnr.1997.6700

[256] A. Rolls, R. Shechter, M. Schwartz, The bright side of the glial scar in CNS repair, Nat. Rev. Neurosci. 10 (2009) 235-241. http://dx.doi.org/10.1038/nrn2591

[257] R. V. Iozzo, I. R. Cohen, S. Grassel, A. D. Murdoch, The biology of perlecan: the multifaceted heparan sulphate proteoglycan of basement membranes and pericellular matrices, Biochem. J. 302 (Pt 3) (1994) 625-639.

[258] U. Hartmann, P. Maurer, Proteoglycans in the nervous system--the quest for functional roles in vivo, Matrix Biol. 20 (2001) 23-35.

[259] Y. Deguchi, H. Okutsu, T. Okura, S. Yamada, R. Kimura, T. Yuge, et al., Internalization of basic fibroblast growth factor at the mouse blood-brain barrier involves perlecan, a heparan sulfate proteoglycan, J. Neurochem. 83 (2002) 381-389. http://dx.doi.org/10.1046/j.1471-4159.2002.01129.x

[260] M. Tenan, G. Fulci, M. Albertoni, A. C. Diserens, M. F. Hamou, M. El Atifi-Borel, et al., Thrombospondin-1 Is Downregulated by Anoxia and Suppresses Tumorigenicity of Human Glioblastoma Cells, J. Exp. Med. 191 (2000) 1789-1798. http://dx.doi.org/10.1084/jem.191.10.1789

[261] B. Jimenez, O. V. Volpert, S. E. Crawford, M. Febbraio, R. L. Silverstein, N. Bouck, Signals leading to apoptosis-dependent inhibition of neovascularization by thrombospondin-1, Nat. Med. 6 (2000) 41-48. http://dx.doi.org/10.1038/71517

[262] J. Lawler, The functions of thrombospondin-1 and-2, Curr Opin Cell Biol 12 (2000) 634-640.

[263] M. Demetriou, C. Binkert, B. Sukhu, H. C. Tenenbaum, J. W. Dennis, Fetuin/alpha 2-HS Glycoprotein Is a Transforming Growth Factor-beta Type II Receptor Mimic and Cytokine Antagonist, J. Biol. Chem. 271 (1996) 12755-12761. http://dx.doi.org/10.1074/jbc.271.22.12755

[264] H. Wang, W. Li, S. Zhu, J. Li, J. D'Amore, M. F. Ward, et al., Peripheral administration of fetuin-A attenuates early cerebral ischemic injury in rats, J. Cereb. Blood Flow Metab. 30 (2010) 493-504. http://dx.doi.org/10.1038/jcbfm.2009.247

[265] R. Minana, E. Climent, D. Barettino, J. M. Segui, J. Renau-Piqueras, C. Guerri, Alcohol exposure alters the expression pattern of neural cell adhesion molecules during brain development, J. Neurochem. 75 (2000) 954-964.

[266] M. Iwai, K. Sato, N. Omori, I. Nagano, Y. Manabe, M. Shoji, et al., Three steps of neural stem cells development in gerbil dentate gyrus after transient ischemia, J. Cereb. Blood Flow Metab. 22 (2002) 411-419. http://dx.doi.org/10.1097/00004647-200204000-00005

[267] A. C. Lepore, I. Fischer, Lineage-restricted neural precursors survive, migrate, and differentiate following transplantation into the injured adult spinal cord, Exp. Neurol. 194 (2005) 230-242. http://dx.doi.org/10.1016/j.expneurol.2005.02.020

[268] S. Zhang, Y. Y. Xia, H. C. Lim, F. R. Tang, Z. W. Feng, NCAM-mediated locomotor recovery from spinal cord contusion injury involves neuroprotection, axon regeneration, and synaptogenesis, Neurochem. Int. 56 (2010) 919-929. http://dx.doi.org/10.1016/j.neuint.2010.03.023

[269] M. A. Nicolelis, D. Dimitrov, J. M. Carmena, R. Crist, G. Lehew, J. D. Kralik, et al., Chronic, multisite, multielectrode recordings in macaque monkeys, Proc. Natl. Acad. Sci. U. S. A. 100 (2003) 11041-11046. http://dx.doi.org/10.1073/pnas.1934665100

[270] A. S. Dickey, A. Suminski, Y. Amit, N. G. Hatsopoulos, Single-unit stability using chronically implanted multielectrode arrays, J. Neurophysiol. 102 (2009) 1331-1339. http://dx.doi.org/10.1152/jn.90920.2008

[271] G. Santhanam, S. I. Ryu, B. M. Yu, A. Afshar, K. V. Shenoy, A high-performance brain-computer interface, Nature 442 (2006) 195-198. http://dx.doi.org/10.1038/nature04968

[272] W. M. Grill, S. E. Norman, R. V. Bellamkonda, Implanted neural interfaces: biochallenges and engineered solutions, Annu. Rev. Biomed. Eng. 11 (2009) 1-24. http://dx.doi.org/10.1146/annurev-bioeng-061008-124927

[273] D. J. Edell, V. V. Toi, V. M. McNeil, L. D. Clark, Factors influencing the biocompatibility of insertable silicon microshafts in cerebral cortex, IEEE Trans. Biomed. Eng. 39 (1992) 635-643. http://dx.doi.org/10.1109/10.141202

[274] M. T. Fitch, J. Silver, Glial cell extracellular matrix: boundaries for axon growth in development and regeneration, Cell. Tissue Res. 290 (1997) 379-384. http://dx.doi.org/10.1007/s004410050944

[275] Y.-T. Kim, R. W. Hitchcock, M. J. Bridge, P. A. Tresco, Chronic response of adult rat brain tissue to implants anchored to the skull, Biomaterials 25 (2004) 2229-2237. http://dx.doi.org/10.1016/j.biomaterials.2003.09.010

[276] K. Jin, Y. Sun, L. Xie, A. Peel, X. O. Mao, S. Batteur, et al., Directed migration of neuronal precursors into the ischemic cerebral cortex and striatum, Mol. Cell. Neurosci. 24 (2003) 171-189. http://dx.doi.org/10.1016/s1044-7431(03)00159-3

[277] D. J. Sharp, G. Scott, R. Leech, Network dysfunction after traumatic brain injury, Nat. Rev. Neurol. 10 (2014) 156-166. http://dx.doi.org/10.1038/nrneurol.2014.15

[278] A. Kutzelnigg, C. F. Lucchinetti, C. Stadelmann, W. Bruck, H. Rauschka, M. Bergmann, et al., Cortical demyelination and diffuse white matter injury in multiple sclerosis, Brain 128 (2005) 2705-2712. http://dx.doi.org/10.1093/brain/awh641

[279] P. G. Matz, A. Lewen, P. H. Chan, Neuronal, but not microglial, accumulation of extravasated serum proteins after intracerebral hemolysate exposure is accompanied by cytochrome c release and DNA fragmentation, J. Cereb. Blood Flow Metab. 21 (2001) 921-928. http://dx.doi.org/10.1097/00004647-200108000-00004

[280] K. A. Potter, A. C. Buck, W. K. Self, M. E. Callanan, S. Sunil, J. R. Capadona, The effect of resveratrol on neurodegeneration and blood brain barrier stability surrounding intracortical microelectrodes, Biomaterials 34 (2013) 7001-7015. http://dx.doi.org/10.1016/j.biomaterials.2013.05.035

[281] A. Denes, S. Ferenczi, K. J. Kovacs, Systemic inflammatory challenges compromise survival after experimental stroke via augmenting brain inflammation, blood- brain barrier damage and brain oedema independently of infarct size, J. Neuroinflammation 8 (2011) 164. http://dx.doi.org/10.1186/1742-2094-8-164

[282] A. Basu, J. K. Krady, M. O'Malley, S. D. Styren, S. T. DeKosky, S. W. Levison, The Type 1 Interleukin-1 Receptor Is Essential for the Efficient Activation of Microglia and the Induction of Multiple Proinflammatory Mediators in Response to Brain Injury, J. Neurosci. 22 (2002) 6071-6082.

[283] T. D. Kozai, A. L. Vazquez, C. L. Weaver, S. G. Kim, X. T. Cui, In vivo two-photon microscopy reveals immediate microglial reaction to implantation of microelectrode through extension of processes, J. Neural Eng. 9 (2012) 066001. http://dx.doi.org/10.1088/1741-2560/9/6/066001

[284] N. T. Markwardt, J. Stokol, R. L. Rennaker, 2nd, Sub-meninges implantation reduces immune response to neural implants, J. Neurosci. Methods 214 (2013) 119-125. http://dx.doi.org/10.1016/j.jneumeth.2013.01.020

[285] W. Tian, A. Sawyer, F. B. Kocaoglu, T. R. Kyriakides, Astrocyte-derived thrombospondin-2 is critical for the repair of the blood-brain barrier, Am. J. Pathol. 179 (2011) 860-868. http://dx.doi.org/10.1016/j.ajpath.2011.05.002

[286] W. Shain, L. Spataro, J. Dilgen, K. Haverstick, S. Retterer, M. Isaacson, et al., Controlling cellular reactive responses around neural prosthetic devices using peripheral and local intervention strategies, IEEE Trans. Neural Syst. Rehabil. Eng. 11 (2003) 186-188. http://dx.doi.org/10.1109/TNSRE.2003.814800

[287] S. Venkatachalam, M. S. Fee, D. Kleinfeld, Ultra-miniature headstage with 6-channel drive and vacuum-assisted micro-wire implantation for chronic recording from the neocortex, J. Neurosci. Methods 90 (1999) 37-46.

[288] J. N. Turner, W. Shain, D. H. Szarowski, M. Andersen, S. Martins, M. Isaacson, et al., Cerebral astrocyte response to micromachined silicon implants, Exp. Neurol. 156 (1999) 33-49. http://dx.doi.org/10.1006/exnr.1998.6983

[289] A. Bignami, D. Dahl, The Astroglial Response to Stabbing. Immunofluorescence Studies with Antibodies to Astrocyte-Specific Protein (Gfa) in Mammalian and Submammalian

Vertebrates, Neuropathol. Appl. Neurobiol. 2 (1976) 99-110. http://dx.doi.org/10.1111/j.1365-2990.1976.tb00488.x

[290] D. J. Wolak, M. E. Pizzo, R. G. Thorne, Probing the extracellular diffusion of antibodies in brain using in vivo integrative optical imaging and ex vivo fluorescence imaging, J. Control. Release 197 (2015) 78-86. http://dx.doi.org/10.1016/j.jconrel.2014.10.034

[291] M. C. Shearer, S. P. Niclou, D. Brown, R. A. Asher, A. J. G. D. Holtmaat, J. M. Levine, et al., The astrocyte/meningeal cell interface is a barrier to neurite outgrowth which can be overcome by manipulation of inhibitory molecules or axonal signalling pathways, Mol. Cell. Neurosci. 24 (2003) 913-925. http://dx.doi.org/10.1016/j.mcn.2003.09.004

[292] P. L. Gabbott, M. G. Stewart, Distribution of neurons and glia in the visual cortex (area 17) of the adult albino rat: a quantitative description, Neurosci. 21 (1987) 833-845.

[293] A. Kharlamov, E. Kharlamov, D. M. Armstrong, Age-Dependent Increase in Infarct Volume Following Photochemically Induced Cerebral Infarction: Putative Role of Astroglia, J. Gerontol. A Biol. Sci. Med. Sci. 55 (2000) B135-B141. http://dx.doi.org/10.1093/gerona/55.3.B135

[294] B. L. Eppley, L. Morales, R. Wood, J. Pensler, J. Goldstein, R. J. Havlik, et al., Resorbable PLLA-PGA Plate and Screw Fixation in Pediatric Craniofacial Surgery: Clinical Experience in 1883 Patients, Plast. and Reconstr. Surg. 114 (2004) 850-856. http://dx.doi.org/10.1097/01.prs.0000132856.69391.43

[295] P. G. Cox, N. Jeffery, Reviewing the morphology of the jaw-closing musculature in squirrels, rats, and guinea pigs with contrast-enhanced microCT, Anat. Rec. (Hoboken) 294 (2011) 915-928. http://dx.doi.org/10.1002/ar.21381

[296] R. Bolander, B. Mathie, C. Bir, D. Ritzel, P. VandeVord, Skull flexure as a contributing factor in the mechanism of injury in the rat when exposed to a shock wave, Ann. Biomed. Eng. 39 (2011) 2550-2559. http://dx.doi.org/10.1007/s10439-011-0343-0

[297] L. E. Corum, V. Hlady, Screening platelet-surface interactions using negative surface charge gradients, Biomaterials 31 (2010) 3148-3155. http://dx.doi.org/10.1016/j.biomaterials.2010.01.025

[298] R. Beigi, E. Kobatake, M. Aizawa, G. R. Dubyak, Detection of local ATP release from activated platelets using cell surface-attached firefly luciferase, Am. J. Physiol. Cell Physiol. 276 (1999) C267-C278.

[299] K. Wulf, M. Teske, M. Lobler, F. Luderer, K. P. Schmitz, K. Sternberg, Surface functionalization of poly(epsilon-caprolactone) improves its biocompatibility as scaffold material for bioartificial vessel prostheses, J. Biomed. Mater. Res. B Appl. Biomater. 98 (2011) 89-100. http://dx.doi.org/10.1002/jbm.b.31836

[300] M. Munder, K. Eichmann, J. M. Moran, F. Centeno, G. Soler, M. Modolell, Th1/Th2-regulated expression of arginase isoforms in murine macrophages and dendritic cells, J. Immunol. 163 (1999) 3771-3777.

[301] R. M. Ritzel, A. R. Patel, J. M. Grenier, J. Crapser, R. Verma, E. R. Jellison, et al., Functional differences between microglia and monocytes after ischemic stroke, J. Neuroinflammation 12 (2015) 106. http://dx.doi.org/10.1186/s12974-015-0329-1

[302] J. A. Ellison, F. C. Barone, G. Z. Feuerstein, Matrix Remodeling after Stroke: De Novo Expression of Matrix Proteins and Integrin Receptors, Ann. N. Y. Acad. Sci. 890 (1999) 204-222. http://dx.doi.org/10.1111/j.1749-6632.1999.tb07996.x

[303] D. Giulian, J. Chen, J. E. Ingeman, J. K. George, M. Noponen, The role of mononuclear phagocytes in wound healing after traumatic injury to adult mammalian brain, J. Neurosci. 9 (1989) 4416-4429.

[304] L. C. Zanetti-Domingues, C. J. Tynan, D. J. Rolfe, D. T. Clarke, M. Martin-Fernandez, Hydrophobic fluorescent probes introduce artifacts into single molecule tracking experiments due to non-specific binding, PloS One 8 (2013) e74200. http://dx.doi.org/10.1371/journal.pone.0074200

[305] R. H. Seevers, R. E. Counsell, Radioiodination techniques for small organic molecules, Chem. Rev. 82 (1982) 575-590. http://dx.doi.org/10.1021/cr00052a002

[306] A. E. Bolton, W. M. Hunter, The labelling of proteins to high specific radioactivities by conjugation to a 125I-containing acylating agent, Biochem. J. 133 (1973) 529-539.

[307] T. W. Gilbert, A. M. Stewart-Akers, S. F. Badylak, A quantitative method for evaluating the degradation of biologic scaffold materials, Biomaterials 28 (2007) 147-150. http://dx.doi.org/10.1016/j.biomaterials.2006.08.022

[308] P. L. Osheroff, V. T. Ling, R. L. Vandlen, M. J. Cronin, J. A. Lofgren, Preparation of biologically active 32P-labeled human relaxin. Displaceable binding to rat uterus, cervix, and brain, J. Biol. Chem. 265 (1990) 9396-9401.

[309] V. Espina, J. D. Wulfkuhle, V. S. Calvert, A. VanMeter, W. Zhou, G. Coukos, et al., Laser-capture microdissection, Nat. Protoc. 1 (2006) 586-603. http://dx.doi.org/10.1038/nprot.2006.85

[310] D. Mustafa, J. M. Kros, T. Luider, Combining Laser Capture Microdissection and Proteomics Techniques, Methods Med. Biol. 428 (2008) 159-178. http://dx.doi.org/10.1007/978-1-59745-117-8_9

[311] T. Dull, R. Zufferey, M. Kelly, R. J. Mandel, M. Nguyen, D. Trono, et al., A third-generation lentivirus vector with a conditional packaging system, J. Virol. 72 (1998) 8463-8471.

[312] R. M. Boehler, R. Kuo, S. Shin, A. G. Goodman, M. A. Pilecki, R. M. Gower, et al., Lentivirus delivery of IL-10 to promote and sustain macrophage polarization towards an anti-inflammatory phenotype, Biotechnol. Bioeng. 111 (2014) 1210-1221. http://dx.doi.org/10.1002/bit.25175

[313] M. S. Moehle, P. J. Webber, T. Tse, N. Sukar, D. G. Standaert, T. M. DeSilva, et al., LRRK2 inhibition attenuates microglial inflammatory responses, J. Neurosci. 32 (2012) 1602-1611. http://dx.doi.org/10.1523/JNEUROSCI.5601-11.2012

[314] R. M. Gower, R. M. Boehler, S. M. Azarin, C. F. Ricci, J. N. Leonard, L. D. Shea, Modulation of leukocyte infiltration and phenotype in microporous tissue engineering scaffolds via vector induced IL-10 expression, Biomaterials 35 (2014) 2024-2031. http://dx.doi.org/10.1016/j.biomaterials.2013.11.036

[315] S. Shin, H. M. Tuinstra, D. M. Salvay, L. D. Shea, Phosphatidylserine immobilization of lentivirus for localized gene transfer, Biomaterials 31 (2010) 4353-4359. http://dx.doi.org/10.1016/j.biomaterials.2010.02.013

[316] A. Mantovani, A. Sica, S. Sozzani, P. Allavena, A. Vecchi, M. Locati, The chemokine system in diverse forms of macrophage activation and polarization, Trends Immunol. 25 (2004) 677-686. http://dx.doi.org/10.1016/j.it.2004.09.015

[317] M. Forlenza, I. R. Fink, G. Raes, G. F. Wiegertjes, Heterogeneity of macrophage activation in fish, Dev. Comp. Immunol. 35 (2011) 1246-1255. http://dx.doi.org/10.1016/j.dci.2011.03.008

[318] M. Rath, I. Muller, P. Kropf, E. I. Closs, M. Munder, Metabolism via Arginase or Nitric Oxide Synthase: Two Competing Arginine Pathways in Macrophages, Front. Immunol. 5 (2014) 1-10. http://dx.doi.org/10.3389/fimmu.2014.00532

[319] S. E. Lakhan, A. Kirchgessner, D. Tepper, A. Leonard, Matrix metalloproteinases and blood-brain barrier disruption in acute ischemic stroke, Front. Neurol. 4 (2013) 1-15. http://dx.doi.org/10.3389/fneur.2013.00032

[320] T. Maier, M. Guell, L. Serrano, Correlation of mRNA and protein in complex biological samples, FEBS Lett. 583 (2009) 3966-3973. http://dx.doi.org/10.1016/j.febslet.2009.10.036

[321] A. S. Zeiger, F. C. Loe, R. Li, M. Raghunath, K. J. Van Vliet, Macromolecular crowding directs extracellular matrix organization and mesenchymal stem cell behavior, PloS One 7 (2012) e37904. http://dx.doi.org/10.1371/journal.pone.0037904

[322] L. Yang, C. F. Fitie, K. O. van der Werf, M. L. Bennink, P. J. Dijkstra, J. Feijen, Mechanical properties of single electrospun collagen type I fibers, Biomaterials 29 (2008) 955-962. http://dx.doi.org/10.1016/j.biomaterials.2007.10.058

[323] J. A. Matthews, G. E. Wnek, D. G. Simpson, G. L. Bowlin, Electrospinning of Collagen Nanofibers, Biomacromolecules 3 (2002) 232-238. http://dx.doi.org/10.1021/bm015533u

[324] F. Meng, V. Hlady, P. A. Tresco, Inducing alignment in astrocyte tissue constructs by surface ligands patterned on biomaterials, Biomaterials 33 (2012) 1323-1335. http://dx.doi.org/10.1016/j.biomaterials.2011.10.034

[325] P. Conti, X. Pang, W. Boucher, R. Letourneau, M. Reale, R. Barbacane, et al., Impact of Rantes and MCP-1 Chemokines on In Vivo Basophilic Cell Recruitment in Rat Skin Injection Model and Their Role in Modifying the Protein and mRNA Levels for Histidine Decarboxylase, Blood 89 (1997) 4120-4127.

[326] J. Jiang, F. R. Willett, D. M. Taylor, Relationship between microelectrode array impedance and chronic recording quality of single units and local field potentials, Conf. Proc. IEEE Eng. Med. Biol. Soc. (2014) 3045-3048. http://dx.doi.org/10.1109/embc.2014.6944265

[327] J. C. Williams, J. A. Hippensteel, J. Dilgen, W. Shain, D. R. Kipke, Complex impedance spectroscopy for monitoring tissue responses to inserted neural implants, J. Neural Eng. 4 (2007) 410-423. http://dx.doi.org/10.1088/1741-2560/4/4/007

[328] G. C. McConnell, R. J. Butera, R. V. Bellamkonda, Bioimpedance modeling to monitor astrocytic response to chronically implanted electrodes, J. Neural Eng. 6 (2009) 055005. http://dx.doi.org/10.1088/1741-2560/6/5/055005

[329] H. Wilms, J. Claasen, C. Röhl, J. Sievers, G. Deuschl, R. Lucius, Involvement of benzodiazepine receptors in neuroinflammatory and neurodegenerative diseases: evidence from activated microglial cells in vitro, Neurobiol. Dis. 14 (2003) 417-424. http://dx.doi.org/10.1016/j.nbd.2003.07.002

[330] A. J. McMorland, M. Velliste, Baseplate for two-stage cranial mounting of BMI connectors, J. Neural Eng. 10 (2013) 034001. http://dx.doi.org/10.1088/1741-2560/10/3/034001

[331] B. T. Rao, R. Kaul, P. Tiwari, A. K. Nath, Inert gas cutting of titanium sheet with pulsed mode CO2 laser, Opt. Lasers Eng. 43 (2005) 1330-1348. http://dx.doi.org/10.1016/j.optlaseng.2004.12.009

[332] H. E. Gotz, M. Muller, A. Emmel, U. Holzwarth, R. G. Erben, R. Stangl, Effect of surface finish on the osseointegration of laser-treated titanium alloy implants, Biomaterials 25 (2004) 4057-4064. http://dx.doi.org/10.1016/j.biomaterials.2003.11.002

[333] D. Puleo, Understanding and controlling the bone–implant interface, Biomaterials 20 (1999) 2311-2321. http://dx.doi.org/10.1016/s0142-9612(99)00160-x